Metallization of Carbon Fibre Reinforced Composites by Lay-up on Cold Sprayed Coatings and by GRIP Metal™ as Bond Coat for Cold Spray

by

Yue Heng Xu

Thesis submitted to the Department of Mechanical Engineering in conformity with the requirements of

Master of Applied Science

University of Ottawa
Ottawa, Canada

January 2018

© Yue Heng Xu, Ottawa, Canada, 2018

Acknowledgements

I would first like to thank my thesis supervisor, Dr. Bertrand Jodoin and co-supervisor, Dr. François Robitaille, for their great guidance in my work. I am thankful for the opportunity that they provided me through which I gained tremendous knowledge. Aside from science, they also showed me how to be more confident and positive in face of failures, which are attributes that I will keep for years to come.

I would like to thank my colleagues for their support, including those who have come and gone. Their knowledge and expertise were truly helpful and valuable. A special thanks to Dr. Mohammed Yandouzi for taking care of the lab equipment, lab supplies, and mess that we made. Without him, Health and Safety Management would be constantly chasing after us.

I would like to thank the people working in the machine shop, Stanley, Leo, Paul and Jacques for their help. Without their dedication and quick response time, my experiments would not have been conducted on time.

Last but not least, I would like to thank my mother who supported me through all these academic years. I am eternally thankful for everything that she has done for me. She has been a true inspiration for me and a great example of what one can achieve with determination, dedication and discipline.

Abstract

The aerospace industry improves safety, reliability and performance of aircrafts through greater incorporation of advanced materials. Carbon fibre reinforced composites (CFRCs), being the most prevalent materials among all, gradually replace many components originally made from aluminium. CFRCs gained their popularity thanks to their high strength-to-weight ratios. Although being strong and light, these materials exhibit vulnerabilities in terms of erosion and limited electrical conductivity. In-flight aircrafts are often subjected to foreign objects such as debris and hail, and to lighting strikes. Damage to critical CFRC components can both cause danger to passengers and put aircraft temporarily out of service. These issues are currently solved by costly methods such as gluing metallic sheets for erosion protection, and embedding copper mesh for lighting strike in relevant areas of the CFRCs.

The purpose of this research was to investigate two potential alternative methods for metallizing, thus protecting CFRC against erosion and lightning strikes. The first approach features the use of a lay-up technique referred to as “Reverse Lay-up Method”. The objectives of this approach were, first, to develop a reliable demoulding process, then a dense and crack-free coating on CFRCs. The second approach, referred to as the “GRIP Metal™ as Bond Coat Method”, features the use of GRIP Metal™ technology as bond coat for cold spray. The objectives of this approach were to characterize the GRIP Metal™ products and to assess their integration into CFRCs.

In the Reverse Lay-up Method, a simple and reliable demoulding process was developed whereby an extra length of CFRC, protruding one edge of the mould, was added to the composite component’s original dimensions. The protrusion served as a cantilever for facilitating the

demoulding process. In term of microstructure, the results revealed that for given surface preparation and spray parameters, copper powder of dendritic morphology could not produce satisfying results due to the presence of microcracks in both as-sprayed and demoulded coatings. Desired coatings were achieved using copper powder of spherical morphology; the as-sprayed coatings were dense and crack-free, and remained undamaged when demoulded along with CFRC.

In GRIP Metal™ as Bond Coat Method, the products were found to be inconsistent in hook height and curvature for some configurations. In term of general consolidation of metal-CFRC, it was found that the hooks of GRIP Metal™ induced fibre distortion leading to the formation of resin-rich zones and porosities. The occurrence, size and concentration of the defects were unpredictable.

Samples from both metallization techniques were tested and compared in term of metal-CFRC adhesion strength. The results indicate that some samples of GRIP Metal™ as Bond Coat Method performed better than samples of Reverse Lay-up Method.

Overall, GRIP Metal™ as Bond Coat Method offers higher metal-CFRC adhesion with trade-off in CFRC consolidation, whereas Reverse Lay-up Method offers lower metal-CFRC adhesion but intact consolidation quality.

Table of Contents

List of Figures

List of Tables

Abbreviations

ASI	Adiabatic Shear Instability
CFRC	Carbon Fibre Reinforced Composite
Cu	Copper
CVD	Chemical Vapor Deposition
EP	Extra Pressure
FOD	Foreign Object Damage
GFRC	Glass Fibre Reinforced Composite
HVOF	High Velocity Oxygen Fuel
MAD	Median Absolute Deviation
PATTI	Pneumatic Adhesion Tensile Test Instrument
PEEK	Polyether Ether Ketone
PTWA	Plasma Transferred Wire Arc Spray
PVD	Physical Vapor Deposition
Ra	Roughness Average
SEM	Scanning Electron Microscope
Sn	Tin
TEC	Thermal Expansion Coefficient
UTS	Ultimate Tensile Strength
WC-Co	Tungsten Carbide – Cobalt
Zn	Zinc

Chapter 1
Introduction

1.1 Background

The aerospace industry continuously improves the safety, reliability and performance of aircrafts in most novel and cost-effective ways. In each generation of aircrafts, manufacturers incorporate lighter and stronger materials to their products, leading to reductions in fuel consumption and carbon emissions that translate into cost-savings for both the airlines and passengers.

Whilst no major changes are made to the fundamental principles of flying machines, all their components are constantly redesigned for improvement through greater incorporation of advanced materials. Among all material systems, carbon fibre reinforced composites (CFRC) are prevalent in the construction of modern aircrafts, replacing many components originally made from aluminium. Outstanding strength-to-weight ratios in tensile loading, minimum fatigue degradation [1, 2] and favourable aging characteristics [3] constitute their main advantages in terms of material properties for aerospace applications. For example, Boeing's 787 Dreamliner features nearly 50% of composite materials in its fuselage, wing and empennage [4]. As another example, General Electric makes use of CFRCs for the fan blades of its GE90 and GE9X engines [5]. Unfortunately, although CFRCs possess some highly desirable mechanical properties, they fall behind in some areas, noticeably their resistance to erosion and their low electrical conductivity.

In-flight environmental conditions generally do not constitute threats to aircrafts. However, the likelihood of erosion by foreign objects such as debris and hail, and damage by lightning strikes on a flying aircraft's exposed structure remains. Considering the low erosion resistance of CFRC, erosion can cause severe damage and put aircraft temporarily out of service, translating to costly service interruptions and delays for the operating airline. Current protective solutions consist in shaping and gluing aluminium or titanium sheets to critical areas of the CFRC structure, such as the leading edge of a wing. Furthermore, in instances of lightning strikes, CFRC's low electrical conductivity causes difficulty in dissipating the high currents and heat generated by the discharge [6]. This vulnerability is currently mitigated by adding a copper mesh sandwiched between glass fibre layers added onto the CFRC. The mesh acts as a conductive medium for facilitating the lightning's electrical current to pass through the aircraft at skin level without ever reaching the internal components such as the fuel system.

It is envisioned that additive manufacturing processes can offer a better solution to metalize CFRCs, particularly titanium coatings with variable thickness. Thermal spray processes such as Plasma Spraying, Wire Arc Spraying and High Velocity Oxygen Fuel (HVOF) Spraying are common techniques for depositing coatings on substrates. Unfortunately, they heat up metallic particles to semi-molten or molten state prior to their impact and solidification on the substrate.

Combining the effect of high temperature with high velocity, these particle impingements against the CFRC substrate often result in degradation by erosion and thermal effect. Additionally, in-flight metallic particle oxidation alters the structure and properties of the feedstock powders used in these processes.

At the lower spectrum of operating temperatures resides the process of Cold Gas Dynamic Spraying (or Cold Spraying). This process enables low temperature additive manufacturing suitable for heat sensitive feedstock powder and substrate materials. First developed in the mid-1980s at the Institute of Theoretical and Applied Mechanics of the Siberian Division of the Russian Academy of Sciences [7], Cold Spraying is a high kinetic energy particle deposition process that utilizes high pressure gas passing through a De Laval nozzle to generate a supersonic gas stream used for accelerating solid particles that plastically deform and bond upon impact on a substrate, consequently creating a coating. Even if the process' gas stagnation temperature can reach hundreds of degrees Celsius, its rapid expansion keeps the in-flight particles cold. This technology offers many advantages, including retention of particles' phase, minimum oxidation and production of dense coatings [8, 9].

However, direct coating deposition by Cold Spraying on CFRCs poses many challenges and requires careful control of deposition parameters as shown by many researchers, including previous work done by the Cold Spray research group at the University of Ottawa [10, 11, 12, 13, 14]. Only a handful of soft metallic materials such as tin have been sprayed directly on CFRCs with coating build-up. No one has yet reported the direct deposition of harder coatings such as copper or titanium on composite materials. The difficulty resides in the low deformability of these feedstock particles compared to tin which tends to lead to erosion of the polymer substrate.

Driven by the aspiration of finding a solution, two novel methods are probed in this research work for protecting CFRCs using cold spraying processes. The first solution is to investigate a technique called “Reverse Lay-up Method”, previously developed by the Cold Spray research group at University of Ottawa to bypass erosion entailed by direct deposition. This technique has shown preliminary success (proof-of-concept level) when using copper particles; however, coating quality remains to be improved and other materials are yet to be probed [14]. The second solution consists in introducing a metallic bond coat on the CFRC substrate as base for coating deposition, which consequently avoids direct deposition of metallic particles on the CFRC. This method is called “GRIP Metal™ as Bond Coat Method”.

1.2 Objectives

The purpose of this research work was to investigate two potential methods for protecting CFRC against erosion and lightning strike. The first approach features the use of a lay-up technique, referred to as “Reverse Lay-up Method”, specially developed by the Cold Spray research group at University of Ottawa to metalize CFRCs with assistance of Cold Spraying process. The method consists of spraying a thin coating on an Invar mould, then laying the uncured laminate onto the coating. Afterwards, the assembly is cured. Once the curing ends, the metal-coated CFRC is demoulded, resulting in a metallized CFRC.

The second approach, referred to as the “GRIP Metal™ as Bond Coat Method”, features the use of GRIP Metal™ technology as bond coat for cold spray. GRIP Metal™ is a thin metallic plate on which strips of metals, namely hooks, are formed by chiselling in patterned intervals. Hooks are formed on one side of the plate only and are exposed to CFRC laminate upon moulding, leaving the other side flat for spraying an extra metallic layer of similar or dissimilar metal. Prior to curing, GRIP Metal™ is compressed into the uncured CFRC laminate, with hooks facing the laminate. The chiselled hooks increase the surface area on which epoxy from the CFRC bonds, with the aim of reaching higher adhesion strengths between GRIP Metal™ and the laminate in comparison with simple, flat sheet metals. It also aims at avoiding gluing, which is currently used commercially. The two approaches differ in terms of manufacturing processes, and therefore in knowledge to be gained.

For the Reverse Lay-up Method, the approach was refined by gaining fundamental knowledge of the physics behind the technique. This technique was originally developed for adding copper coatings on to CFRCs for lighting strike protection. Initial implementation demonstrated the proof of concept [14]. Nonetheless, examination of coating quality after demoulding revealed cracking in the coatings, which translated to inter-coating failure when copper-coated CFRCs were tested in interfacial adhesion. It was believed that the spray parameters and/or powder morphology were not optimized for coating quality; hence, some fundamental studies allowing process parameters refinement were needed. Furthermore, demoulding proved to be challenging due to the absence of reliable guidance developed for this special technique. Therefore, work on Reverse Lay-up Method focused on studying the key parameters enabling dense coatings after demoulding and developing a reliable demoulding method.

GRIP Metal™ is a recent technology originating from the automotive industry, used for mounting brake pads on callipers. As such, the work on GRIP Metal™ as Bond Coat Method focused on exploring the feasibility/proof of concept of integrating GRIP Metal™ as a bond coat, and on assessing the quality of the laminates. GRIP Metal™ is available in many configurations characterized by different hook materials, hook sizes, hook curvatures and hook densities. A selected range of configurations was tested. Due to current availability, aluminium and steel GRIP Metal™ were probed.

1.3 Thesis Outline

Chapter 2 presents a review of literature on related topics, which include introductory knowledge on carbon fibre reinforced composites, alternative solutions to metalize CFRC with comments on their advantages and limitations, introductory knowledge to Cold Spray process, product presentation on GRIP Metal™, and other relevant topics. Chapter 3 details all materials and equipment used in conducting experimental trials, followed by a presentation of experimental procedures for the two metallization approaches. Chapters 4 presents all the results. In Chapter 5, the results are discussed and compared. Finally, Chapter 6 offers conclusions on all results and observations.

1.4 Contributions

Following along the trend of greater adoption of advanced composite materials in aerospace industry, this research addresses some important issues concerning CFRC weaknesses. The contributions explicitly include the exploration and refinement of technologies for metallizing CFRC that would ultimately be aimed at protection against erosion and lightning strikes. The Reverse Lay-up Method presents a unique use of the Cold Spray process that bypasses issues encountered with direct coating deposition. The GRIP Metal™ as Bond Coat Method examines a new alternative solution for metallizing composite materials; the benefits and challenges represent important elements of knowledge. Overall, the two techniques potentially engender possibilities of coating materials other than copper.

Chapter 2

Literature Review

2.1 Carbon Fibre Reinforced Composites

Carbon Fibre Reinforced Composite (CFRC) is a general term associated with materials made of a combination of carbon fibres and a polymer, metal or ceramic matrix. In recent decades, materials of this type saw increasing demand thanks to their high strength-to-weight ratio, and they have been widely used as primary structural components in many applications in aerospace and automotive industries. Different matrix materials suit different needs for physical and chemical properties; for example, carbon fibre reinforced titanium can operate at temperatures that greatly exceed those of polymer and aluminium matrices [15]. In this work, epoxy matrix was used, therefore the term *CFRC* henceforth refers specifically to carbon fibre reinforced, epoxy matrix composites in this thesis. Like any other material, CFRCs have their strengths and weaknesses. Nevertheless, their weaknesses can be mitigated by introducing extrinsic materials to their surface and/or structure. This research focuses on surface modification of CFRCs by introducing coating materials.

2.1.1 Strengths

The strength of CFRCs arises mainly from the inlayed carbon fibres of high ultimate tensile strength (UTS). The UTS of consumer grade fibres can easily exceed 1000 MPa [16], which is twice as strong as aerospace grade 7000 series aluminium [17], and UTS of aerospace grade carbon fibres can reach up to 5000 MPa [18]. The fibres are usually paired with a thermoset polymer as a matrix due to latter's workability and performance which satisfy most needs. Thermoset resins offer much better formability in its uncured state in comparison with molten metals and ceramics which pose many challenging composite manufacturing problems such as low permeability, critical cooling rate and potential corrosive behaviour affecting the carbon fibres [15].

CFRCs are light thanks to the low densities of the inlayed fibres and epoxy matrix. Both materials usually weigh less than 2 grams per cubic centimetre [16, 19], which is around 30 percent lighter than aluminium [17]. The combination of high strength and low weight gives the CFRCs their well-known characteristic of high strength-to-weight ratios.

CFRCs have proven to perform well under fatigue loading. Studies have shown that CFRCs deteriorate, in a non-corrosive environment, at most by 15% in strength amplitude after 10 million cycles (Fig. 1) [1]. In comparison, carbon steel and aerospace grade 7075-T6 aluminium deteriorate nearly 30% for the same number of loading cycles [2, 20].

CFRCs also have proven to perform well in resistance to crack growth. In the same studies, it is noted that the crack growth in notched samples only becomes critical after 3 million fatigue loading cycles [1]. Other studies on this matter have shown that crack propagation is slowed down by interfacial bonding between fibres and matrix. Fissures in CFRC begin by fracture of fibres, then fibre-matrix interfacial delamination and creation of new crack sites (Fig. 2) [21].

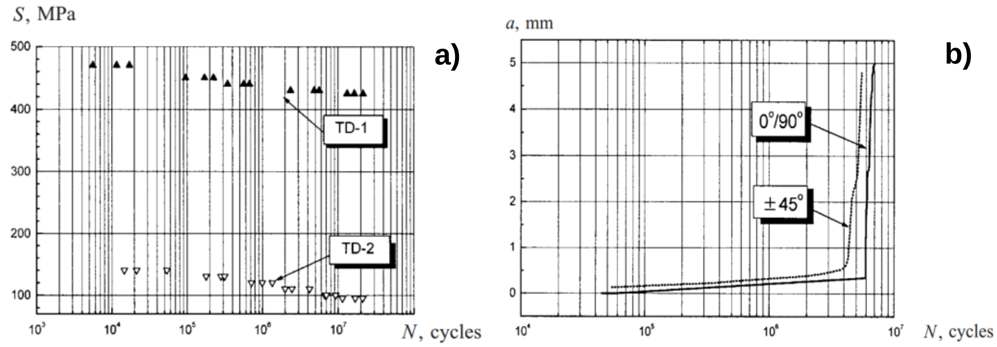

Figure 1 - a) S-N graph of (unnotched) carbon fibre reinforced epoxy (TD-1: 0°/90°, TD-2: ±45°); b) Fatigue crack growth versus number of cycles [1]

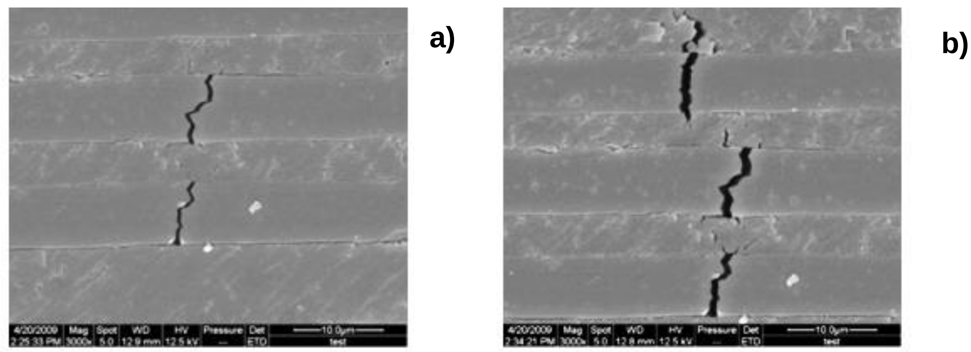

Figure 2 - SEM images of a) fibre fracture in epoxy matrix; b) extension of existing cracks and creation of new crack sites [21]

Finally, CFRCs perform well in aging. Studies have shown that mechanical properties of CFRCs made of unidirectional plies only changed slightly after being exposed to UV radiation and water condensation for 2160 h [3].

2.1.2 Weaknesses

Properly fabricating a high quality CFRC laminate is challenging. Stacking prepreg plies requires careful alignment between plies for ensuring correct mechanical properties [22]. During laydown of each ply, inter-layer air bubbles should be extracted for ensuring no trapped air remains. These air pockets would not only act as crack initiation sites, but also alter fibre orientations. Fibres misalignment causes deviation of mechanical properties from intended design. Studies have shown that the compressive strength of CFRCs decreases significantly when limited fibre waviness and/or misalignment induced through manufacturing errors are present in the laminate [23].

Another weakness of CFRCs is their low resistance to erosion. Studies on erosion behaviour of materials have shown that a material's yield strength plays an important role in its erosion resistance, with the general rule being that higher yield strength leads to reduced erosion [24]. Polymers, more specifically epoxies, have low strengths in comparison to metals and ceramics, making them prone to faster erosion degradation. This weakness is highly significant in aircraft structures exposed to in-flight external environments whereby flying debris and water droplets frequently impinge the exposed CFRC components.

Additionally, CFRCs generally have a low electrical conductivity. Since carbon fibres are good conductors, this characteristic mainly results from the poor electrical conductivity of the epoxy matrix. Even though CFRCs are more electrically conductive than polymers alone thanks to their fibre content, their conductivity does not come close to that of metals. In an event of high electrical discharge on CFRCs, for instance a lightning strike, the composite would not be able to transfer the incoming electrical current easily across its structure for overall dissipation, resulting in local heating and thermal degradation of the polymer matrix. Figure 3 shows an example of an inadequately protected CFRC damaged in a lightning strike test; the electrical discharge burned a hole through the composite laminate.

Figure 3 - Example of damaged CFRC by lightning strike test [25]

2.2 Carbon Fibre Reinforced Composites in Aerospace Industry

2.2.1 Usage

Ever since commercial air travel debuted in the late 1900s [26], airlines have seen unbroken year-to-year increase in numbers of air passengers. In 2016, the total number of all passengers around the globe reached 3.7 billon [27], an increase of 800 million from 2012 [28]. This rising demand sparks fierce competition between the airlines that seek any possible cost savings that could translate into reductions in air fare, attracting price-conscious customers.

Airlines spend on average 33% of their operation costs on fuel; therefore, fuel efficiency is a critical factor that determines the ticket price [28]. Reduction in fuel consumption can be achieved by refining aircraft aerodynamics, improving jet-engine combustion efficiency and most importantly, cutting the weight of aircrafts. Without compromising on structural strength, weight lost requires careful integration of advanced materials such as CFRCs that possess both characteristics of low density and high strength. For this reason, CFRCs are widely used as primary structures in modern aircraft fuselages, wings and empennages. The benefits of CFRCs extend to their weather-resistance and fatigue resistance as discussed in section 2.1.1, which ensure the long-term durability of the aircrafts.

Nonetheless, it is mandatory to protect carefully the CFRC structures from any form of damage, as it is difficult to execute good repairs of CFRCs. Repair is a lesser problem for metals whereby repair material can be fused to damaged zones; but for CFRCs, this type of repair is very challenging due to the impossibility of reconnecting the fibres. Furthermore, there is no proper way to repair internal fractures without damaging their surrounding areas. Therefore, established critical damage to CFRCs could put an aircraft out of service.

2.2.2 Erosion Protection

One of the most common form of damage to aircrafts is Foreign Object Damage (FOD). It comprises surface erosion and impact on aircrafts caused by foreign objects in flight; examples include: water droplets, hail, birds and gravels impingement on the aircraft's skin. While many airlines keep and publish statistics on bird strikes [29], they generally do not publicly disclose any data on erosion. Nevertheless, a recent example of severe erosion damage is the emergency landing of Delta Air Lines' Flight 1889 at Denver International Airport in 2015. Caught in a severe thunderstorm, the aircraft was struck by hail, causing serious damage to the front facing area of the aircraft, mainly the nose cone and cockpit's windshields [30]. A picture from the event (Fig. 4) shows that the nose cone was completely eroded, exposing plane's internal structure through open cavities. Type and occurrence of erosion vary depending on geographical location, hence aircrafts could encounter diverse situations according to their zones of operation, for instance: sandstorm in desert regions.

Figure 4 - Image of Delta Air Lines Flight 1889, erosion damage by hailstones [31]

To protect the CFRCs from erosion, airplane manufacturers glue metal sheets on critical areas of the aircraft where erosion resistance is needed. For example, Boeing's 787 Dreamliner features an aluminium protective layer added to the leading edges of its wings and empennage

(Fig. 5) [4]. Other metals such as titanium and steel are often used for the fan blades of jet-engines. Engine maker General Electrics has been using titanium leading edges in their GE90 series engines for protecting CFRCs against FOD [5]. These metallic layers are usually glued onto the CFRCs.

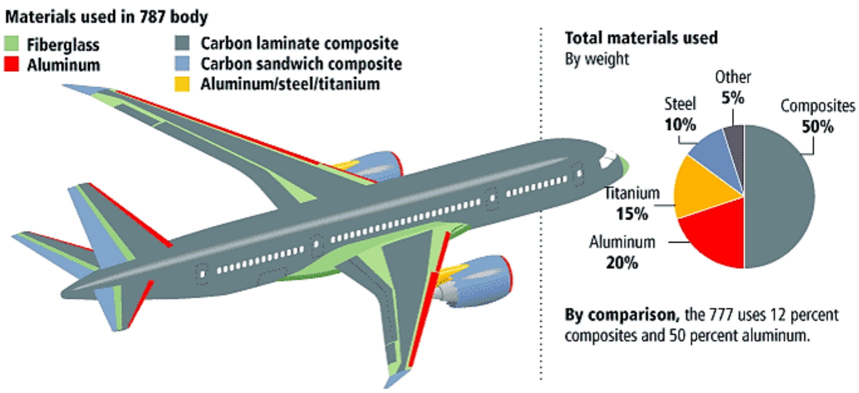

Figure 5 - Diagram of materials used in 787 Dreamliner's body [4]

To produce these geometrically accurate protective layers, the process of stretch-forming is used whereby metal sheets are bent and stretched in a mould (Fig. 6). For broad components like the wings, this process requires large pieces of equipment that are costly to purchase and operate. Due to the geometric complexity of components and cost limitations of this process, multiple short sections of the protective layer are often glued side-by-side on the leading edge instead of a continuous layer [32]. Even though stretch-forming has been widely adopted, it remains a costly way of satisfying the need. Moreover, different areas of aircrafts need different levels of protection; the production of a variable-thickness layer poses challenges.

Figure 6 - Process of stretch-forming [33]

2.2.3 Lightning Strike Protection

Clouds are a mixture of air and water in vapor, liquid and solid forms. Two phenomena naturally occur and lead to an eventual lightning strike. First is the continual evaporation and condensation of water molecules inside the clouds. Second is the rise of warm and moist air from lower atmosphere that moves towards the clouds. The combination of the two phenomena induce collision between particles, causing a loss of electrons in some collided molecules. As the electrical imbalance builds up inside the clouds, the charged particles separate into positive and negative sides, generating a capacitor-like effect with the negative and positive charges stored at the bottom and top of the clouds respectively [34]. Eventually, the strong negative charge gains sufficiently high potential to repel the earth's superficial electrons, charging the ground surface as positive (Fig. 7). Negative charges in the clouds then begin to move towards the ground by branching in zigzag patterns, while positive charges from ground surface migrate upward. When these opposite charges meet, a conductive path is created, letting electrons to flow rapidly. Lightning strikes also happen within and between clouds, but with less intensity. Clouds use in-flight aircrafts as a conductive medium for discharge; this phenomenon is usually observed in the form of a visible light strip entering one end, then exiting the other end of an aircraft (Fig. 8).

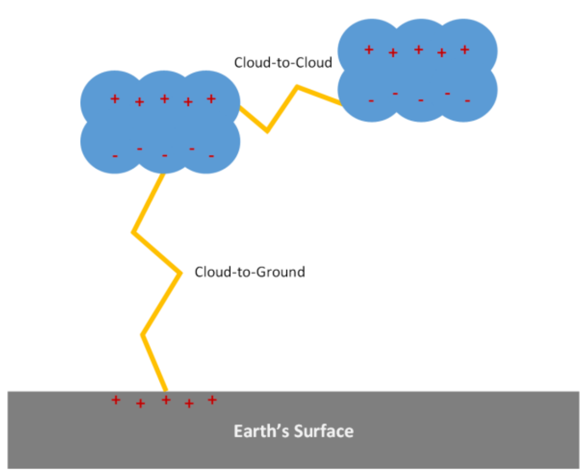

Figure 7 - Illustration of mechanisms of lightning strikes

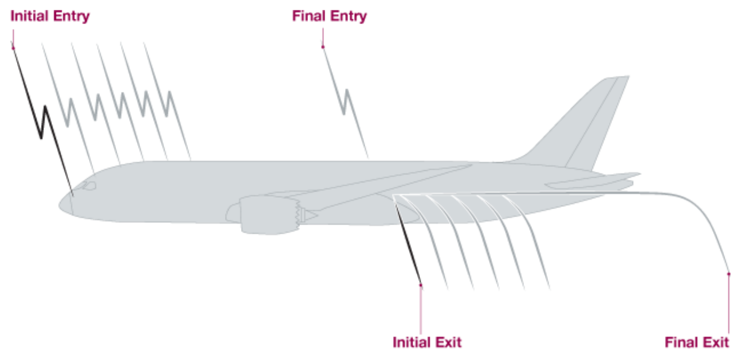

Figure 8 - Lightning strike attachment to an aircraft [35]

The natural behaviour of lightning strikes reveals that, geographical locations with high moisture content and warm temperatures are more prone to such incidents in comparison to drier regions (Fig. 9); and that, lightning strikes happen in different forms. Recent statistics published by airlines reported that lightning predominantly strikes on aircrafts in clouds (Fig. 10) [36]. These statistics mean that short- and medium-haul aircrafts repeatedly performing take-off and landing would likely suffer more from lightning strikes than long-haul airliners that stay mostly above the clouds during their journeys. For this reason, a durable protective solution is essential to ensure safety of the affected aircrafts.

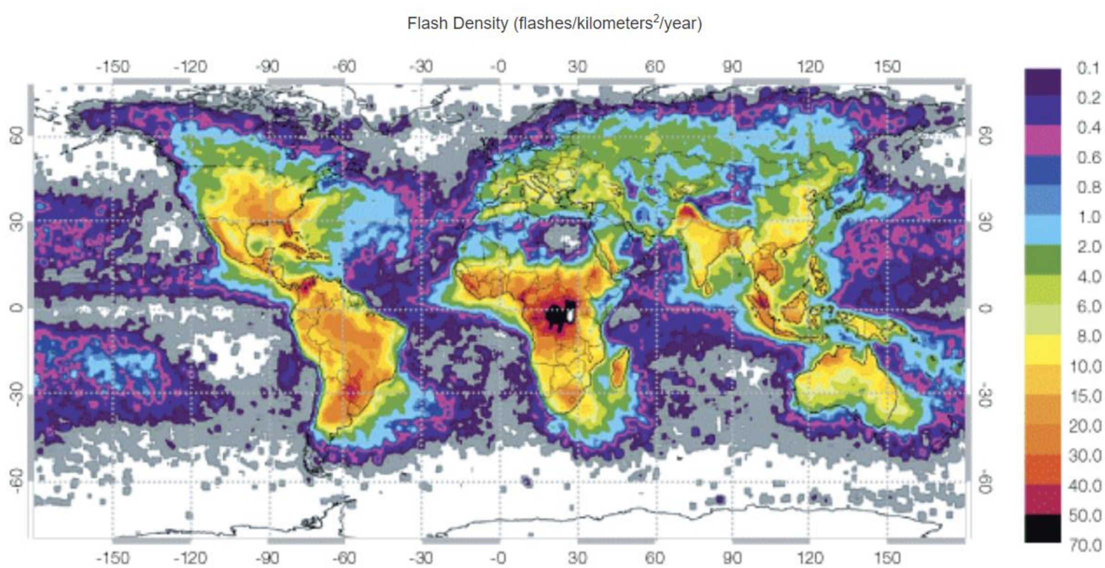

Figure 9 - Schematic of worldwide lightning activity: April 1995 through February 2003 [35]

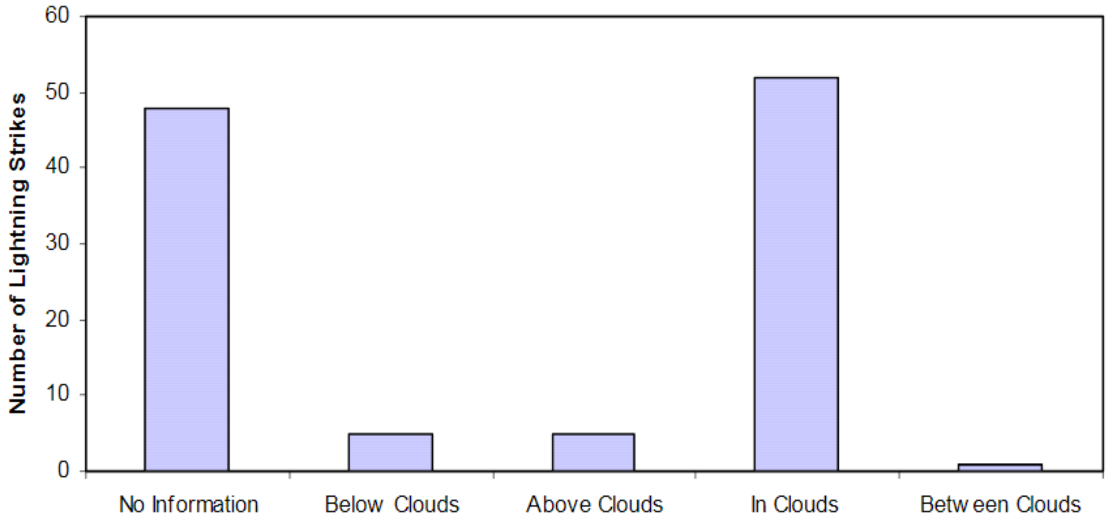

Figure 10 - Number of lightning strikes versus aircraft's position [36]

Current protective solutions include the incorporation of wire mesh, metallic frames, metallic foil liners, expanded foils, bonded aluminium foils or aluminium flame spray coatings [35]. Figure 11 shows a schematic view and an example of an embedded copper mesh. While solutions exist, they solve the problem inadequately due to their inefficient method of application.

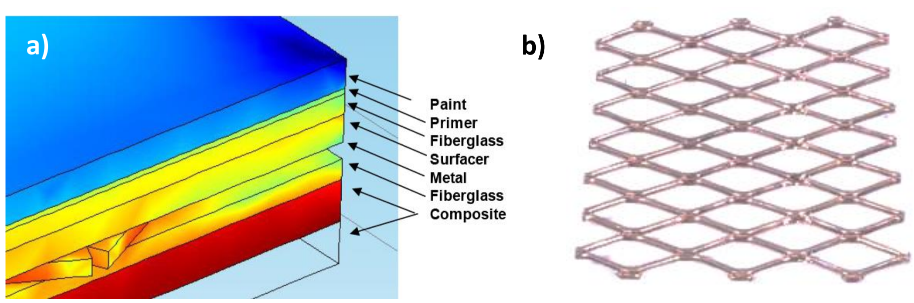

Figure 11 - a) Schematic view of embedded copper mesh [37], b) Example of copper mesh [38]

All solutions, with the exception of flame spray coatings, demand accurate shaping and fitting of the conductive layer conforming to the profile of the protected components. While wire mesh and foil can be draped onto the components, technical challenges remain when draping complex geometries. Thus, it is believed that a better solution would be to metallize the CFRCs by surface coating technologies.

2.3 Currently Available Coating Technologies for Metallizing CFRCs

Many surface coating technologies can be used for metallizing CFRCs. However, some outperform others based on characteristics and results. Before presenting the coating technologies currently available for metallizing CFRCs, it is important to understand some of the common factors that determine the ability of a coating technology to meet the requirements.

There are three essential factors through which coating processes can be evaluated and compared: coating performance, coating process characteristics, and cost. Coating performance is defined as the coating's ability to meet specifications, for instance the minimum value of adhesion strength on a substrate. Coating process characteristics are defined as the complexity of the process and its advantages versus disadvantages. Coating cost is defined as the cost-per-coating produced. Although costs and exact specifications vary greatly for diverse aerospace applications, they do not impede some degree of comparison based on logical assumptions.

As CFRCs exhibit sensitivity to both thermal degradation and erosion, some coating technologies would inevitably induce damage on the composite substrates. Even if the damage appears to be superficial, properties of the CFRC might have changed during the coating process. In the aerospace industry, material certification is a costly and lengthy procedure, hence any involuntary damage to the CFRCs would require thorough material reassessment.

2.3.1 Non-thermal Spray Processes

Spray processes can be divided into two categories: non-thermal spray processes and thermal spray processes. In the first category, numerous researchers have shown that surface coating technologies such as electroplating, physical vapor deposition (PVD) and chemical vapor deposition (CVD) can metallize CFRCs and offer potential value for aerospace applications.

2.3.1.1 Electroplating

Electroplating utilizes electricity to help depositing coating on a substrate material. This process works by configuring an electrical circuit formed by an electrical source, cathode, anode and electrolyte (Fig. 12). The coating material acts as the anode whereas the substrate material acts as the cathode, with the electrolyte connecting the two parts. The electrolyte is a liquid solution containing partially the same substance as the coating material, for instance: copper sulphate solution for electroplating brass substrate with a copper coating. For plating polymer materials, the surface of the substrate must be etched prior to electrodeposition. Typically, this preparation process consists in cleaning the CFRC substrate surface, then boiling it in NHO_3 at 83°C [39, 40, 41].

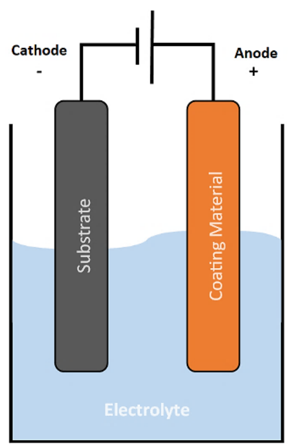

Figure 12 - Simplified illustration of the electroplating process

The main disadvantage with electroplating is the low adhesion strength of coatings on the substrates. Studies have shown that an electroplated copper coating on CFRCs fails at 450 kPa in adhesion [40]. Other studies have shown that nickel coatings electroplated on CFRCs had an adhesion strength of only 78.5 kPa [41]. To put these numbers in perspective, miscellaneous tests done as part of this research work showed that slightly roughened copper sheet glued using Gorilla Glue® onto roughened CFRC substrates outperformed both results.

2.3.1.2 Physical Vapor Deposition

Physical Vapor Deposition (PVD) refers to a series of vacuum deposition techniques. The techniques are generally performed in a vacuum chamber wherein the coating material is evaporated, then deposited on the substrate material. An example of PVD process is the deposition of photovoltaic material on metallic substrates for thin-film solar cells [42].

This process uses an electrical power source to charge the coating material negatively, so-called target, to liberate free electrons from the latter. Argon is injected into the deposition chamber. Argon molecules have their electron knocked off by collisions with the flowing free electrons. Positively charged argon particles are attracted towards the negatively charged target and in turn knock off atoms from the latter. These liberated atoms are subsequently deposited on the substrate (Fig. 13).

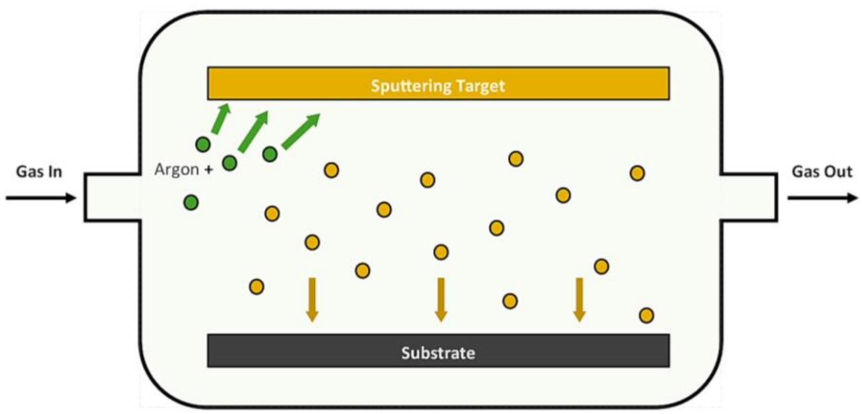

Figure 13 - Simplified illustration of the sputtering process

Researchers have demonstrated the feasibility of depositing titanium based PVD coatings on CFR-PEEK at a temperature of 130°C (Fig. 14) [43]. Nevertheless, the dimensions of the vacuum chamber scale up with those of the substrates; the equipment would be costly for large components. Furthermore, PVD is commonly a line-of-sight coating process, unsuitable for complex substrate geometries.

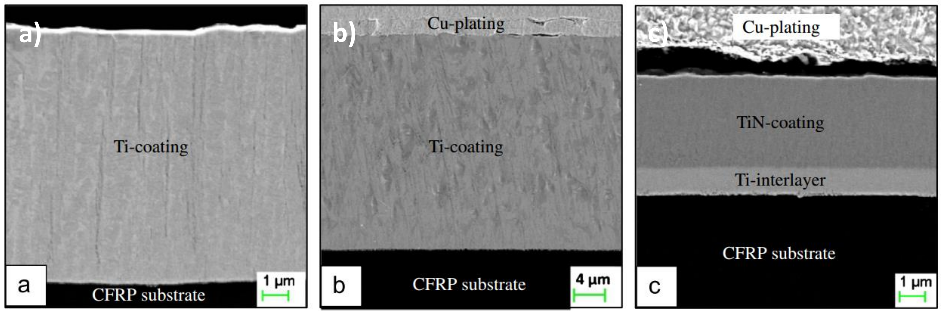

Figure 14 - SEM images of cross-sections of PVD coatings on CFR-PEEK substrates: a) 10 μm titanium, b) 30 μm titanium, c) 5 μm titanium nitride [43]

2.3.1.3 Chemical Vapor Deposition

Chemical Vapor Deposition (CVD) refers to a series of techniques that use chemical reactions to deposit coatings on substrates. This type of process plays an important role in coating thin-films on silicon wafers in the semiconductor industry. Figure 15 shows an illustration of the process. CVD utilizes precursors in vapor phase that are introduced into the deposition chamber where they adsorb on the substrate. The precursors diffuse on the surface of the substrate and form a solid thin film. The by-products of this chemical reaction are then exhausted out of the coating chamber [44]. Traditionally, this technique operates at high temperatures unsuitable for many substrate materials, however the introduction of plasma-enhanced CVD allows the process to perform equivalently well at much lower temperatures [44].

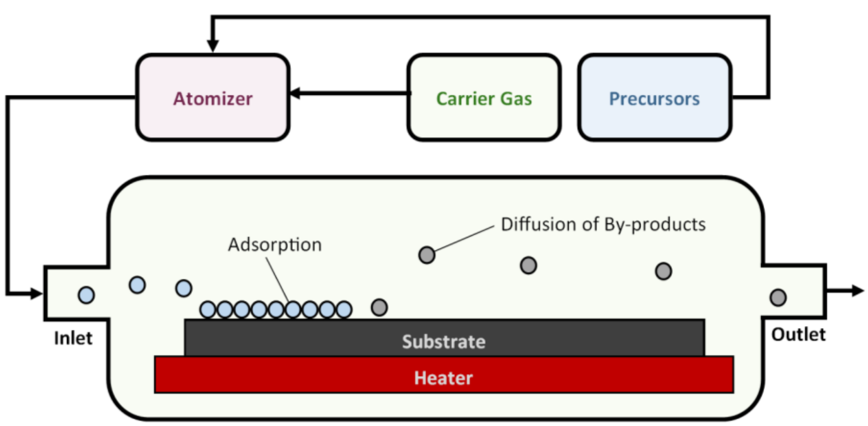

Figure 15 - Simplified illustration of the CVD process

Studies reported the feasibility of copper thin films on CFRCs by plasma-enhanced pulsed CVD deposition [45]. Although the film growth rate was in the range of nanometres per hour, continuous copper thin films were successfully produced at a temperature of 100°C. Another research work attempting metallization of CFRCs was done; it took the unique approach of metallizing only the carbon fibres instead of the epoxy matrix [46]. The line-of-sight limitation of PVD does not apply to CVD; however, a meaningful disadvantage of CVD is the production of often toxic by-products.

2.3.2 Thermal Spray Processes

Thermal spray processes comprise many techniques, notably plasma spray, wire arc spray, flame spray, high velocity oxy-fuel coating spray (HVOF) and cold spray. Most work by projecting on a substrate a stream of softened or molten coating material in powder form, carried by a gas stream. The coating material deforms upon impact on the substrate, then quickly cools down and solidifies. Among all thermal spray processes, cold spray stands as the least temperature intensive technique. Nonetheless, high temperature coating techniques can be tweaked to maintain a relatively low substrate temperature.

2.3.2.1 Plasma Spray

Plasma spray works by generating a plasma stream that propels powder towards a substrate. The equipment consists of a cathode and an anode charged using high electrical potential (Fig. 16).

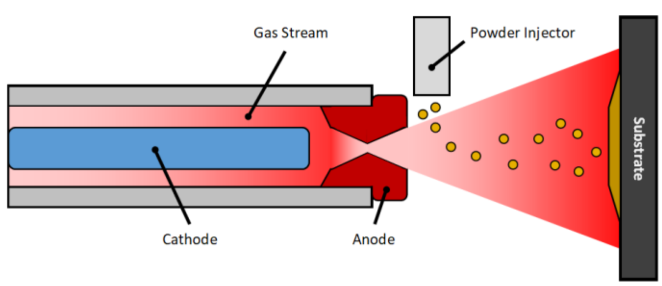

Figure 16 - Simplified illustration of the plasma spray process

A gas stream passes between the them, through the electric arc created between the electrodes, and reacts as an electrical conductive medium causing the gas to ionize. Coating material in powder form is injected into the plasma stream. Propelled by the hot and rapid stream, the powder quickly heats up and accelerates. Upon impact on the substrate, the powder deforms, then consolidates as it cools down.

Researches demonstrated the feasibility of depositing pure aluminium coatings by atmospheric plasma spray on CFRCs (Fig. 17) [47]. To reduce thermal degradation of the CFRCs, the spray distance was selected to enable sufficient cooling. Furthermore, studies have demonstrated the feasibility of depositing pure copper coatings by atmospheric plasma spray on CFRCs [48]. In both cases, the plasma sprayed coatings were used as an interlayer for subsequent cold spray deposition. The bonding strength of plasma-cold sprayed copper coatings on CFRCs remains comparatively low; it was determined to be around 2 MPa. Nevertheless, these results might already satisfy some applications whereby the operating environment does not promote coating delamination.

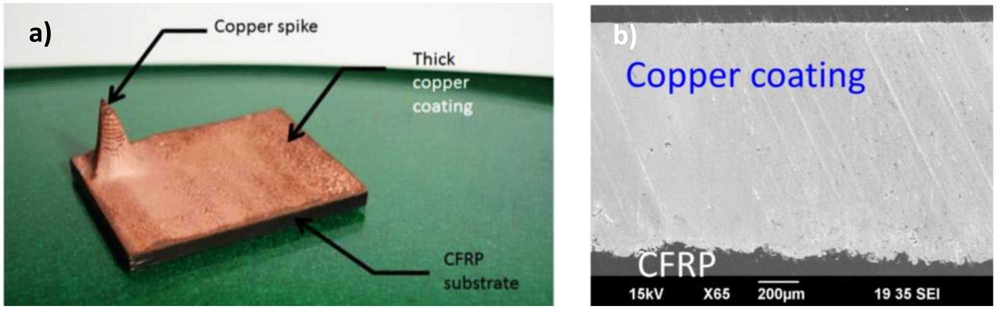

Figure 17 - Copper coating by cold spray over copper interlayer by plasma spray on CFRCs: a) isometric view, b) SEM image of coating-CFRC cross-section [48]

2.3.2.2 Wire Arc Spray

Wire Arc Spray operates by feeding two feedstock wires towards each other with one wire being charged positively and the other charged negatively; then, a gas stream passes between the wires, acting as both an electrically conductive medium and a propellant (Fig. 18). The arc's high temperature transforms the tip of the feedstock wires into molten state. The molten material is then propelled by the gas stream towards the substrate. A more advanced technique is called Plasma Transferred Wire Arc Spray (PTWA). This technique is generally used in the automotive industry for depositing mineral coatings on engine cylinder bores [49].

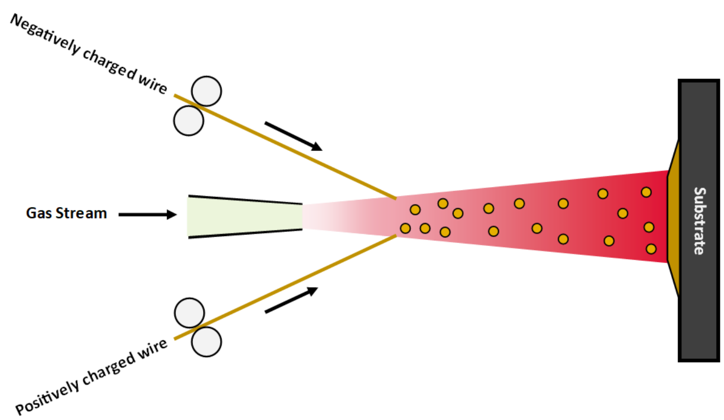

Figure 18 - Simplified illustration of the wire arc spray process

Research work has demonstrated the feasibility of wire arc deposition on CFRC substrates by mixed coating materials composed of steel, nickel, chromium, boron and silicon (Fig. 19). The substrates were either grit blasted or roughened with sand paper for increased surface roughness, prior to coating deposition [50]. Although successful deposition was achieved, the process operates at high temperatures, and the integrity of CFRCs after spray remains unknown.

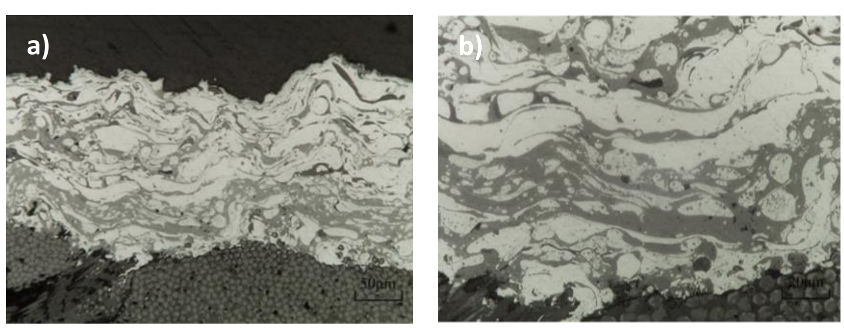

Figure 19 - Microstructure of mixed-metal coating on CFRC: a) low magnification; b) coating-substrate interface [50]

2.3.2.3 High Velocity Oxy-Fuel (HVOF) Spray

HVOF Spray utilizes the combustion of oxygen and gas, or of a liquid fuel mixture, to generate a high temperature gas that exits a De Laval nozzle at supersonic velocity. In parallel, feedstock powder is injected into the exiting stream by means of an inert carrier gas (Fig. 20).

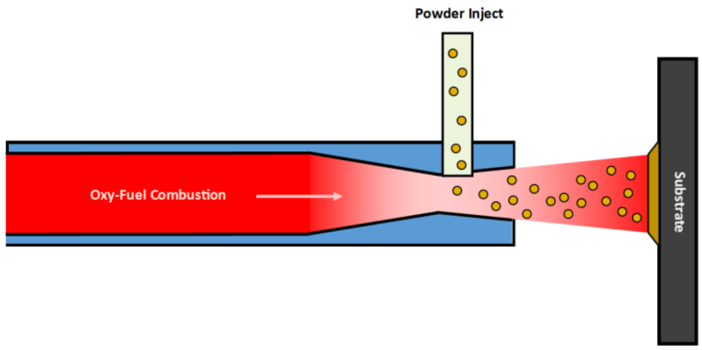

Figure 20 - Simplified illustration of the HVOF spray process

Research work demonstrated the feasibility of applying a tungsten carbide-cobalt (WC-Co) topcoat on polyimide interlayer on CFRC substrate (Fig. 21) [51]. A mixture was used for avoiding tungsten-carbide particles eroding the CFRC substrate, as its high modulus prevents it from undergoing substantial deformations. The general microstructure of region C, illustrated in Figure 21, was composed of 46% polyamide, 26% WC-Co and 28% voids. High polymer and void contents make the coating vulnerable as erosion protection layer.

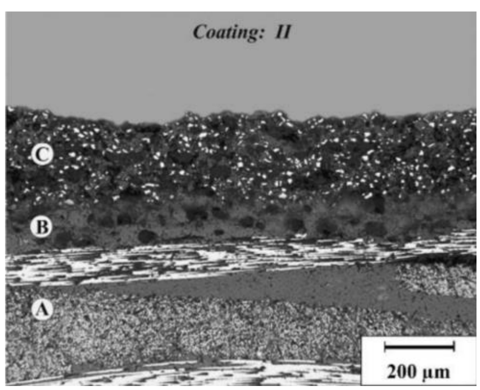

Figure 21 - Microstructure of a two-layer HVOF sprayed coating composed of a WC-Co/polyimide outer layer (C) and a pure polyimide layer (B) on a CFRC substrate (A) [51]

2.3.2.4 Flame Spray

Flame Spray is similar to HVOF but operates at lower temperatures and does not use a converging-diverging nozzle (Fig. 22). The propellant gas is formed by combusting a mixture of oxygen and fuel gas.

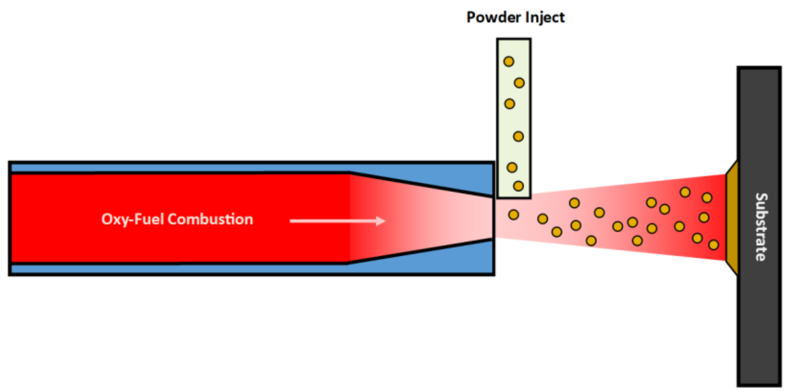

Figure 22 - Simplified illustration of the flame spray process

Research work demonstrated the feasibility of depositing aluminium on glass fibre reinforced composites (GFRCs) by flame spray (Fig. 23) [52]. A continuous coating of 165 μm in thickness was successfully built on the composite tube and no deterioration of the substrate was observed. Coating with materials other than aluminium remains to be investigated.

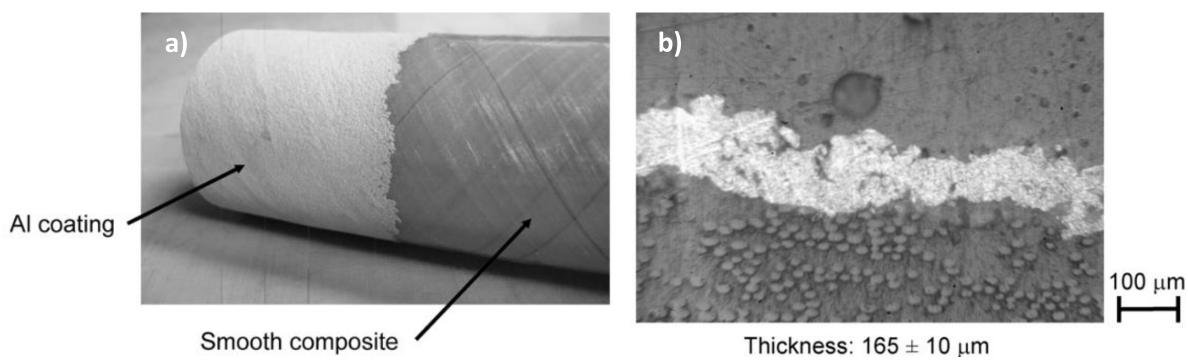

Figure 23 - Images of: a) GFRC tube, partially coated in aluminium using flame spray b) microstructure of coating created on CFRC using five passes of the flame spray torch [52]

2.4 Cold Spray

Cold Spray is a process developed during the mid-1980s at the Institute of Theoretical and Applied Mechanics of the Siberian Division of the Russian Academy of Sciences. During a study involving copper particles in a two-phase supersonic flow in a wind tunnel, scientists found traces of copper deposited on the model's surfaces. They subsequently realized that fast-moving particles can be deposited by deformation upon impact on a substrate without heating them to elevated temperatures, and consequently named the process Cold Spray [53].

2.4.1 Process & Characteristics

The process resembles HVOF but replaces the oxygen-fuel mixture combustible with a high-pressure inert gas (Fig. 24). Since the carrier gas does not combust, it is heated by electrical heaters. The high-pressure heated gas flows towards a De Laval nozzle's exit while powder is being injected into the accelerating stream by means of an inert carrier gas. Inserted particles are accelerated by the gas stream, then deform both themselves and the substrate upon impact.

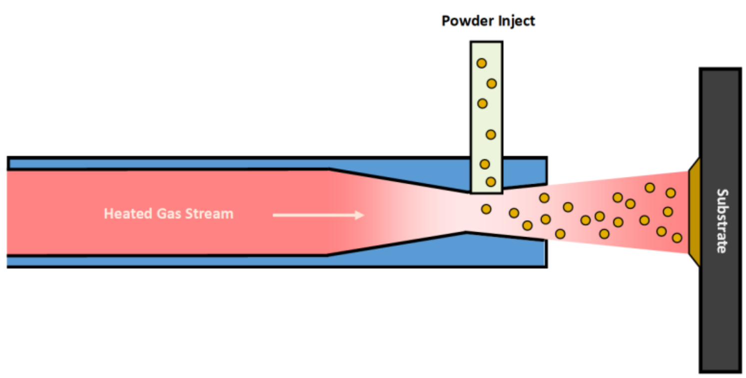

Figure 24 - Simplified illustration of the cold spray process

One common misconception relates to the misinterpretation of Cold Spray process: operation temperatures. Although Cold Spray operates at temperatures much lower than other spray techniques, the gas stagnation temperature can still reach up to 1000°C by heat transfer from electrical heaters. Figure 25 illustrates the temperature and pressure profiles of a gas stream inside a De Laval nozzle, where the symbol M is the Mach number. The high-pressure heated gas accelerates from subsonic to supersonic velocities across the nozzle, while pushing the injected particles to high velocity.

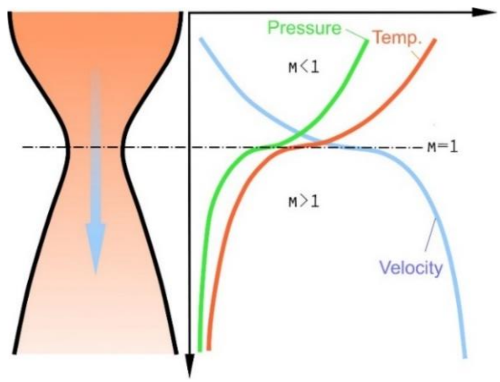

Figure 25 - Temperature and pressure distributions of gas stream inside a De Laval nozzle [54]

The accelerated particles possess high kinetic energy which, upon impact on the substrate, transforms mostly into heat. This sudden transformation increases temperature of the particles in their impact zones, resulting in local thermal softening that allows these affected regions to shear. This phenomenon is called Adiabatic Shear Instability (ASI) [55].

The complete spectrum of particle bonding mechanisms in Cold Spray is not well understood; however, it is known that two types of mechanisms exist for the deposition of metallic particles on metallic substrates: metallurgical bonding and mechanical anchoring [56]. On one hand, the impact and deformation break any potential oxide layer grown on the substrate material prior to spray, leading to new and clean substrate surfaces to which the particles could bond metallurgically. On the other hand, particle impacts induce localized deformation of the substrate. In case where both the particles and substrate deform plastically, mechanical anchoring is created between the two materials, allowing the particles to be retained on the surface of the substrate. To facilitate this type of anchoring, substrate surfaces are often roughened prior to coating deposition, to induce superficial valleys that are called anchoring sites [57]. Research work showed that the likelihood of bonding is dependant of particle velocity [58]. For a given set of coating and substrate materials, the particles need to exceed a certain speed called critical velocity, for them to bond on the substrate. These concepts do not apply directly to the deposition of metallic coatings on polymer substrates [10]; these challenges are explained in more detail in section 2.4.2.

Overall, cold spray offers many advantages: minimum to no powder oxidation, no powder melting, no change in the microstructures of the powder and substrate. These positive traits explain cold spray use for damaged surface repair, structural repair, as well as corrosion and erosion protection [59, 60, 61, 62]. Furthermore, cold spray has gained increasing popularity as an additive manufacturing technology suitable for building thick and dense components. General Electric has demonstrated cold spray technology to build gear teeth (Fig. 26) [53]. Other applications include the manufacturing of Inconel turbine rotors [63], titanium pipes for chemical processing [64], aluminium fins for heat exchangers [65] and copper rotating bands for artillery shells [66].

Figure 26 - Cold spray gear teeth on shaft [53]

2.4.2 Current Challenges and Solutions in CFRC Metallization Using Cold Spray

The only bonding mechanism between a metallic coating and a polymer substrate is mechanical anchoring, due to the impossibility of forming a metallurgical bond between these two types of materials.

Many researchers have reported both successful and unsuccessful attempts at metallizing CFRCs using cold spray. The difficulty lies in the brittleness and low strength of the CFRC matrix. Impinging particles first erode the epoxy matrix during deposition, leading to exposure of carbon fibres which then fracture under repeated particles impacts [10]. Figure 27 shows the results of eroded CFRC surfaces after cold spray of aluminium and copper powders, respectively. In such cases, the notion of critical velocity does not apply due to the substrate being continuously eroded; in other words, to bond to the substrate, the particles must possess a critical velocity lower than the value at which erosion becomes imminent.

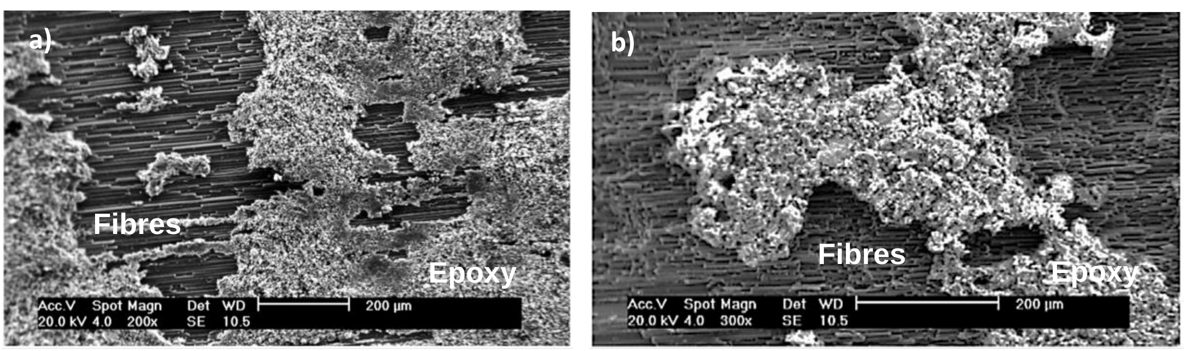

Figure 27 - SEM images of CFRC surfaces, showing eroded composites after cold spray of: a) aluminium powder, b) copper powder [10]

Studies have shown that only soft materials can deform on CFRC substrates without erosion. For this reason, successful metallization of CFRCs by direct cold spray deposition has been reported with tin powders only [11, 12, 13, 47, 67]. Studies on the deposition of spherical aluminium and copper particles on CFRCs have shown that powders do not deform upon impact on substrates due to their relatively higher stiffness. Only traces of powder embedment were found, with no coating build-up (Fig. 28). The inability to deform ultimately translates to substrate erosion.

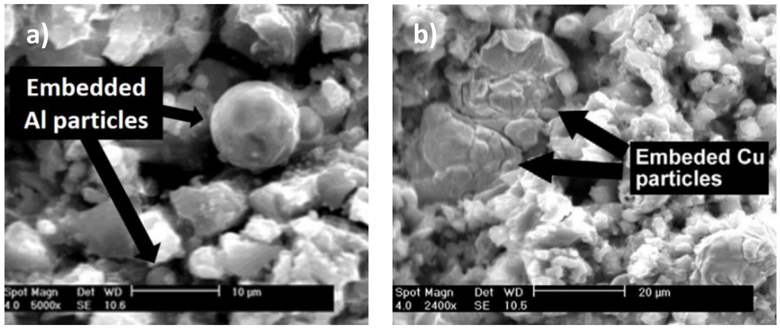

Figure 28 - Embedded particles in CFRCs: a) spherical aluminium, b) spherical copper [10]

On the contrary, tin is a soft material that can deform easily upon impact on a substrate, enabling coating build-up on a CFRC. Figure 29 shows an example of a dense tin coating deposited on a CFRC. Furthermore, the melting point of tin is within the range of gas temperatures used for the cold spray process, and therefore the tin particles start melting when heated sufficiently. Figure 30 shows this phenomenon for different spray temperatures; traces of semi-molten particles were found on the top surface of the coating. It is noticeable in both figures that the tin particles, initially spherical, became extensively stretched and/or fused due to melting. The surface of coatings sprayed at 310°C features satellite-like attachments to the main particles, potentially due to splashing of molten tin material. Melting drastically softens the particles, enabling larger deformations than seen in the full solid state.

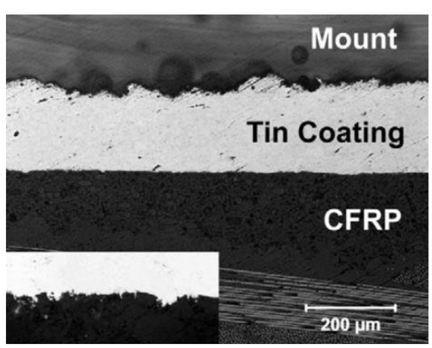

Figure 29 - Cross-section image of cold sprayed tin coating on CFRC [10]

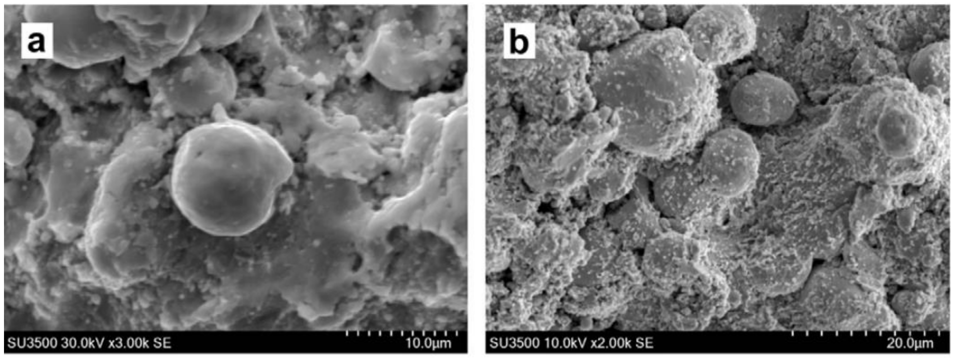

Figure 30 - SEM images showing tin particles at the top surfaces of coatings cold sprayed at gas temperatures of: a) 280 °C, b) 310 °C

To mitigate erosion, studies have demonstrated the feasibility of depositing an interlayer prior to the final/top coating [47, 67]. The interlayer is either a tin coating deposited by cold spray or a coating of the same material as the top coat, deposited using a high temperature thermal spray process. Figure 31 a) illustrates an aluminium interlayer deposited on a CFRC substrate using plasma spray, which facilitates subsequent deposition of an aluminium top coat by cold spray, shown in b).

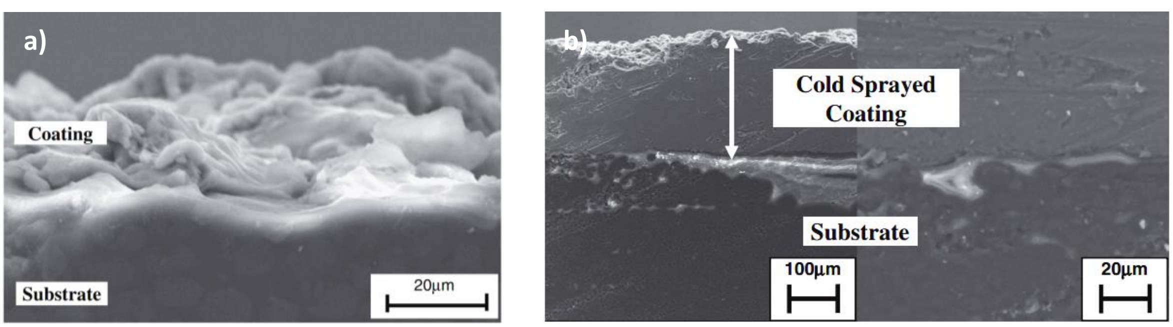

Figure 31 - SEM images of: a) atmospheric plasma-sprayed aluminium (interlayer) on CFRC substrate, b) aluminium cold sprayed coating on CFRC substrate with atmospheric plasma sprayed interlayer [47]

Another common method to lessen erosion consists in using powder mixtures: one stiff and one soft, with the aim of using the soft powder to generate an initial/base layer on the CFRC substrate, on top of which both the stiff and soft powders can build up. Studies have shown the feasibility of depositing copper-PEEK mixtures on CFRC substrates [68]. Figure 32 illustrates two different metal-PEEK combinations deposited on CFRC substrates. Figure 32 c) shows that spherical copper particles exhibited plastic deformation only when impacting each other [68]. An anchoring mechanism was proposed whereby the PEEK builds the first layer on the substrate, for subsequent copper particles to adhere. As shown in Figure 33 a), copper particles alone cannot anchor on CFRC, hence rebound from the substrate after impact. The presence of PEEK allows the copper particles to embed into already deposited PEEK, as shown in Figure 33 b).

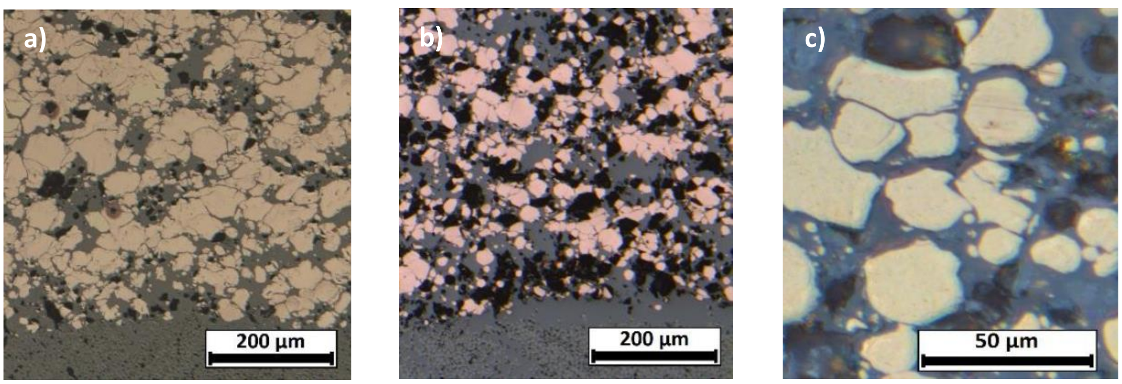

Figure 32 - Microstructures of copper-peek coating with a) irregular copper particles, b) spherical copper particles, c) magnified view of b) [68]

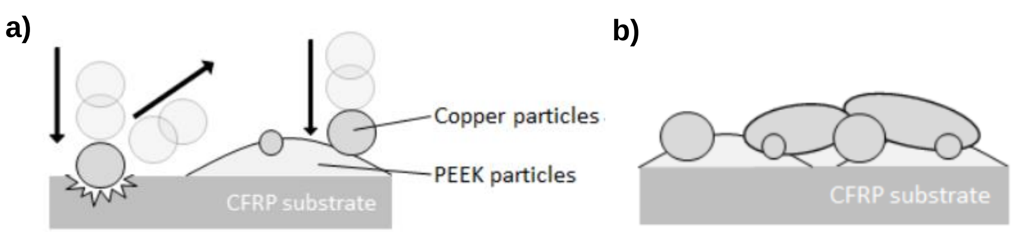

Figure 33 - Proposed anchoring mechanism of copper-tin mixed powders [68]

Other research work has demonstrated the feasibility of depositing zinc-tin and copper-tin mixtures on CFRCs [69]. The investigations were conducted using mixture of irregular tin, dendritic copper and irregular zinc. All mixtures had tin as the main component, then a secondary material was added. Figure 34 illustrates all pure and mixed powders used. The results indicate that zinc-tin powders produced nearly pure tin coating whereas copper-tin powders produced a homogeneously mixed coating on CFRC substrates (Fig. 35), for the potential reason being that the dendritic copper particles, having many branches, are easier to retain than the rounded irregular zinc particles.

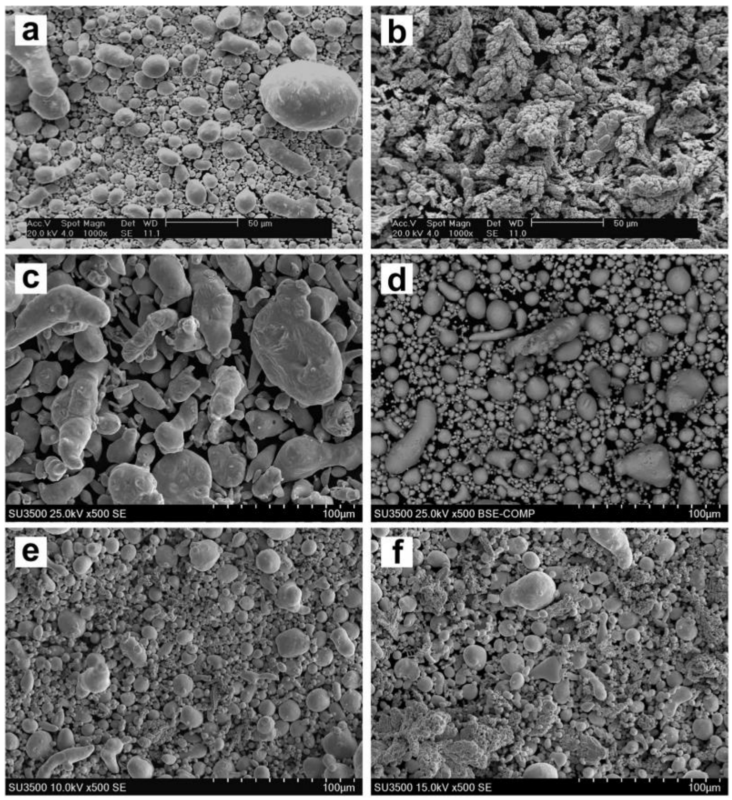

Figure 34 - SEM images showing the single-component powders and mixed powders: (a) irregular Sn, (b) dendritic Cu, (c) irregular Zn, (d) 10wt% Zn-Tin, (e) 10wt% Cu-Tin, and (f) 30wt%Cu-Tin

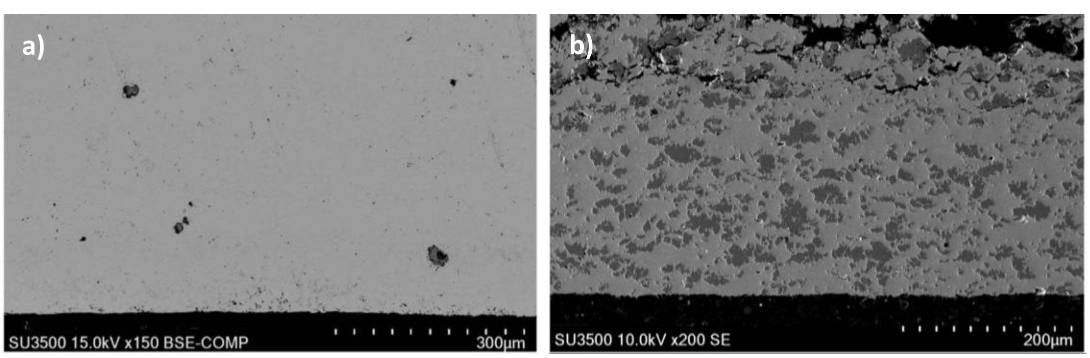

Figure 35 - Microstructures of a) zinc-tin mixture coating, b) copper-tin mixture coating [69]

2.4.3 Reverse Lay-up Method

Although coating formation is possible using many thermal spray techniques, processes where coatings are sprayed directly on CFRC substrates do not eliminate the possibility of damage induced by particle impingement and/or high temperature gas flow. The Reverse Lay-up Method was developed for avoiding this damage issue, and for an easier integration of Cold Spray technology into manufacturing processes for CFRC components. This method also eliminates the need for the additional steps of producing metal sheets that are to be glued on the CFRC structure.

The method consists of four steps: 1) Mould surface preparation, 2) Spraying metal coating on the mould, 3) Laying uncured CFRC laminate on coating followed by cure of the assembly, 4) demoulding the cured copper-coated CFRC (Fig. 36).

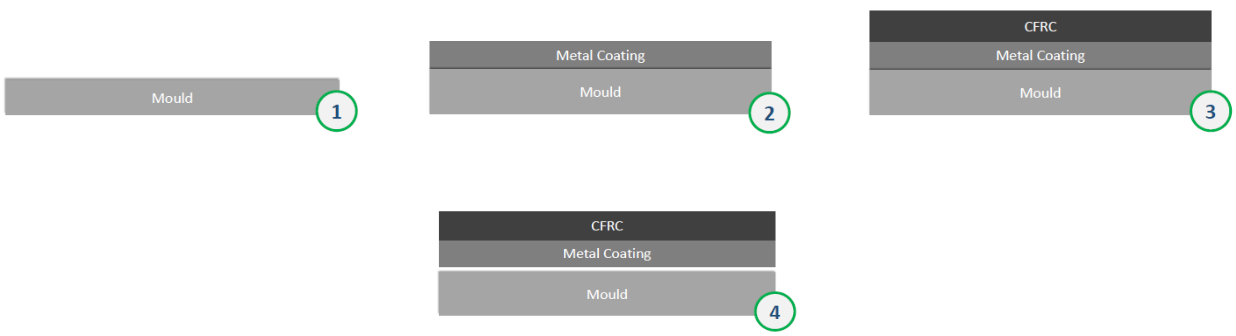

Figure 36 - Schematic of Reverse Lay-up Method

This method eliminates the erosion issue by spraying coating on the mould instead of the CFRC, avoiding the erosion phenomenon mentioned in the previous section (2.4.2). Figure 37 illustrates the manufacturing steps and images of a sample produced. Previous work on this subject demonstrated this method. Copper powder of dendritic morphology was successfully sprayed on a grit blasted Invar mould and was then demoulded along with the CFRC after cure. Coating on

CFRC was dense but with visible presence of micro-cracks (Fig. 38). The adhesion of the coating on the CFRC was tested and its results showed intra-coating (cohesive) failure at 2.6 MPa [14].

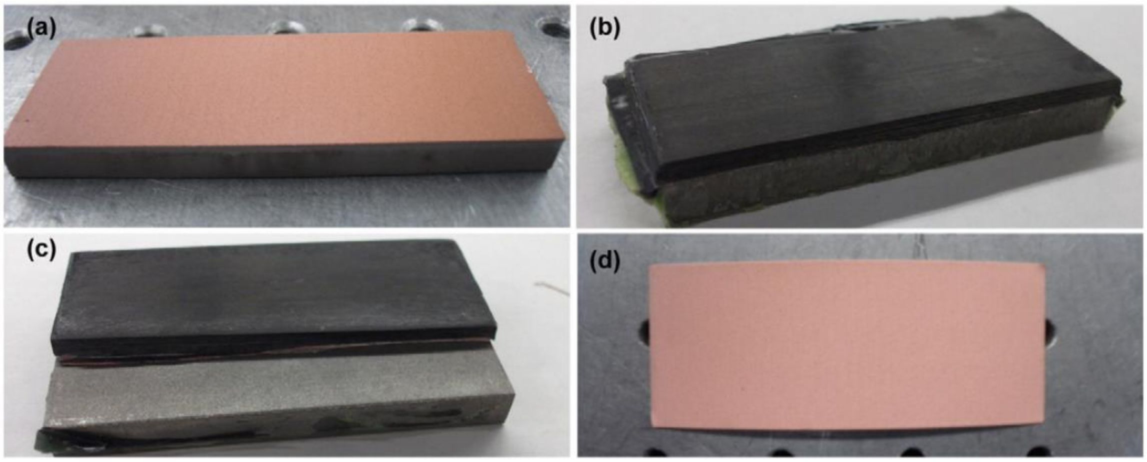

Figure 37 - Images of: a) sample at Step 2, b) sample at Step 3, c) sample at Step 4, d) top surface of the demoulded copper-coated CFRC [14]

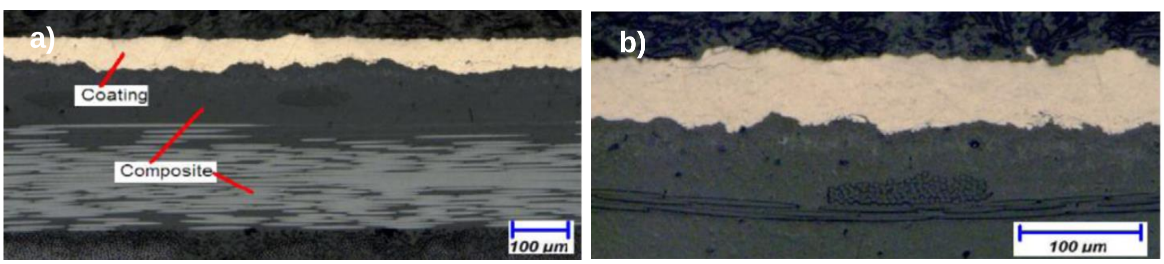

Figure 38 - Microstructures of demoulded copper coating produced by Reverse Lay-up Method on CFRC: a) cross-section, b) magnified cross-section [14]

Some issues were identified towards further development. These issues make up core points of this research work. The first issue is coating quality. Despite many attempts at modifying the spray parameters with the aim of improving coating quality, micro-cracks remained and led to intra-coating failure during bond strength tests. Past research work wherein the same copper powder was used for other applications showed much higher failure strengths than that observed as described. It was believed that the surface roughness of the mould and the powder morphology are the two key factors dictating the cohesive strength of the coatings, besides spray parameters. On one hand, coating adhesion on the mould is greatly dependant on the mould's surface roughness, with the general knowledge that adhesion increases with surface roughness. If the coating adheres too well to the mould, it potentially impedes the demoulding process and leads to damage in form of micro-cracks. On the other hand, powder morphology may also play a role in cohesive strength. The morphology dictates the amount of deformation required for particles to bond on the substrate and between themselves during deposition [70, 71, 72]. Copper of dendritic morphology used here is known for easy coating formation because of its tree-like shape [70]. This characteristic trades off cohesive strength for coating formation, in comparison to powders of spherical morphology that require much more deformation for forming a coating [70]. Additionally, spray was performed at low gas temperatures and pressures, which could affect negatively the cohesive strength of the coating from a lack of sufficient kinetic energy for intensive deformation of the particles.

The second issue is the difficulty of demoulding the cured CFRC without applying excessive forces that might damage the coating-CFRC assembly. As the previous work was a proof of concept, no emphasis was put towards developing an effective technique to demould the CFRC easily. The idea was to initiate a crack at the coating-mould interface from one edge of the assembly, that would allow the coating to detach itself from the mould. This method was proven to be arduous and unreliable.

2.5 GRIP Metal™

Originated from the automotive industry where brake pads delaminate upon use, GRIP Metal™ is the solution developed by the company Nucap whereby the surface of the backing plate is chiselled using industrial knives to form hooks that prevent delamination of the brake pad (Fig. 39). The size, height, curvature and density of hooks can be tuned for specific requirements. The idea of using hooks is to increase the interfacial shear strength between the backing plate and brake pad, in such a way that the hooks help interfacial glue to bear shear stresses. Even in the case of a critical failure at the interface, the hooks hold the pad in place (Fig. 40). This technology has seen great success in automotive industry; many companies such as VW group, FCA and GM use this product in their vehicles [73].

Figure 39 - NUCAP NRS™ backing plate [73]

Figure 40 - Advertised results of NUCAP NRS™ technology [74]

The difference between NRS and GRIP Metal™ lies in the thickness of the base materials whereby GRIP Metal™ products are made from thin metal sheets (Fig. 41). Prior to this work, no research had been published regarding the transfer of this technology to aerospace applications. Most information is available in the results section on this work, where results using GRIP Metal™ products are reported.

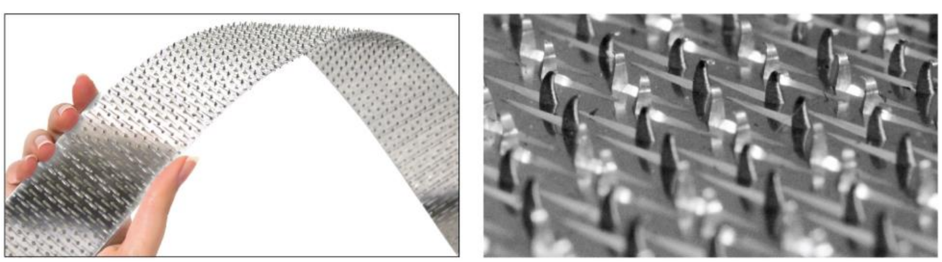

Figure 41 - GRIP Metal™ [74]

Chapter 3

Material, Equipment & Experimental Procedures

In this chapter, the materials and equipment used in this work are presented, followed by experimental procedures. In section 3.1 Materials and section 3.2 Equipment, all items are described along with their specifications. In section 3.3 Experimental Procedures, all experiments conducted in this work are listed according to the metallization method, then all procedures from sample preparation to sample manufacturing, final analysis and testing are explained in detail.

3.1 Materials

Section 3.1 features descriptions and specifications of all materials used in this work. Each sub-section presents a brief description of one or a set of materials, followed by specifications and images. Some materials were used in both metallization methods.

3.1.1 Invar Mould Material

Invar 36 was used as a substrate material and served as a mould for curing CFRC laminates along with a coating in the Reverse Lay-up Method. The material is composed of 36% nickel and 64% iron in mass fractions (Table 1). Its low thermal expansion coefficient minimizes dimensional variations during curing, making it suitable for high temperature and repetitive curing cycles. This material is often used for manufacturing aerospace grade CFRC components [75], and was therefore chosen as a substrate/mould for this study.

The dimensions of Invar samples varied according to the type of the analysis. Coating to mould adhesion strength was tested on 25.4 mm x 25.4 mm (1" x 1") samples whereas coating to CFRC tests were conducted using 25.4 mm x 76.2 mm (1" x 3") long samples (Fig. 42). All samples were ground before any further surface modification.

Table 1 - Specifications of Invar mould material

Invar 36	
Composition (wt.%)	Nickel, 36% Iron, 64%

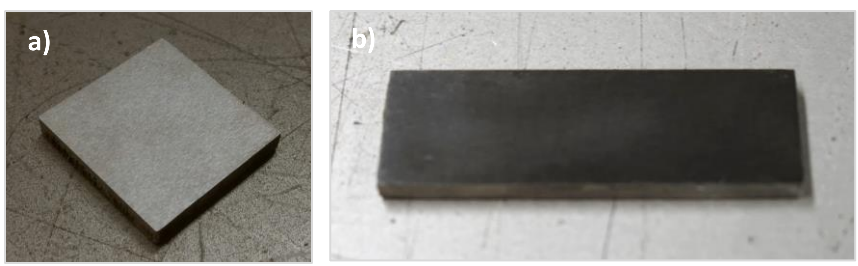

Figure 42 - Images of ground Invar sample: a) 1" x 1", b) 1" x 3"

3.1.2 Metallic Powders

Two metallic powders were probed for the Reverse Lay-up Method: SST-C5003 by Centerline (Windsor) Ltd and Cu-159 by Praxair (Table 2). The first powder is a copper powder of dendritic morphology produced by electrolytic forming with manufacturer-claimed minimum purity of 99.7% [76]. These particles are of tree-like shapes. The second is a copper powder of spherical morphology produced by gas atomization with manufacturer-claimed minimum of 99% purity [77]. The morphologies of both powders are shown in Figure 43.

Table 2 - Specifications of metallic powders

Metallic Powders		
Commercial Name	SST-C5003	Cu-159
Material, Morphology	Copper, Dendritic	Copper, Spherical
Manufacturing Method	Electrolytic Forming	Gas Atomization
Purity	>99.7%	>99.0%
Particle Size	<44 µm	6-31 µm
Manufacturer	Centerline (Windsor) Ltd.	Praxair

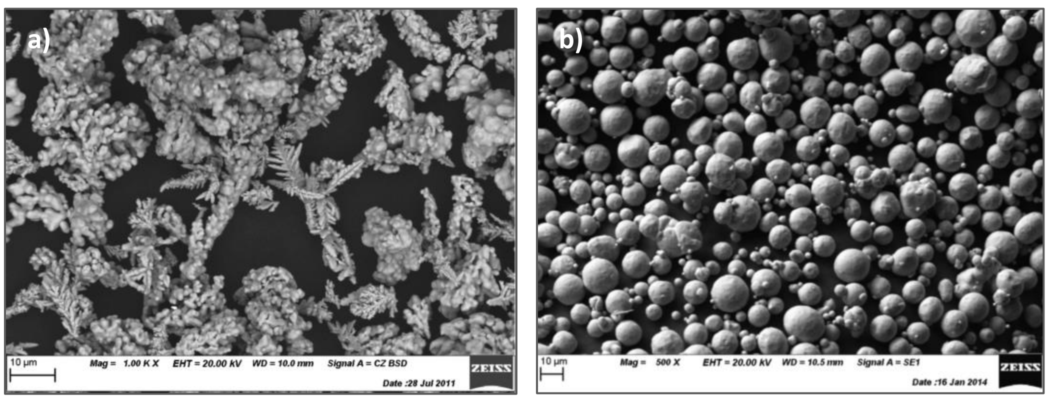

Figure 43 - SEM images of copper powder: a) SST-C5003, b) Cu-159 [67]

3.1.3 GRIP Metal™

GRIP Metal™ was used in the second part of this work. All GRIP Metal™ sheets were manufactured by Nucap. GRIP Metal™ consists of sheet metals on which hooks are formed by chiselling with automated industrial grade knives. Hook curvature, density and height are customizable, as shown in Figure 44. It should be noted that the names for each configuration are arbitrary and do not relate to any form of dimensional scale in International System of Units. Figure 45 shows examples of GRIP Metal™ sheets used in this work. Two materials were probed in this research: aluminium 5052-H38 and AISI 1010 steel.

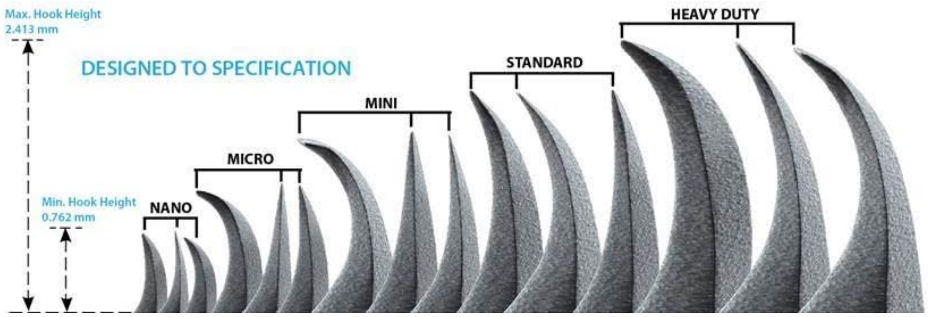

Figure 44 - Advertised GRIP Metal™ specs [78]

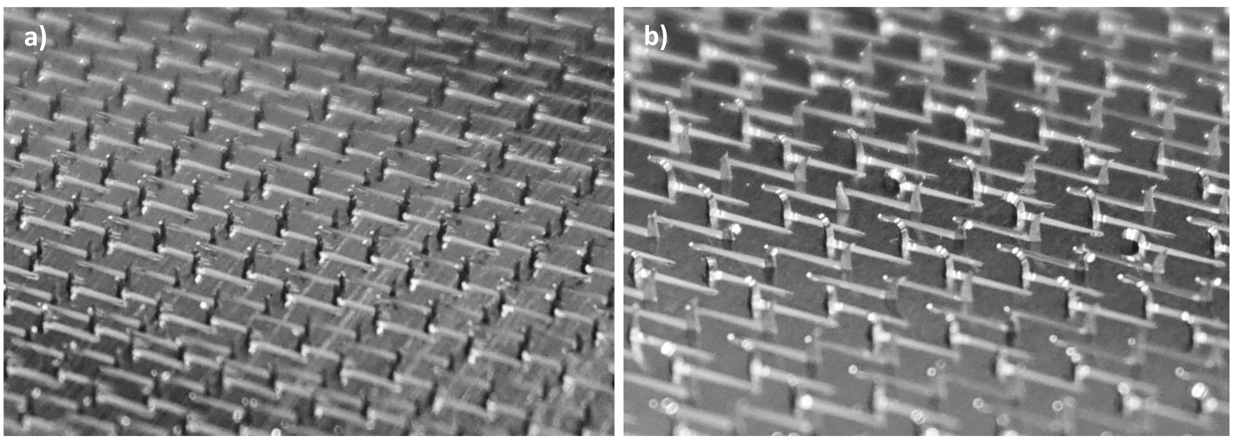

Figure 45 - Examples of as-received aluminium 5052-H38 GRIP Metal™ sheets: a) Nano hook size, b) Standard hook size

The work was divided into two phases (section 3.3.4). In phase 1, both aluminium and steel were probed whereas in phase 2, experiments focused on testing different hook curvatures for aluminium only. The complete list of GRIP Metal™ materials probed appears in Table 3. The two phases used different batch of materials, as all GRIP Metal™ sheets were made upon demand.

Table 3 - Specifications of GRIP Metal™ for experiments of phase 1 and phase 2

GRIP Metal™ - Phase 1				
Material	Al 5052-H38	Al 5052-H38	AISI 1010 Steel	AISI 1010 Steel
Hook Size	Nano	Standard	Nano	Standard
Hook Curvature	Standard	Standard	Standard	Standard

GRIP Metal™ - Phase 2						
Material	Al 5052-H38	Al 5052-H38	Al 5052-H38	Al 5052-H38	Al 5052-H38	Al 5052-H38
Hook Size	Nano	Nano	Nano	Standard	Standard	Standard
Hook Curvature	Straight	Standard	Over-bent	Straight	Standard	Over-bent

3.1.4 Carbon Fibre Prepreg & Epoxy Adhesive Film

Both the carbon fibre prepreg and epoxy adhesive film were manufactured by Gurit, Table 4. The prepreg features unidirectional fibres impregnated in uncured resin [79]. The same prepreg was used in all experiments. The epoxy adhesive film consists of uncured resin featuring the same chemical composition as that used in the prepreg [80]. Structural integrity of the film is ensured by the presence of one layer of light woven glass fibre. Figure 46 shows images of the prepreg and epoxy adhesive film.

Table 4 - Specifications of CFRC prepreg and epoxy adhesive film

Carbon Fibre Prepreg	
Type	Unidirectional Carbon Fibre Prepreg
Model	SE 70
Manufacturer	Gurit
Epoxy Adhesive Film	
Type	Epoxy with one layer of glass fibre
Model	SA 70
Manufacturer	Gurit

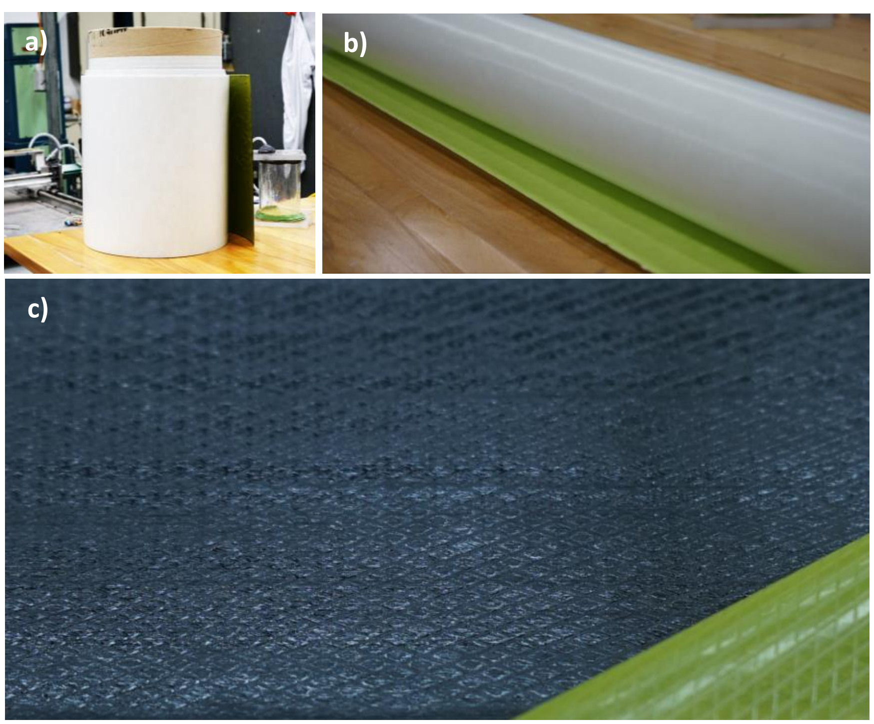

Figure 46 - a) CFRC prepreg in roll, b) epoxy film in roll, c) magnified CFRC prepreg

3.2 Equipment

Section 3.2 features descriptions and specifications of all equipment used in this work. Each sub-section presents a brief description of one or a set of equipment, followed by specifications.

3.2.1 Surface Grinding

Surface grinding was performed on the Invar substrates as-received, by means of an automated grinding machine equipped with a #46 grit grinding wheel. This process aimed at smoothing the surface of the substrates uniformly prior to grit blasting. Table 5 and Figure 47 show the specifications and image of the machine, respectively.

Table 5 - Specifications of surface grinding equipment

Grinding Machine	
Model	NB
Manufacturer	The Churchill Machine Tool Company
Grinding Wheel	
Model	AA60-N6-V10
Material, Grit Size	SiC, 46 Grit
Manufacturer	Carborundum

Figure 47 - Grinding machine

3.2.2 Grit Blasting of Invar Mould

For the Reverse Lay-up Method, control of roughness was required to achieve the desired adhesion. All Invar substrates were grit blasted prior to coating deposition. Two grit sizes were used in this work: #20 copper slag and #80 aluminium oxide. Table 6 lists the specifications and Figure 48 shows the setup. Images of the grits and samples after grit blasting are presented in Figure 49.

Table 6 - Specifications of grit blasting equipment

Grit Blasting Cabinet		
Model	Bench Model Sandblasting Cabinet	
Manufacturer	PowerFist	
Grit Blasting Gun		
Model, Container Size	18 oz. Hopper Gravity Feed Abrasive Spot Blaster Gun	
Feeding Type, Propelling Gas	Gravity-fed, Compress air or nitrogen	
Manufacturer	PowerFist	
Grits		
Model	Aluminium Oxide	Ebonygrit™
Manufacturer	Opta Minerals	Opta Minerals
Grit Size	# 80	#20
Material Composition (wt. %)	Al2O3: 92-96.5% TiO2: 1-4% FeO3: 0.1-1.5% SiO2: 0.15%	Fe2O3: 53-60% SiO2: 32-37% Al2O3: 3-6% CaO: 1-3% MgO: 1-2% Zn: <1.0% Quartz: <1.0%

Figure 48 - Grit blasting setup

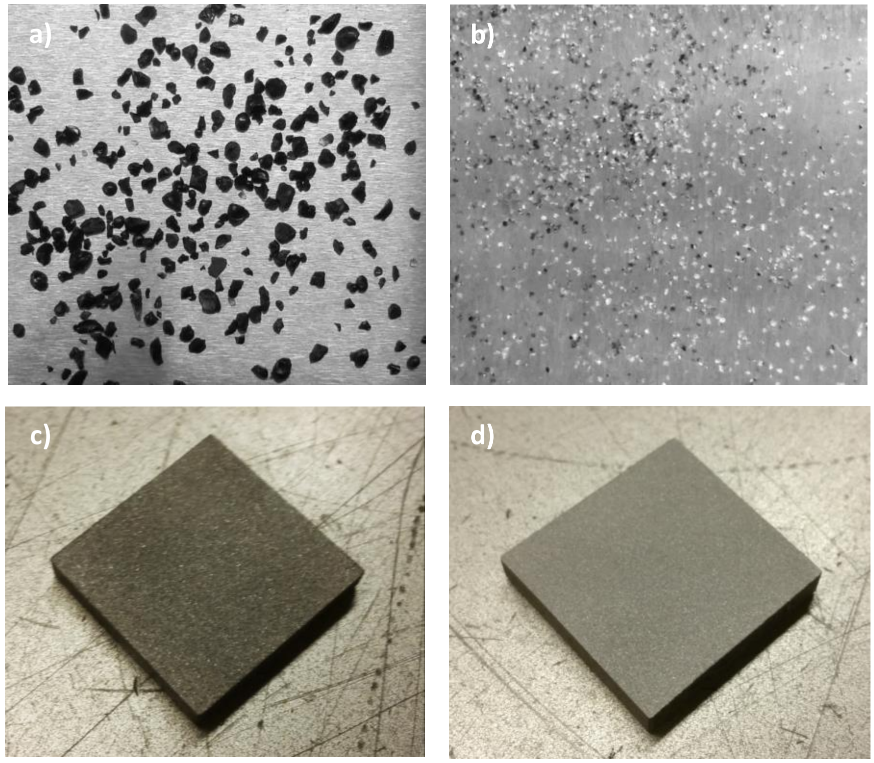

Figure 49 - Image of: a) Ebonygrit™, b) aluminium oxide, c) Invar sample grit blasted by Ebonygrit™, d) Invar sample grit blasted by aluminium oxide

3.2.3 Cleaning of Invar Mould and GRIP Metal™ Sheets

After grit blasting, Invar substrates were drenched in a beaker filled with a solution of ethanol and cleaned using a vibratory ultrasonic bath for 10 minutes. The substrates were dried by compressed air after cleaning. Table 7 and Figure 50 show the specifications and image of the equipment.

Table 7 - Specifications of cleaning equipment

Vibratory Ultrasonic Bath	
Type	Single Frequency
Model	TS 540 Transonic Bath
Manufacturer	Elma
Cleaning Fluid	
Type	Ethanol
Concentration	95%

Figure 50 - Vibratory ultrasonic bath

Cleaning was mandatory for Invar substrates due to grit residuals on their roughened surface. Residues could affect coating deposition due to their high hardness and potential weak bonding on substrates that alter particle deformation.

Cleaning was also mandatory for removing grease and dust from GRIP Metal™ sheets before integrating them into uncured CFRC prepreg stacks. The metallic sheets were cleaned using ethanol. No vibratory ultrasonic bath was used with GRIP Metal™ as it did not undergo grit blasting.

3.2.4 Surface Roughness Measurement

Surface roughness measurement was performed on Invar substrates after cleaning. The profilometer outputs an average of measurements in arithmetical mean deviation (Ra) taken across a certain length of the surface. In pursuance of consistency, at least eight measurements were performed per sample at randomly selected locations within zones of interest. Table 8 and Figure 51 show the specifications and image of the instrument.

Table 8 - Specifications of surface profile measurement instrument

Surface Profile Measurement Instrument	
Type	Profilometer
Model	SRG-4000
Manufacturer	Phase II

Figure 51 - Profilometer on top of an Invar sample

3.2.5 Coating Thickness Measurement

Coating thickness measurements were performed on metal-coated Invar samples after coating deposition in the Reverse Lay-up Method. This non-destructive testing gauge utilizes electromagnetic induction and voltage feedback to measure the coating thickness. As instructions suggest, the probe was first calibrated on an uncoated substrate (Invar in this case), then the thickness measurement was taken by pressing the probe's tip lightly against the coating. The measurement, displayed in units of micrometres, indicates the thickness at that specific point of contact. For a fair representation of the thickness, at least 8 measurements were taken across each zone of interest. Table 9 and Figure 52 show the specifications and image of the instrument.

Table 9 - Specifications of coating thickness measurement tool

Coating Thickness Measurement	
Model	456
Operation Temp.	-10 to 50°C
Accuracy	± 2.5 µm
Manufacturer	Elcometer®

Figure 52 - Coating thickness measurement instrument: Elcometer®

3.2.6 Cold Spray System

A cold spray system was used for depositing coatings on Invar substrates. The setup consisted of four components: gas bottles, control unit, powder feeder and spray chamber (system & De Laval nozzle). The system can reach gas temperature up to 500°C and gas pressure up to 3.5 MPa (500 psi). Table 10 and Figure 53 show the specifications and image of the system.

Table 10 - Specifications for cold spray system

Gas Bottles		
Type	High Pressure Nitrogen Gas	
Model	11-Bottles Pack	
Manufacturer	Linde	
Control Unit		
Type	Gas Dynamic Cold Spray System	
Model	SST Extra Pressure (EP)	
Manufacturer	Centerline (Windsor) Ltd.	
Powder Feeder		
Type	Pressure-fed Powder Feeder	
Model	1264	
Manufacturer	Praxair	
Nozzle(s)		
Type	De Laval Nozzle	De Laval Nozzle
Material	Stainless Steel	Tungsten Carbide
Orifice Diameter	2mm	2mm
Manufacturer	Centerline (Windsor) Ltd.	Centerline (Windsor) Ltd.

Figure 53 - Cold spray system used for all experiments

3.2.7 Hydraulic Press

A manually operated hydraulic press equipped with an analogue pressure gauge was used for compressing GRIP Metal™ hooks into CFRC laminates in experiments performed as GRIP Metal™ as Bond Coat - Phase 1 (section 3.3.6). Table 11 and Figure 54 show the specifications and image of the hydraulic press.

Table 11 - Specifications of hydraulic press

Hydraulic Press	
Type	Manual operation with pressure gauge
Model	SW-1000-14
Manufacturer	Rodgers Hydraulic

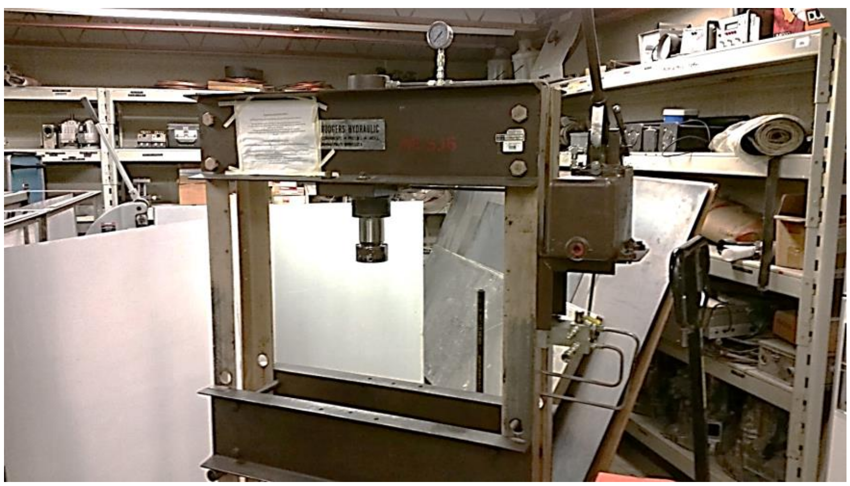

Figure 54 - Hydraulic press with analogue pressure gauge

3.2.8 Instron

An Instron universal testing frame equipped with a 10 kN load cell was used in GRIP Metal™ as Bond Coat method - Phase 2 experiments for two purposes: assembling GRIP Metal™ onto CFRC laminates and testing the adhesion of GRIP Metal™-CFRC assemblies (section 3.3.6). The Instron frame is operated by computer, hence offering more accuracy compared with the manually operated hydraulic press. Table 12 and Figure 55 show the specifications and image of the machine.

Table 12 - Specifications of Instron machine

Material Testing Machine	
Model	4482
Load Cell Capacity	10 kN
Manufacturer	Instron

Figure 55 - Instron universal testing frame

3.2.9 Vacuum Bagging and Curing

Vacuum bagging and curing were performed as follows. First, an aluminium plate was used as a base, over which was a release film. On top of the latter was the uncured laminate. Then, a layer of perforated release film and a layer of breather were added over the CFRC. Cure-resistant adhesive tape was used in conjunction with an oversized release film to seal the assembly. A two-component vacuum valve of was placed on the oversize release film, with one section inside and the other outside the bag.

By means of a hose connected to vacuum pump, air was drawn out of the bag. Finally, the entire assembly was placed inside a controlled oven for curing, following a manufacturer-specified curing cycle of +2°C/minute ramping up, dwelling at 120°C for 1 hour, then -5°C/minute ramping down until ambient temperature was reached.

Table 13 lists the specifications of all components used in the vacuum bagging and curing processes. Figure 56 and 57 show a schematic view and actual image of the setup.

Table 13 - Specifications of vacuum bagging and curing equipment

Vacuum Bagging					
Type	Perforated Film	Non-perforated film	Breather	Adhesive Tape	Aluminium Tool
Model	P-3 Dahlar® Release Bag 125	Dahlar® Release Bag 125	Econoweave 44	SM 5126 Tacky Tape®	N/A
Manufacturer	Airtech	Airtech	Airtech	Schnee-Morehead	N/A
Controlled Convection Oven					
Model	PF120				
Manufacturer	Carbolite Inc.				
Vacuum Pump					
Type	Belt-Drive Vacuum Pump				
Model	1399 Duoseal Vacuum Pump				
Manufacturer	Welch				

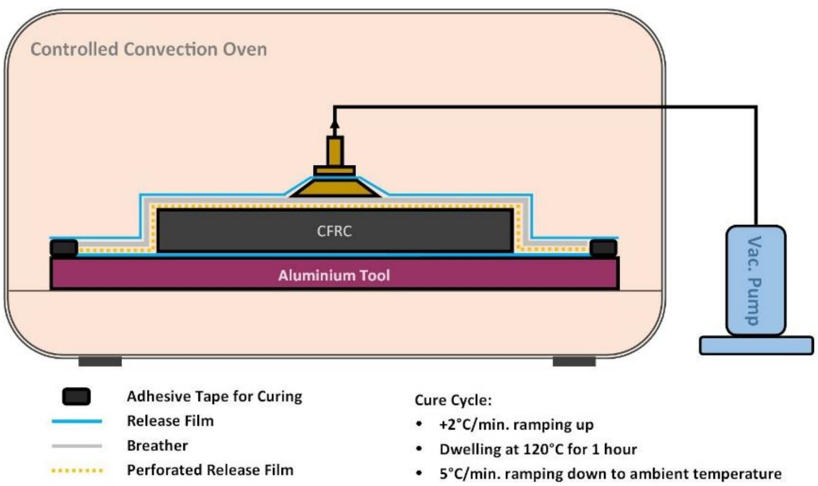

Figure 56 - General layout for vacuum bagging and curing

Figure 57 - Vacuum bagged assembly in controlled convection oven

3.2.10 Pneumatic Adhesion Tensile Test Instrument (PATTI)

PATTI was used for testing coating to mould, coating to CFRC and GRIP Metal™ to CFRC adhesion strength. The setup consists of first gluing a metallic chess-like piece, called Dolly, on a zone of interest, then isolating it from surrounding coating by manually cutting off coating material around the Dolly, using a circular saw. Using the PATTI, the dolly is pulled upward while pressing its surrounding downward, creating a tensile loading. Table 14 lists the specifications of the instrument and the dolly. Figure 58 shows the PATTI and an example of sample ready to be tested.

Table 14 - Specifications of PATTI and dollies

Pneumatic Adhesion Tensile Test Instrument (PATTI)	
Model	PosiTest AT-T
Dolly Size (Diameter)	20 mm
Manufacturer	Defelsko

Figure 58 - Image of: a) PATTI, b) dolly glued and secured on copper coated CFRC

3.2.11 Sample Cutting, Mounting and Polishing

Samples were cut into smaller pieces for analysis using an automated cut-off machine. A diamond coated blade was used for minimizing blade wear and maintaining cutting consistency. The automated cut-off process offers steady and accurate cutting. Cut pieces were then mounted using cold mounting resin & hardener, and polished using an automated polishing machine. Table 15 and Figure 59 show the specifications and images of the mentioned components.

Table 15 - Specifications of sample cutting, mounting and polishing

	Cut-off Machine	Cut-off Blade	Cold Mounting	Polishing
Manufacturer	Struers	Struers	Struers	Struers
Model	Secotom-10	Diamond Coated Stainless Steel Blade	Epoxy Resin & Hardener	Combination of TegraPol-31, TegraForce-5 and TegraDoser-5

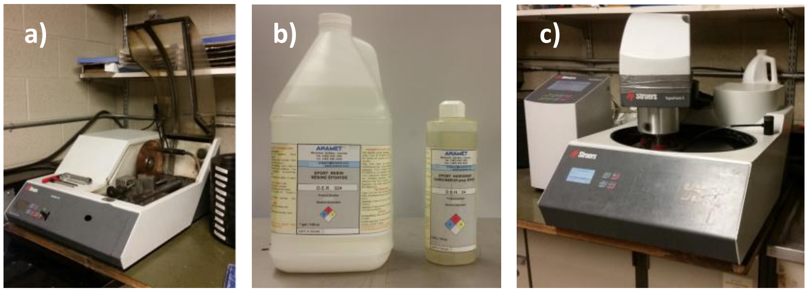

Figure 59 - Image of: a) cut-off machine, b) resin & hardener, c) polishing machine

3.2.12 Digital Optical Microscope

A digital optical microscope features a layer-by-layer 2D image capturing capability that digitally combines the data to portrait a 3D topography illustration. Sample consolidation and microstructure were also examined on cross-sections using this equipment. Additionally, the microscope was used for characterizing hooks in different GRIP Metal™ configurations. Table 16 and Figure 60 show the specifications and image of the microscope.

Table 16 - Specifications of digital microscope

Digital Microscope	
Model	VHX-2000
Manufacturer	Keyence

Figure 60 - Digital microscope

3.3 Experimental Procedures

This section presents lists of experiments conducted for this work along with their setups, procedures and analysis approaches. The work was divided into two separate parts, one for each metallization method mentioned.

3.3.1 Experiments Conducted for the Reverse Lay-up Method

Work for the Reverse Lay-up method was split along two objectives (Table 17); Objective 1: Easy and Reliable Demoulding Technique and Objective 2: Coating Quality Improvement. The demoulding technique developed in experiment RL 1.3 was employed throughout Objective 2. Details of each experiment are presented in the following sub-sections.

Table 17 - List of experiments conducted for the Reverse Lay-up Method

Objective 1: Easy and Reliable Demoulding Technique	Code
Metal Tape as Crack Initiation Site	RL 1.1
Dual Roughness Zones	RL 1.2
Single Roughness Zone	RL 1.3
Objective 2: Coating Quality Improvement	**Code**
Series No.1 - Dendritic Copper (SST-C5003)	
Low Spray Parameters	RL 1.4
Combination of Spray Parameters	RL 1.5
High Spray Parameters	RL 1.6
Combination of Spray Parameters with Increased 2nd Layer Traverse Speed	RL 1.7
Combination of Spray Parameters with Double 1st Layer	RL 1.8
Combination of Spray Parameters with Double 2nd Layer	RL 1.9
Series No.2 - Spherical Copper (Cu-159)	
Attempt with Praxair Cu-159 Powder	RL 1.10

3.3.1.1 Metal Tape as Crack Initiation Site

In this experiment, aluminium and copper tapes were probed. The tapes consisted of thin metal foils attached to a thin layer of glue. The tapes measuring 3 mm in width were applied manually to the edge of the Invar substrate. After setting the tape, SST-C5003 copper powder was sprayed over the samples. If a coating was generated successfully, then a CFRC laminate would be mounted over the latter. Figure 61 shows a schematic view of the concept.

Table 18 lists the spray parameters of this experiment. Values were extracted from previous work whereby a successful copper coating was produced on an Invar substrate [14]. The surfaces of the substrates were grit blasted to Ra values of 4.4 ± 0.54 µm prior to deposition, achieved using a gas pressure of 0.62 MPa (90 psi) and a grit size of #20.

Table 18 - Spray parameters, experiment RL 1.1

Spray Parameters	Description
Gas Temperature	350°C
Gas Pressure	1.7 MPa
Powder Feeding Rate	4 RPM
Powder Feeding Wheel Type	320 Holes
Powder Feeding Gas Flow Rate	25 SCFM
Nozzle Type	Stainless Steel
Standoff Distance	15 mm
Traverse Speed	45 mm/s
Step Size	1 mm
Number of Passes	1

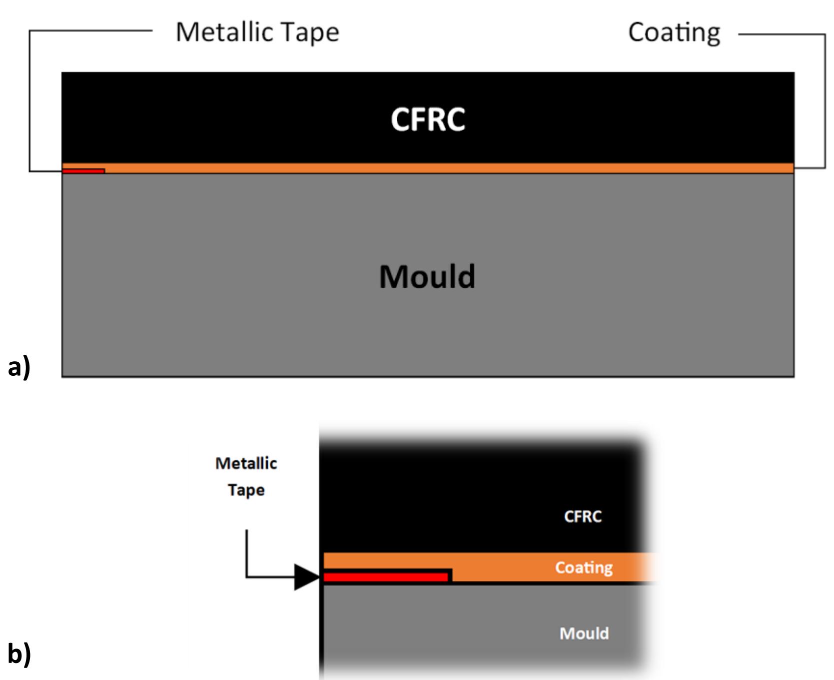

Figure 61 - Illustration of a) Metal Tape as Crack Initiation Site, b) magnified view of a)

3.3.1.2 Dual Roughness Zones

The approach consisted of 4 steps: 1) grit blast the mould's surface and obtain two zones of different roughnesses, 2) spray the coating on the mould, 3) mount the uncured CFRC laminate with its extra length protruding one edge of the mould, then cure the assembly, 4) demould the CFRC along with coating by applying a force on the protruded portion of the composite laminate. Spray parameters remained identical to those from previous experiment (RL 1.1). Figure 62 illustrates the concept of this approach. A similar method has been employed for studying coating-substrate crack propagation [81].

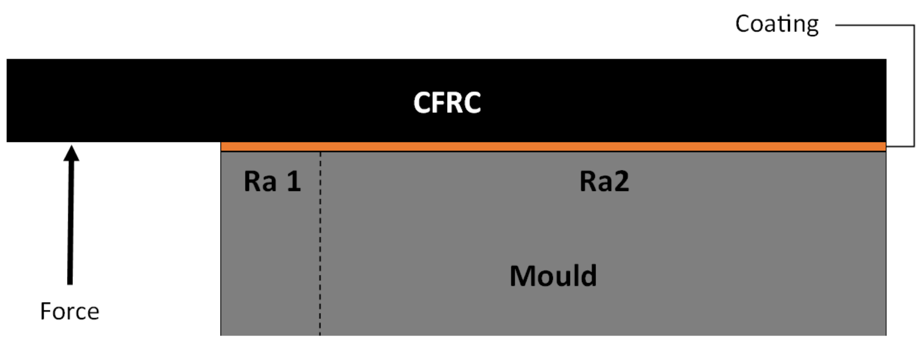

Figure 62 - Illustration of Dual Roughness Zones

The width of zone Ra 1 was arbitrarily set to 3 mm. No investigation was done to determine the optimal width of zone Ra 1 as the next experiment (RL 1.3) demonstrated that dual roughness is not mandatory for achieving this cantilever-effect approach. As for the CFRC, its additional length was arbitrarily set to 50.8 mm (2 inches).

Prior to coating deposition, the two different surface roughnesses were generated using grit blasting with #20 grits and 0.62 MPa (90 psi) gas pressure. By masking the opposite zone with tape and controlling each surface's exposure time to grit bombardment, different surface roughnesses were achieved. Ra values were measured for both zones using the profilometer. The average Ra for zone Ra 1 and Ra 2 were 2.52 ± 0.66 µm and 4.5 ± 0.55 µm respectively.

In addition to producing complete copper coated CFRC samples, some supplementary samples of 31.75 mm x 31.75 mm (1.25” x 1.25”) in dimensions were produced for testing the coating to mould bond strength via PATTI test. These samples did not have CFRC mounted on them and had one surface roughness only: either Ra 1 or Ra 2.

3.3.1.3 Single Roughness Zone

Surface preparation and all spray parameters remained identical to those in RL 1.2 with the exception of zone Ra 1 being discarded, as shown in Figure 63. The protrusion in CFRC also remained 50.8 mm in length.

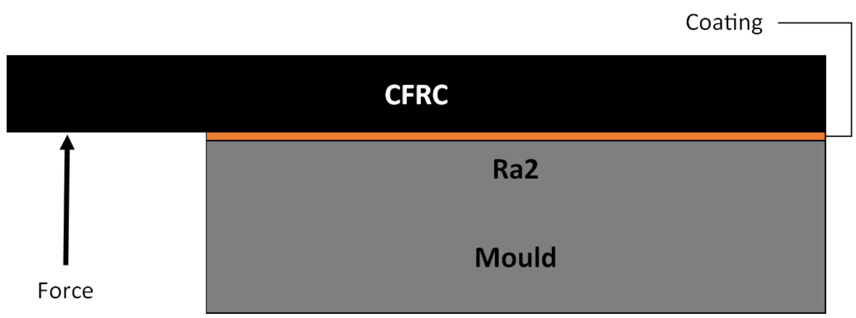

Figure 63 - Illustration of Single Roughness Zone

3.3.1.4 Low Spray Parameters

The successful development of a reliable demoulding technique in experiment RL 1.3 fulfilled Objective 1, and therefore led the research focus towards coating quality improvement. Experiment RL 1.4 was the first trial towards Objective 2.

With the exception of the spray parameters, this approach was identical to that of experiment RL 1.3 (Fig. 64). Spray parameters (Table 19) were extracted from previous work whereby a series of tests were performed to obtain a fully dense and crack-free coating on an Invar substrate [14]. The surface of the Invar mould was grit blasted with #20 grit to an average roughness Ra of 3.9 ± 0.2 μm, according to specification presented along those parameters.

No CFRC was mounted on the samples due to the presence of undesirable microcracks observed in as-sprayed coatings (section 4.1.4). Some supplementary samples were produced for testing coating to mould adhesion strength.

Table 19 - Spray parameters, experiment RL 1.4

Parameters	Description
Gas Temperature	300°C
Gas Pressure	2.2 MPa
Powder Feeding Rate	4 RPM
Powder Feeding Wheel Type	320 Holes
Powder Feeding Gas Flow Rate	25 SCFM
Nozzle Type	Stainless Steel
Standoff Distance	15 mm
Traverse Speed	50 mm/s
Step Size	1 mm
Number of Passes	1

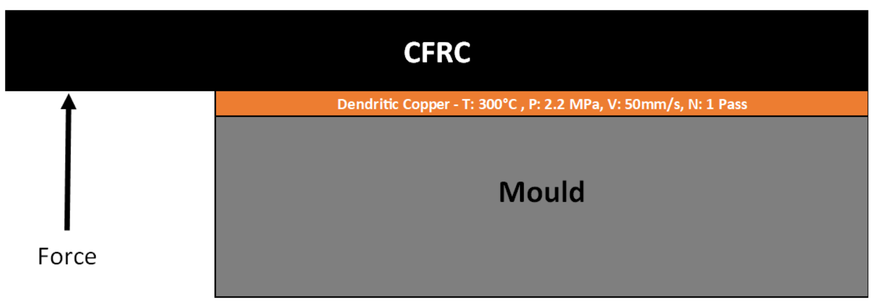

Figure 64 - Illustration of Low Spray Parameters

3.3.1.5 Combination of Spray Parameters

A new approach was proposed whereby two coating layers with different parameters were subsequently sprayed. Spray parameters from the previous experiment (RL 1.4) were used for depositing the first layer, and high gas temperatures and pressures were used for the second layer. Figure 65 shows a schematic view of the concept. The spray parameters are listed in Table 20. The surface roughness of the Invar mould remained identical to that in the previous experiment (Experiment RL 1.4 Low Spray Parameters).

Table 20 - Spray parameters, experiment RL 1.5

Common Parameters for 1st and 2nd Layers	Description
Powder Feeding Rate	4 RPM
Powder Feeding Wheel Type	320 Holes
Powder Feeding Gas Flow Rate	25 SCFM
Nozzle Type	Stainless Steel
Standoff Distance	15 mm
Traverse Speed	50 mm/s
Step Size	1mm
Number of Passes	1
Parameters of 1st Layer	
Gas Temperature	300°C
Gas Pressure	2.2 MPa
Parameters of 2nd Layer	
Gas Temperature	500°C
Gas Pressure	3.45 MPa

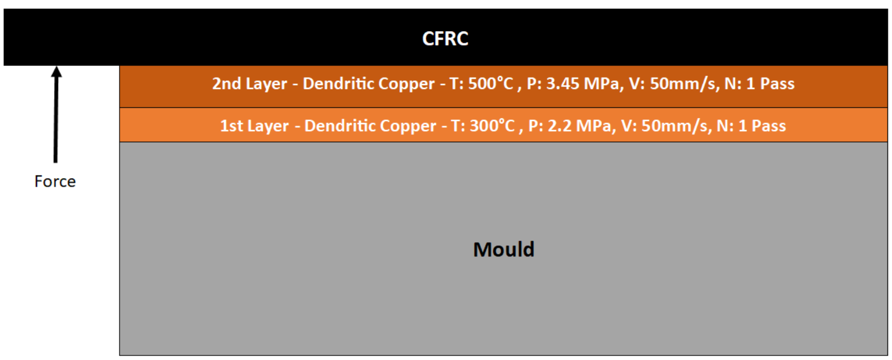

Figure 65 - Illustration of Combination of Spray Parameters

3.3.1.6 High Spray Parameters

In this experiment, only one layer of copper coating was deposited (Fig. 66). The roughness of the substrates' surfaces remained identical to that in experiment RL 1.4. Spray parameters were those used for the second layer in experiment RL 1.5, with the traverse speed increased from 50mm/s to 100mm/s and the number of passes from 1 to 2. Table 21 lists the spray parameters for this experiment. Some supplementary samples were produced for testing coating to mould adhesion strength.

Table 21 - Spray parameters, experiment RL 1.6

Parameters	Description
Gas Temperature	500°C
Gas Pressure	3.45 MPa
Powder Feeding Rate	4 RPM
Powder Feeding Wheel Type	320 Holes
Powder Feeding Gas Flow Rate	25 SCFM
Nozzle Type	Stainless Steel
Standoff Distance	15 mm
Traverse Speed	100 mm/s
Step Size	1 mm
Number of Passes	2

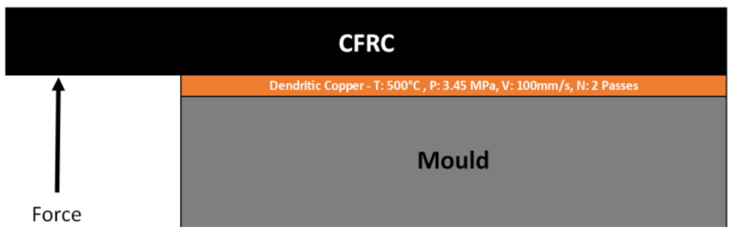

Figure 66 - Illustration of High Spray Parameters

3.3.1.7 Combination of Spray Parameters with Increased 2nd Layer Traverse Speed

Similarly to experiment RL 1.5, two layers of different spray parameters were subsequently deposited on the substrate (Fig. 67). However, the traverse speed used for the second layer was increased to 100mm/s, and the number of passes to 2 (Table 22). Surface Ra of the substrates also remained identical to that in experiment RL 1.5. In addition to cross-section analysis, some coating to mould samples were etched for inspection of particles deformation and coating consolidation.

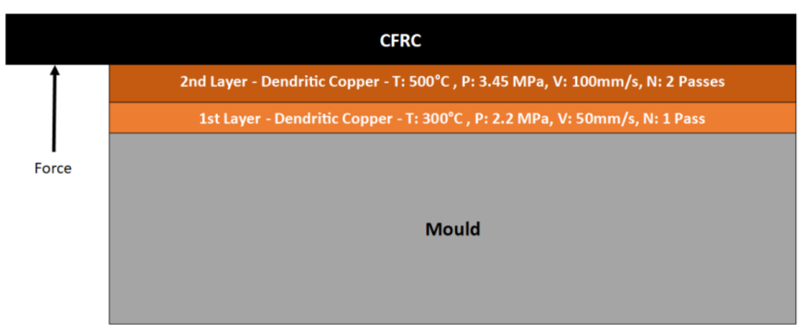

Figure 67 - Illustration of Combination of Spray Parameters with Increased 2nd Layer Traverse Speed

Table 22 - Spray parameters, experiment RL 1.7

Common Parameters for 1st and 2nd Layers	Description
Powder Feeding Rate	4 RPM
Powder Feeding Wheel Type	320 Holes
Powder Feeding Gas Flow Rate	25 SCFM
Nozzle Type	Stainless Steel
Standoff Distance	15 mm
Step Size	1mm
Parameters of 1st Layer	
Gas Temperature	300°C
Gas Pressure	2.2 MPa
Traverse Speed	50 mm/s
Number of Passes	1
Parameters of 2nd Layer	
Gas Temperature	500°C
Gas Pressure	3.45 MPa
Traverse Speed	100 mm/s
Number of Passes	2

3.3.1.8 Combination of Spray Parameters with Double 1st Layer

In this experiment, the number of passes for the first layer was increased from 1 to 2 without modifying any other parameters from experiment RL 1.7. Figure 68 shows the schematic view.

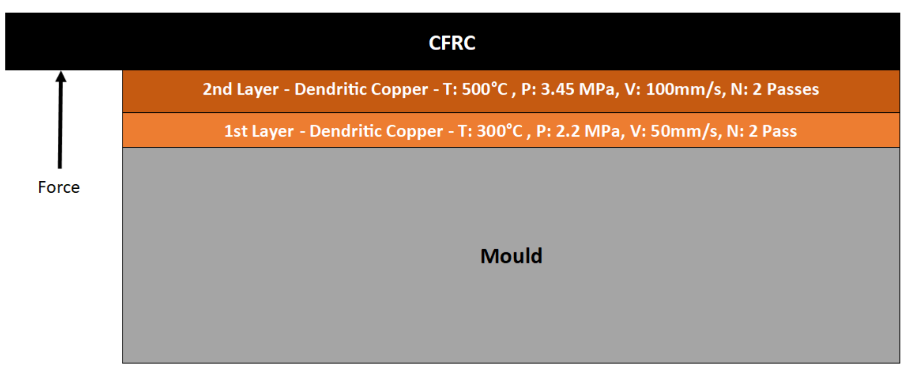

Figure 68 - Illustration of Combination of Spray Parameters with Double 1st Layer

3.3.1.9 Combination of Spray Parameters with Double 2nd Layer

In this experiment, the number of passes for the second layer was increased from 2 to 4 without modifying any other parameters from the experiment RL 1.7 (Fig. 69).

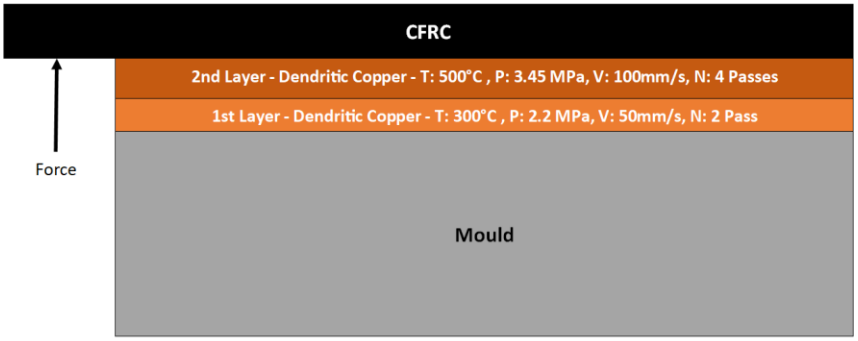

Figure 69 - Illustration of Combination of Spray Parameters with Double 2nd Layer

3.3.1.10 Attempt with Praxair Cu-159 Powder

In this experiment, only one coating layer was deposited using a new surface roughness and set of spray parameters (Fig. 70). These new parameters (Table 23) were extracted from previous work on this subject, that did not investigate spherical copper beyond determining a coating to mould adhesion value [14].

Table 23 - Spray parameters, experiment RL 1.10

Parameters	Description
Gas Temperature	350°C
Gas Pressure	1.7 MPa
Powder Feeding Rate	1 RPM
Powder Feeding Wheel Type	320 Holes
Powder Feeding Gas Flow Rate	25 SCFM
Nozzle Type	Tungsten Carbide
Standoff Distance	15 mm
Traverse Speed	50 mm/s
Step Size	1 mm
Number of Passes	2

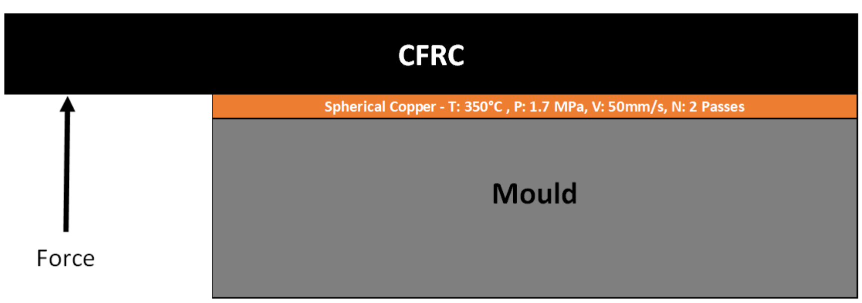

Figure 70 - Illustration of Attempt with Praxair Cu-159 Powder

The surface of the Invar mould was grit blasted using #80 grits to an average roughness Ra of 1.38 ± 0.12 μm by 0.62 MPa (90 psi) pressure. Similarly to many experiments in the Reverse Lay-up Method, some supplementary coating to mould samples were produced for investigating the microstructure of as-sprayed coatings under optical microscope. Coating-CFRC samples generated from the main experiment were also inspected. PATTI tests were performed on both coating to mould and coating to CFRC samples.

3.3.2 Sample Manufacturing Procedures for the Reverse Lay-up Method

The manufacturing procedures featured 5 steps: preparation, cold spray, CFRC lay-up, CFRC curing and demoulding. Each step features sub-steps that were performed consecutively. Figure 71 illustrates the manufacturing procedures for the Reverse Lay-up Method.

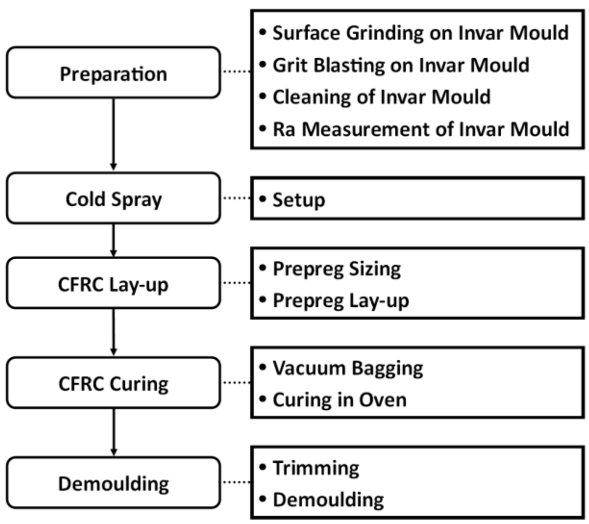

Figure 71 - Diagram of manufacturing procedures for the Reverse Lay-up Method

In preparation, the moulds were ground then roughened using grit blasting to the desired Ra value. The moulds were then soaked in a beaker filled with ethanol and placed in a supersonic vibratory bath for cleaning. After 10 minutes, the moulds were dried using compressed air, and their surface roughness was measured using a Profilometer. Afterwards, the coatings were deposited on the surface of the moulds using prescribed spray parameters and powder. After spray, CFRC laminates were stacked using prepreg, following a stacking sequence of $[0°,90°]_6$. Once done, an epoxy adhesive film was added to the top surface of the laminates. Before assembling the CFRCs onto the coated moulds, the sides and bottom of the latter were wrapped in release-tape to prevent excessive resin from the CFRC from sticking on the mould during curing. Once warped, each mould was mounted on its designated CFRC laminate, with the coating facing the composite. Figures 72 and 73 illustrate the stacking and mounting process. Finally, the assemblies were placed inside a vacuum bag then cured inside an instrumented convection oven following a curing cycle of +2°C/minute ramping up, 1-hour dwelling at 120°C and -5°C/minute ramping down to ambient temperature (Fig. 74). The cured samples were demoulded in a vice by lifting the protruding CFRC.

Figure 72 - Illustrations of prepreg stacking and substrate mounting processes

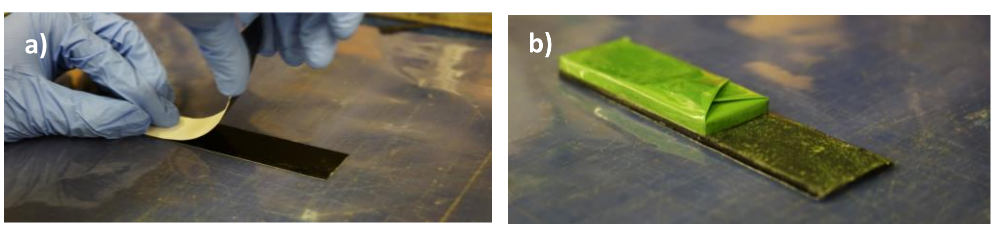

Figure 73 - Image of: a) process of stacking CFRC, b) final assembly before vacuum bagging

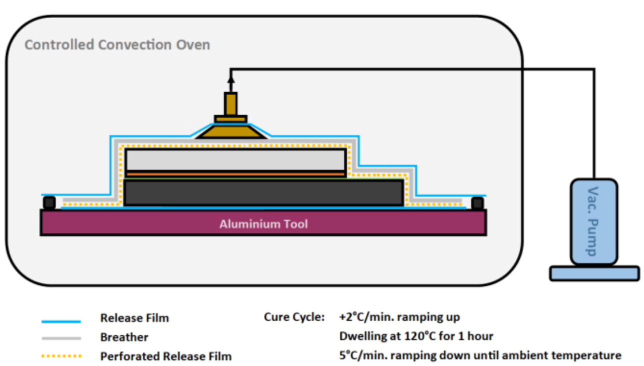

Figure 74 - Illustration of curing process for the Reverse Lay-up Method

3.3.3 Analysis Procedures of the Reverse Lay-up Method

Samples were examined using cross-section analysis whereby they were first cut with an automated cutting machine, cold-mounted in resin, polished using an automated machine, then observed under digital optical microscope. For samples that were to be tested in adhesion, a PATTI was used whereby dollies were glued onto the surface of the samples, then pulled in tensile stress. The stress increased by 0.2MPa/second and stopped when the coating detached from the mould.

3.3.4 Experiments Conducted for the GRIP Metal™ as Bond Coat Method

Since GRIP Metal™ had never been investigated for any aerospace application, the work was split into two phases, each targeting different objectives. Table 24 presents the list of all experiments conducted for the GRIP Metal™ as Bond Coat Method.

Phase 1 focused on designing the assembly procedures and the testing setups for the GRIP Metal™-CFRC integration. Due to the high cost and complexity of changing the manufacturing setup of GRIP Metal™ sheets from the manufacturer, only aluminium 5052-H38 and AISI 1010 steel were provided for this research. Two types of assembly procedures were probed: with and without pre-compression. Pre-compression consists in pressing the GRIP Metal™ sheet onto the uncured laminate before vacuum bagging. Afterward, GRIP Metal™-CFRC samples were cut into smaller pieces for cross-section analysis under microscope and for adhesion test using PATTI.

Phase 2 discarded AISI 1010 steel due to presence of corrosion at the metal-CFRC interface observed in Phase 1 (section 4.2.4). The performance of different aluminium GRIP Metal™ hook sizes and curvatures was investigated. A new patch of GRIP Metal™ sheets were received for these experiments. It contained a total of six different configurations with two hook sizes: Nano and standard, and three hook curvatures: straight, standard and over-bent. The hook height measurement method was changed from using 3D topography to a so-called 2D image-focus technique that allowed faster and more accurate measurements (section 3.3.5). The setups were modified for better precision and control in the steps of pre-compression and of adhesion testing. The modifications consisted in replacing both the hydraulic press and the PATTI by an Instron machine. This in turn allowed the PATTI test to be replaced by a standardized test, ASTM C297, specifically designed for flatwise tensile tests [82].

Table 24 - List of experiments conducted for the GRIP Metal™ as Bond Coat Method

	Material	Pre-compression	Hook Size	Hook Curvature	Code
Phase 1	Al 5052-H38	Yes	Nano	Standard	GM P1 Al1
		No	Nano	Standard	GM P1 Al2
		Yes	Standard	Standard	GM P1 Al3
		No	Standard	Standard	GM P1 Al4
	AISI 1010 Steel	Yes	Nano	Standard	GM P1 ST1
		No	Nano	Standard	GM P1 ST2
		Yes	Standard	Standard	GM P1 ST3
		No	Standard	Standard	GM P1 ST4
	Material	Pre-compression	Hook Size	Hook Curvature	Code
Phase 2	Al 5052-H38	Yes	Nano	Straight	GM P2 Al1
		Yes	Nano	Standard	GM P2 Al2
		Yes	Nano	Over-bent	GM P2 Al3
		Yes	Standard	Straight	GM P2 Al4
		Yes	Standard	Standard	GM P2 Al5
		Yes	Standard	Over-bent	GM P2 Al6

3.3.5 As-received GRIP Metal™ Sheet Characterization

As-received GRIP Metal™ sheets were examined under digital microscope for determining average hook height, curvature and density for each configuration. The characterization techniques were identical in both phases except for hook height measurements.

In phase 1, hook height was measured using 3D imaging of the sheets. The microscope took 2D images at different depths, from which it composed, a three-dimensional representation. The height of each hook was determined using a built-in software (Fig. 75). For each configuration, 60 hooks were randomly selected and measured. It was detected that this approach could not match the heights measured using cross-sections images. 3D images often came nearly 200 μm short.

An alternative approach was used in Phase 2 whereby the height was determined by calculating the depth-of-focus difference between the plate's surface and the hook's tip with the aid of a built-in tool. For each measurement, the image was first focused on the plate then moved up to the tip (Fig. 76). Considering the step size of the moving lens, a precision of +/- 5 μm at each focal point could be obtained under 300x magnification. As the technique required focusing twice per hook, the sum of deviations was +/- 10 μm per hook measurement. A total of 18 hooks per sample and 9 samples per configuration were evaluated in Phase 2.

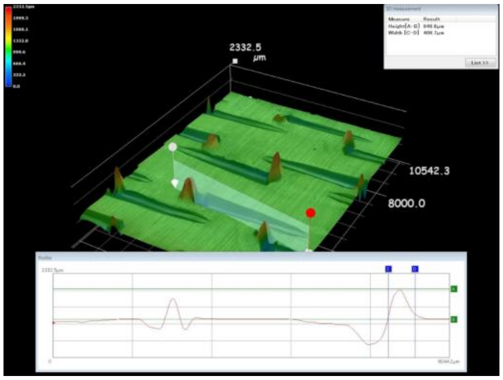

Figure 75 - Example of hook height measurement by 3D topography

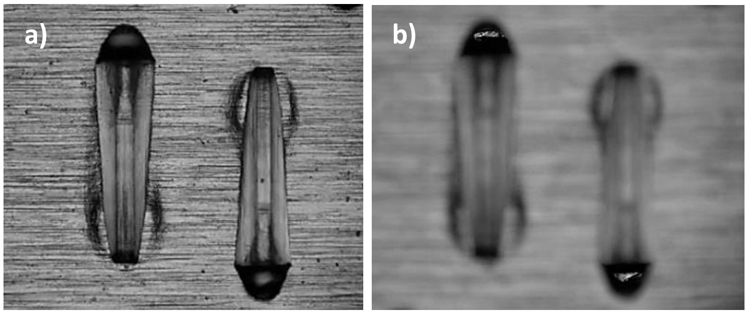

Figure 76 - Example of hook height measurement using depth-of-focus:
a) focus on plate, b) focus on hook's tip

Hook curvature was measured using cross-section images of the GRIP Metal™ sheets. Hooks often needed more than one curvature to describe their profile; as the hook's tip is the portion that made the first contact with the CFRC laminate upon integration, the inner curvature measurement was taken near the tip instead of the base, e.g.: in Fig. 77, the curvature is 725 μm. In phase 1, for each configuration, 4 samples from different plates were selected randomly for inspection; in each sample, a total of 9 hooks in cross-section were measured. In Phase 2, 3 hooks per cross-section, 3 cross-sections per sample and 6 samples per configuration were inspected.

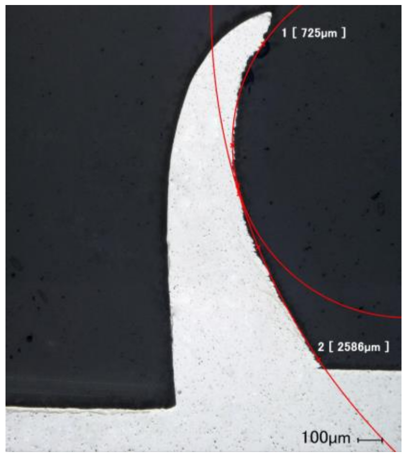

Figure 77 - Example of hook curvature measurement

Hook density was measured using 2D imaging of the sheets. The microscope took 2D images from the top view of the sheets and created stitched images (Fig. 78). Hook density in each image was calculated by counting the number of visible hooks divided by the area of the image. For both phases, 9 samples were selected randomly from 3 plates per configuration.

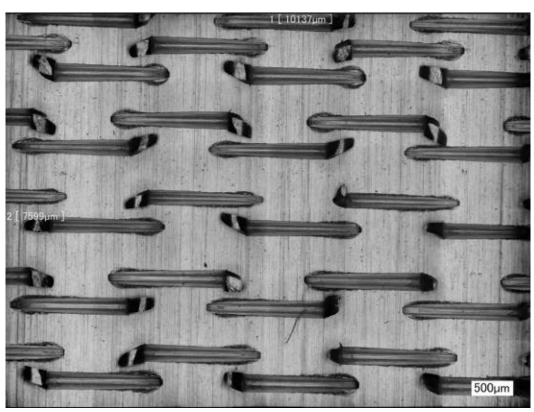

Figure 78 - Example of hook density measurement

3.3.6 Sample Manufacturing Procedures for the GRIP Metal™ as Bond Coat Method

CFRC laminates were stacked following a sequence of $[0°,90°]_8$. The GRIP Metal™ sheets were cleaned with ethanol, then pressed against the laminates with hooks facing towards the CFRCs. Afterward, these assemblies were put in a vacuum bag and cured in a convection oven. Figures 79 and 80 show schematic views of these procedures.

In phase 1, the pre-compression was performed using a manually operated hydraulic press equipped with an analogue pressure gauge, whereas an Instron machine was used in phase 2. Figure 81 shows the different setups. The pre-compression stress was set to 10 atm and held for 5 minutes before release. The assembly was then cured following the cycle: +2°C/minute ramping up, 1-hour dwelling at 120°C and -5°C/minute ramping down to ambient temperature.

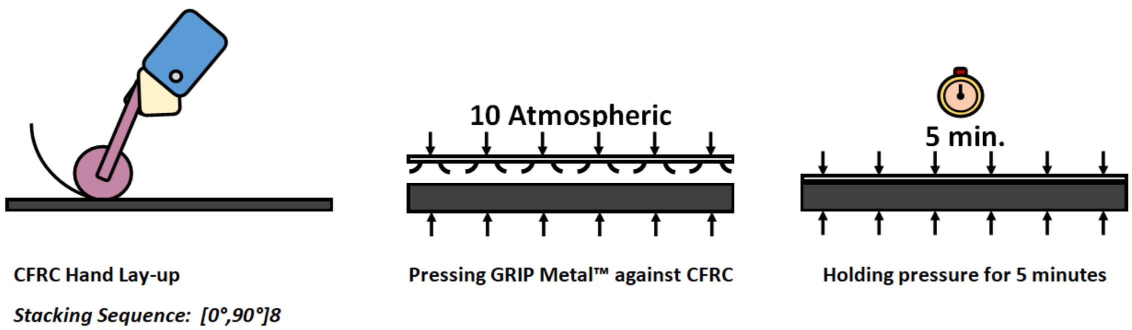

Figure 79 - Illustration of GRIP Metal™ - CFRC integration procedures

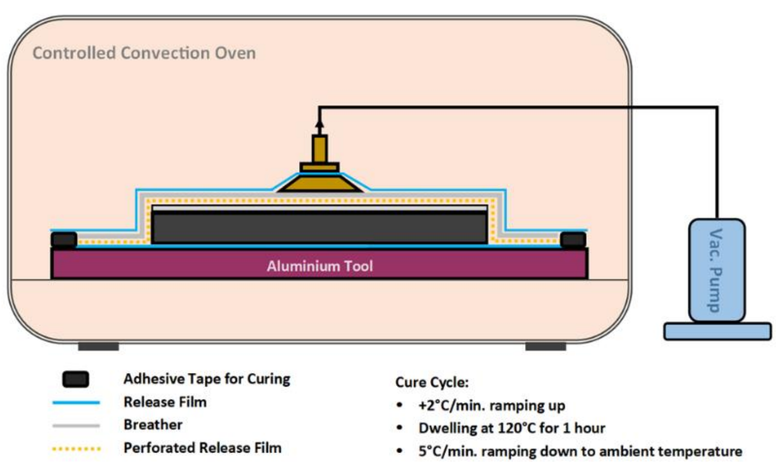

Figure 80 - Illustration of curing process for GRIP Metal™ as Bond Coat Method

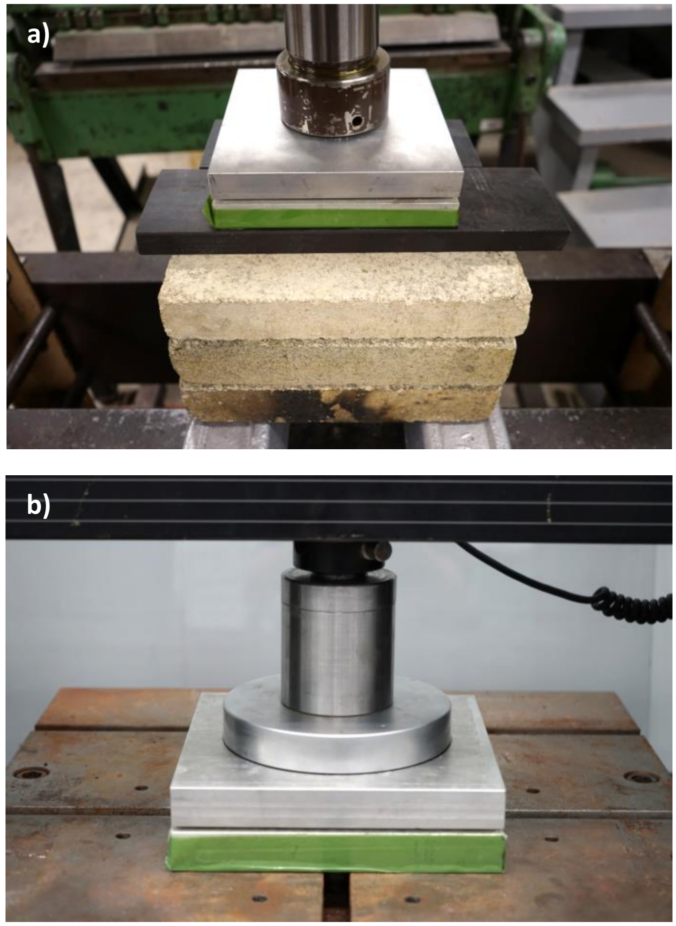

Figure 81 - Pre-compression setup of: a) Phase 1, using hydraulic press, b) Phase 2, using Instron

3.3.7 Analysis Procedures for the GRIP Metal™ as Bond Coat Method

In both phases, samples were examined using cross-section analysis whereby they were first cut using an automated cutting machine, cold-mounted in resin, polished using an automated machine, then observed under digital microscope.

In Phase 1, PATTI tests were performed on GRIP Metal™-CFRC samples. Similar to what was done in the Reverse Lay-up Method, the tests consisted of first gluing the dollies on the samples' metallic side, then isolating the dollies by cutting off surrounding material, in this case the aluminium or steel of the GRIP Metal™. Afterwards, the dollies were pulled using the pneumatic instrument.

In phase 2, ASTM C297 flatwise tensile test was performed using an Instron machine in lieu of PATTI tests. This test is designed specifically for samples of sandwich structures like the GRIP Metal™-CFRC. Samples were cut to 25.4 mm x 25.4 mm (1” x 1”) dimensions, conforming to the minimum sample size suggested in the standard, and tested using square bond-plugs. Figure 82 shows the setup used for testing and the setup recommended in the standard. The difference between the actual and recommended bond plugs lies in the geometry of their edges; the actual ones had rounded edges for fitting into round tensile test adapters.

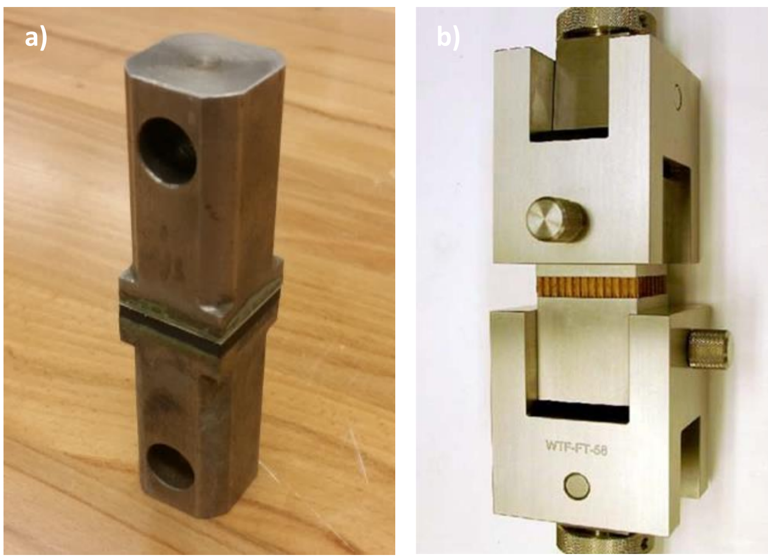

Figure 82 - Image of: a) bond plugs used, b) ASTM C297 suggested setup

Chapter 4
Results

4.1 Results for the Reverse Lay-up Method

As mentioned in the literature review, the main issues and challenges related to this metallization method consisted in the lack of a convenient demoulding technique and unsatisfied coating quality. More specifically, a sharp tool was used for initiating crack propagation at coating to mould interface for demoulding the coated CFRC; the procedure was determined to be unreliable. Also, in demoulded copper coated CFRC samples, microcracks were observed within the coating. To solve these issues, the work was split into two parts, each targeting one of the two issues: Objective 1: Easy and Reliable Demoulding Technique and Objective 2: Coating Quality Improvement. Considering the convenience of having a reliable demoulding technique that would facilitate the proceedings of latter experiments, the work began by targeting Objective 1.

Ultimately, the ideal coating would be one that has a low coating to mould adhesion strength, featuring a dense and crack-free microstructure, and retains all its properties after demoulding the CFRC.

4.1.1 Metal Tape as Crack Initiation Site

Gluing a strip of metallic tape at the edge of the Invar mould prior to coating deposition was envisaged as a potential solution (Fig. 83 a) and b)). The tape had low adhesion and could therefore function as a pre-induced defect at the coating to mould interface.

Both experiments with aluminium and copper tapes were unsuccessful (Fig. 83 c) and d)). The tapes peeled off during spraying. As a result, no further investigations were undertaken for this approach.

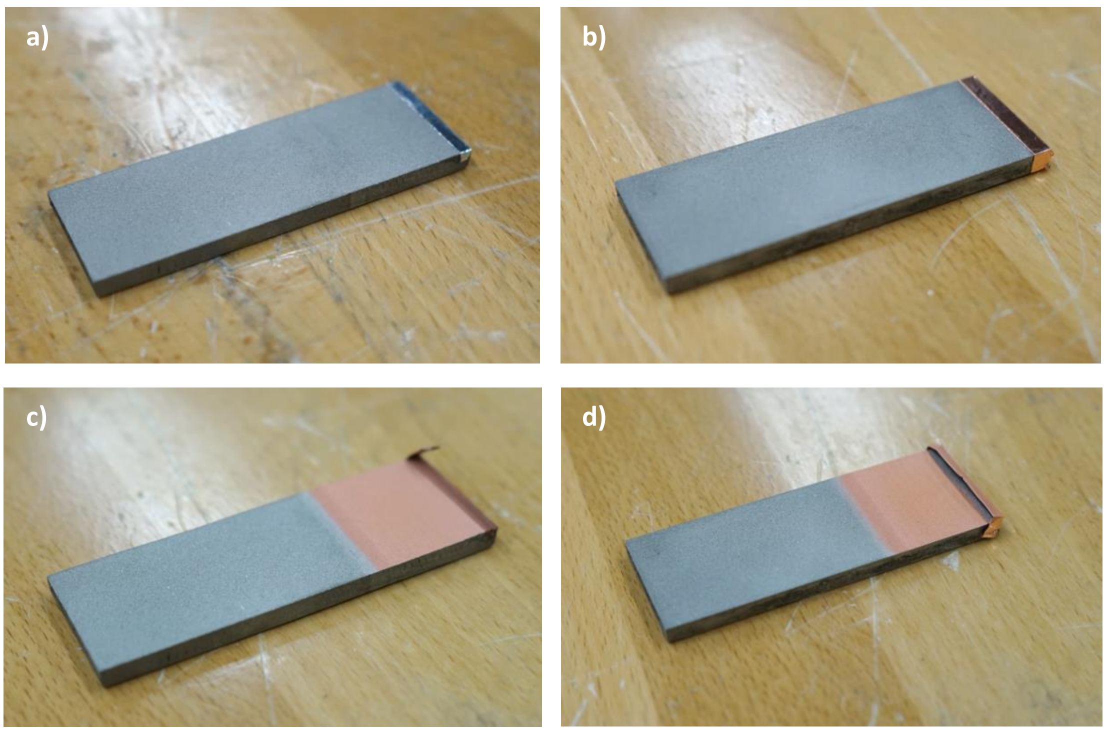

Figure 83 - RL 1.1: Images of aluminium tape on substrate: a) before spray, c) after spray; image of copper tape on substrate: b) before spray, d) after spray

4.1.2 Dual Roughness Zones

This approach was proven to be successful. CFRCs demoulded easily and the coating showed no sign of severe damage when examined by eyes (Fig. 84). The dual zones were identifiable through a minor colour variation (Fig. 85).

Upon closer examination, small coating fragments were found near the edge of the mould. The exact reason for leftover fragmentation is unclear; however, it is believed that the coating in zone 1 could have delaminated during deposition, leaving gaps between the coating and mould for resin in the CFRC to infiltrate, consequently gluing affected areas firmly onto the mould.

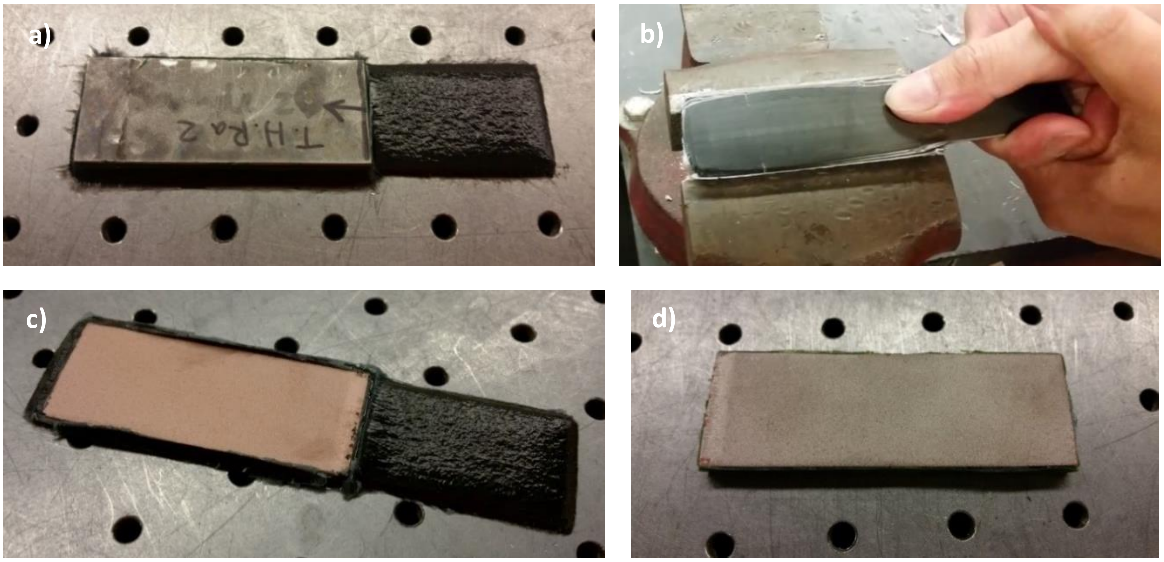

Figure 84 - RL 1.2: a) Assembly before demoulding, b) Assembly in a vice, ready for demoulding, c) Demoulded copper coated CFRC, d) Mould after demoulding

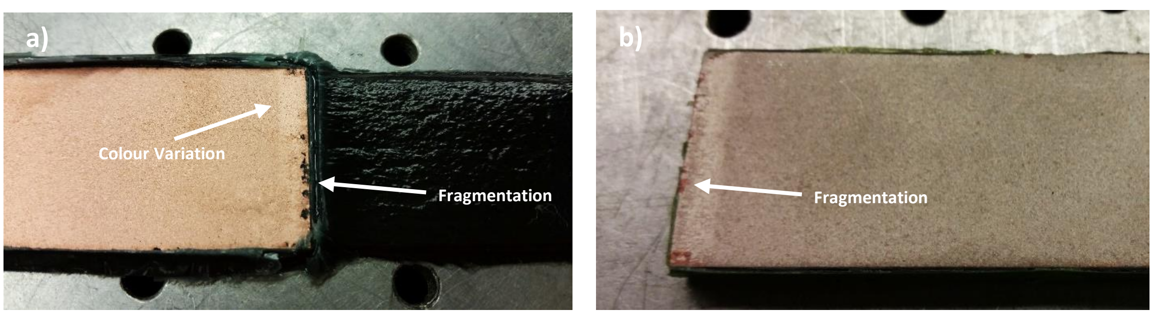

Figure 85 - RL 1.2: Magnified image of: a) copper coated CFRC showing copper colour variation between zones Ra 1 and Ra 2, and coating fragmentation at edge, b) Invar mould after demoulding, showing copper coating fragmentation at edge

To evaluate the coating quality after demoulding, zones Ra 1 and Ra 2 were assessed by examining coating to CFRC sample cross-sections. Overall, the coatings seemed to retain their shape after demoulding (Fig. 86 a) and b)). No distinguishable difference could be observed between sections of the contrasting zones (Fig. 86 a)). It was difficult to identify clearly the transition point between the two zones without referring to their superficial colour difference.

Microcracks were observed near the surface and within the coating (Fig. 86 c)). These cracks occurred throughout the coating, with no predictable zones of concentration. A PATTI test was wherefore performed on the coated CFRC samples to assess the consolidation of the coatings. All coatings fractured in cohesive failure at an average stress of 2.61 ± 0.5 MPa. The presence of microcracks would be studied later as part of Objective 2.

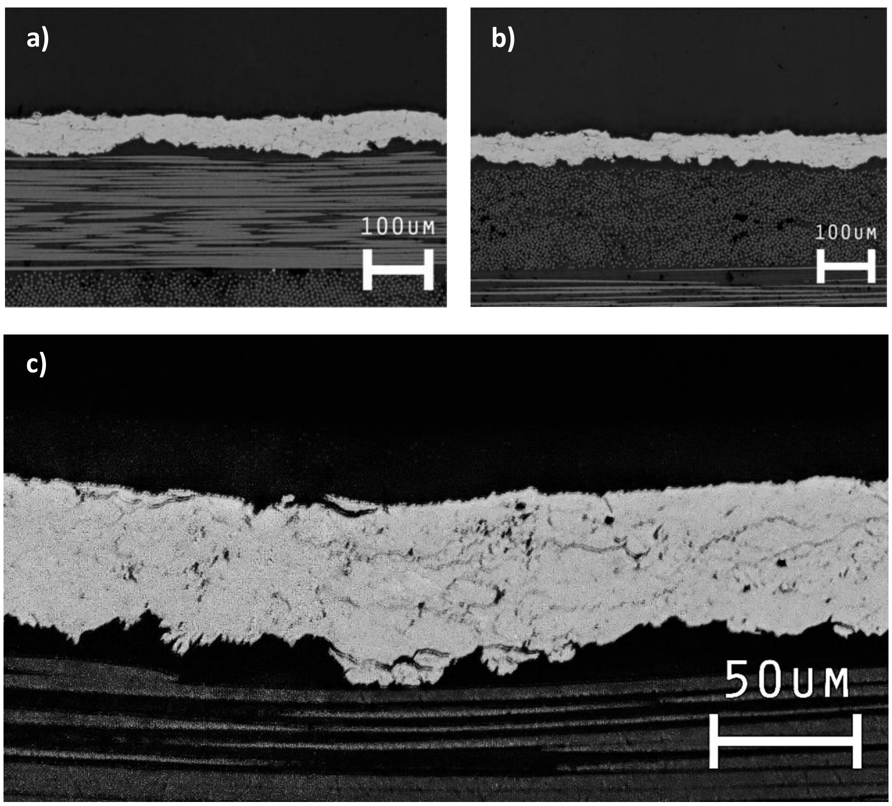

Figure 86 - RL 1.2: Cross-section image of: a) transition between zones Ra 1 and 2, b) zone Ra 2, c) zoomed zone Ra 2 showing microcracks in coating

Coating to mould PATTI results showed that all coatings failed in adhesion, with bonding strength in zone Ra 2 averaging 2.48 ± 0.44 MPa and near zero for zone Ra 1. When testing samples with roughness Ra 1, their adhesion was so low that all coatings debonded during setup.

By comparing all PATTI tests performed in this section, it could be noticed that zone Ra 2 coating to mould test (adhesion failure) returned similar values to that of coating to CFRC test (cohesion failure). This indicates that the demoulding process could have induced or amplified defects within the coating for the reason that if the coating retained its microstructure after demoulding, then the coating to CFRC failure strength would have been higher as the coating could sustain stresses higher than what was obtained from coating to mould adhesion strength test.

4.1.3 Single Roughness Zone

The success of the previous experiment pointed towards a clear direction for further development. It was envisaged that a similar result could be obtained without the complication of producing two zones of contrasting roughness. Hence, an improvement was proposed whereby a single surface roughness would yield an equivalent outcome.

The improvement proved to be successful and the demoulding process remained essentially effortless. Figure 87 shows one of the samples produced. The coating surface no longer contained colour variation due to roughness difference. When examined closely, no coating fragments were observed near the mould's edge; the coating's edge looked sharp and undamaged. The absence of fragmentation could mean that the coating did not delaminate during spray.

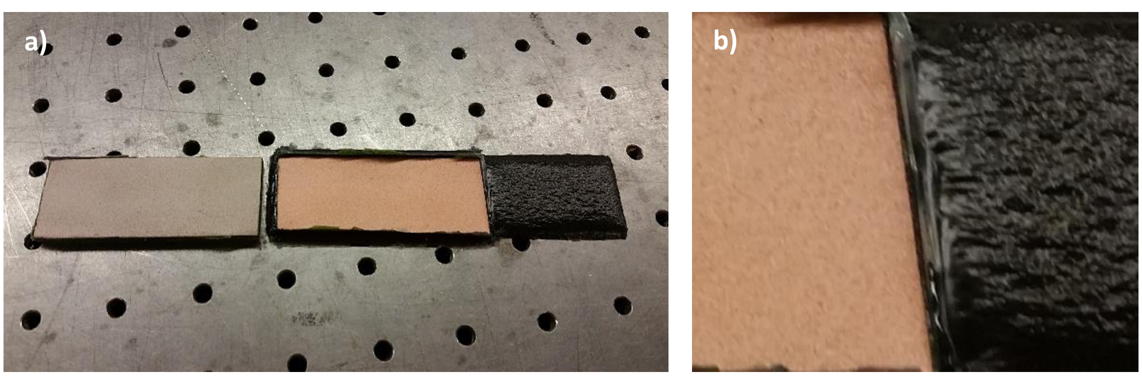

Figure 87 - RL 1.3: Image of: a) demoulded sample and mould, b) magnified copper coated CFRC showing undamaged edge of the coating.

In the hope of identifying the origin of microcracks observed in experiment RL 1.2, cross-section analyses were performed on as-sprayed coatings and on demoulded coatings (Figure 88 a) and b)). From these inspections, it was noticed that the microcracks were already present in the as-sprayed coating (Fig. 88 a)). The defects remained after demoulding (Fig. 88 b)). The fact that microcracks happened before addition of uncured CFRC laminate implied that the spray parameters selected could not generate a crack-free coating microstructure. Nevertheless, the coating retained its shape during demoulding. Since the single-roughness-zone approach was reliable, it was used in all experiments performed towards Objective 2.

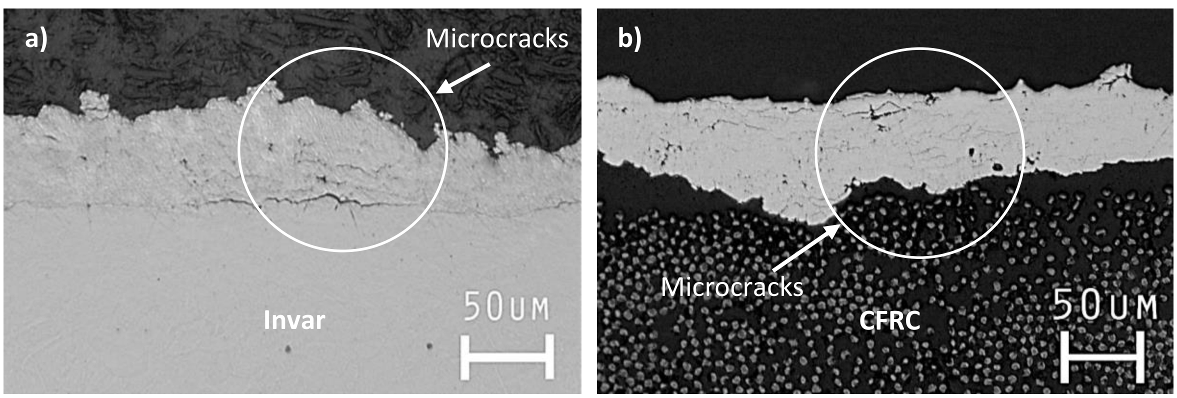

Figure 88 - RL 1.3: Cross-section image of: a) coating as-sprayed on mould; b) coating after demoulding

4.1.4 Low Spray Parameters

In this experiment, coatings were produced on Invar moulds using a set of spray parameters identified in previous work, obtained through a series of partial optimizations aiming at generating a fully dense and crack-free coating [14]. Inspection on cross-sections showed that the coating featured a dense microstructure with minor microcracking in some areas (Fig. 89). The presence of microcracks indicated that this trial could not reproduce the same results as those shown in previous work. The exact reason for this discrepancy is unclear. Visual inspection on the powder showed that the copper still possessed a light orange colour, indicating that no severe oxidation had taken place that led to an alternation in performance. In coating to mould PATTI test, all samples failed in adhesion at an average stress of 2.19 ± 0.37 MPa.

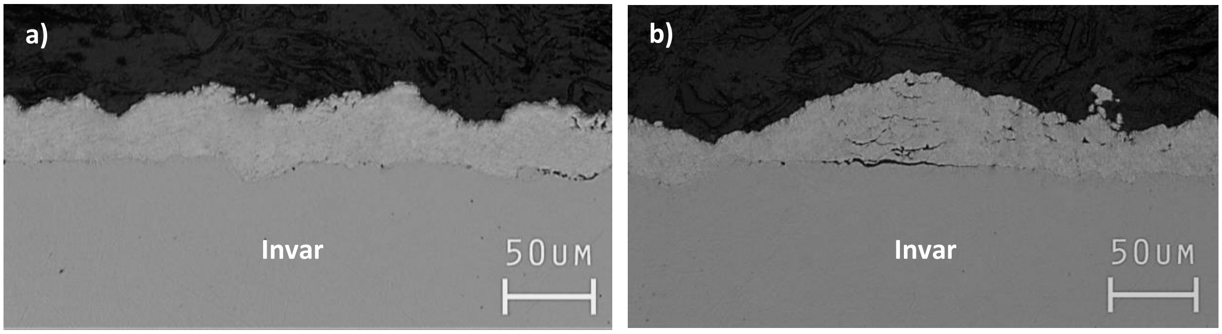

Figure 89 - RL 1.4: Cross-section image of: a) fully dense and crack-free as-spray coating on mould, b) as-sprayed coating containing microcracks

4.1.5 Combination of Spray Parameters

Aiming at eliminating the coating quality issue, an alternative approach was considered: to spray two coating layers, one with low and the other with high spray parameters. The idea consisted of first depositing a layer that adhered poorly on the mould, then adding a second layer possessing the desired microstructure.

Such combination would likely allow the first layer to detach easily from the mould while retaining the dense second layer on CFRC. If the second layer was to remain dense and crack-free on the CFRC after demoulding, the first layer would be removed by machining so as to keep only the desired microstructure.

Inspection of as-sprayed sample cross-sections showed that the coatings possessed a fully dense microstructure (Fig. 90 a)). No distinction could be made between the first and second layers, meaning that the first layer was likely densified by the deposition of the second layer. However, vertical cracks were observed in some regions of the coatings (Fig. 90 b)).

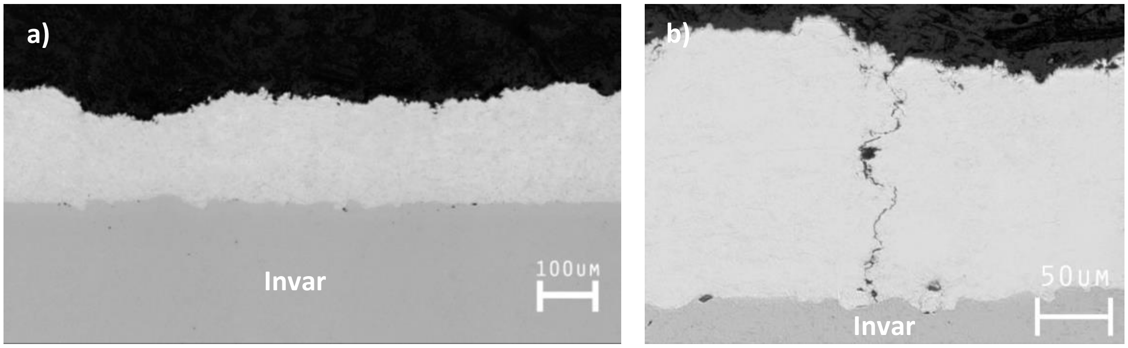

Figure 90 - RL 1.5: Cross-section image of: a) as-sprayed coating on mould, b) vertical crack in as-sprayed coating due to TEC mismatch

These vertical cracks are believed to originate from a thermal expansion coefficient (TEC) mismatch between the copper coating and the Invar mould, as that copper thermally expands much more than Invar. The copper coatings were hot during spray and were cooled after deposition. The cooling induced a volumetric contraction to both materials. The contraction of copper was restricted by that of the Invar due to their substantial difference in TEC (Copper: 16 x 10^{-6}m/m°C; Invar: 1.3 x 10^{-6} m/m°C [83, 84]). This generated significant tensile stresses in the copper coating and led to vertical cracking.

Such fractures happen in areas of the coating where the internal stresses exceed the cohesive strength between particles. Once a crack is initiated, it continues to propagate through particle boundaries. The cracking only occurred as a result of in-plane contraction as no limitation prevented the coating from shrinking along its thickness.

The heating that induced these defects was caused by the long exposure time to the gas stream that transferred heat to the coating and mould during spray. TEC mismatch can be alleviated by decreasing the time during which the gas stream touches the sample. Such phenomenon was not observed in RL 1.2 to 1.4 as gas temperatures were much lower.

4.1.6 High Spray Parameters

This experiment focused on determining whether a combination of layers produced using different parameters (Experiment RL 1.5 Combination of Spray Parameters) was beneficial. To this end, only one layer was sprayed on the mould, using high temperatures and high pressures to produce well consolidated coatings. The spray parameters were those used for the second layer in Experiment RL 1.5, with gun traverse speed and number of spray passes modified from 50mm/s and 1 pass to 100mm/s and 2 passes in order to avoid TEC mismatch.

Inspection of both as-sprayed and demoulded coating samples showed that the coatings were fully dense on the Invar mould, with no sign of microcracks, but they fractured during demoulding. Large cracks were observable throughout the demoulded samples (Fig. 91).

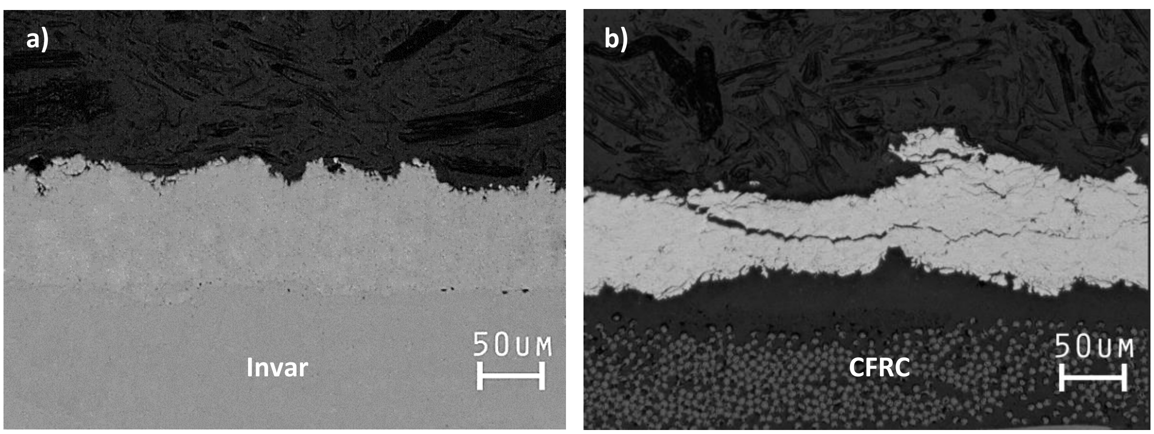

Figure 91 - RL 1.6: Cross-section image of: a) as-sprayed coating on mould, b) coating on CFRC after demoulding

In coating to mould adhesion tests, all samples failed in interfacial adhesion at an average stress of 6.12 ± 0.36 MPa. When comparing this value to the coating to mould adhesion strength obtained from experiment RL 1.4, it is clear that the cause of damage in this experiment originated from coating adhesion, meaning that a compromise exists between adhesion strength and coating quality after-demoulding.

4.1.7 Combination of Spray Parameters with Increased 2nd Layer Traverse Speed

This experiment continued the investigation of combined coating layers, introduced in Experiment RL 1.5 Combination of Spray Parameters. In this case, the second layer was sprayed with a doubled gun traverse speed: 100 mm/s and 2 passes This modification aimed at preventing the temperatures of the coatings and moulds from increasing dramatically, and letting the layers cool down. Inspection on coating to mould cross-sections showed that the coating was fully dense with no signs of vertical cracks (Fig. 92), meaning that the faster traverse speed did have a beneficial effect in avoiding extensive heating of the coating to mould assembly by the carrier gas stream exiting the spray nozzle. The increased speed allowed coatings deposited in of each pass to cool sufficiently down before the next layer was applied. Additionally, an absence of microcracks means that two faster spray passes for the second layer densified the first layer in a similar manner as one single pass did in experiment RL 1.5.

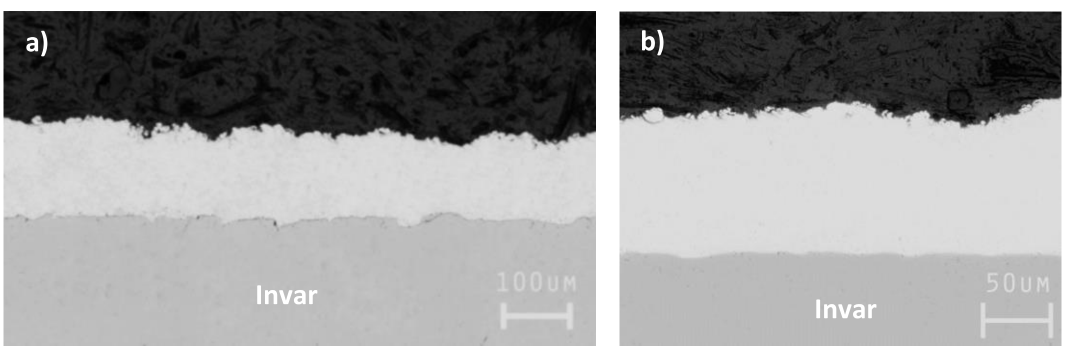

Figure 92 - RL 1.7: Cross-section image of coating to mould: a) fully dense and crack-free microstructure, b) magnified image of fully dense and crack-free microstructure

When examining magnified etched cross-sections (Fig. 93), the first observation made is that the first and second layers have nearly undistinguishable microstructures. This is due to the numerous ramifications of the dendrites that make the assessment of particle deformation challenging. The second observation made is that many particles folded on themselves, possibly during their impact or after being impinged by incoming particles. The dendritic morphology has been known to adhere more easily than spherical, thanks to its tree-like ramifications that allow the particles to be easily deformed upon impact, facilitating their anchoring on the surface of the substrate [70].

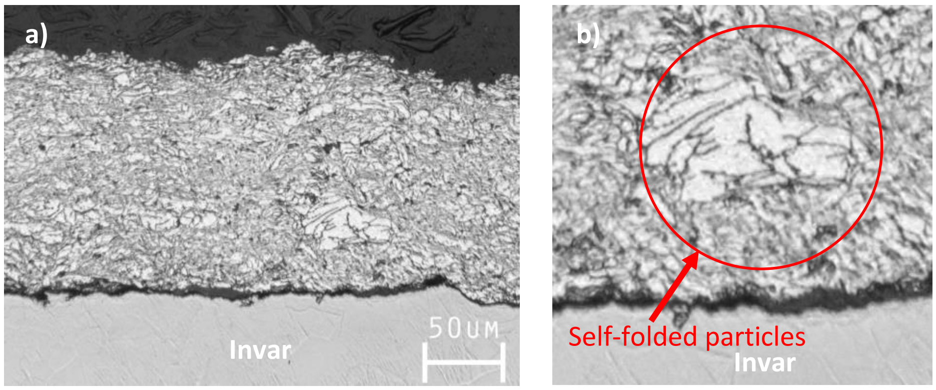

Figure 93 - RL 1.7: Cross-section image of etched coating-mould sample: a) coating microstructure, b) zoomed of a), showing self-folded particles

Inspection of coating to CFRC cross-sections showed that the coatings contained a mixture of cracked and crack-free microstructures (Fig. 94). The cracks originated from the first layer, then propagated towards the second. This behaviour could be observed as a decrease in propagation intensity through the thickness of the coating. In some areas the cracks made their way unfortunately through the second layer. These results indicated that the second layer possessed a higher cohesive strength than the first; if the opposite were true, then the crack initiation would have taken place within the second layer.

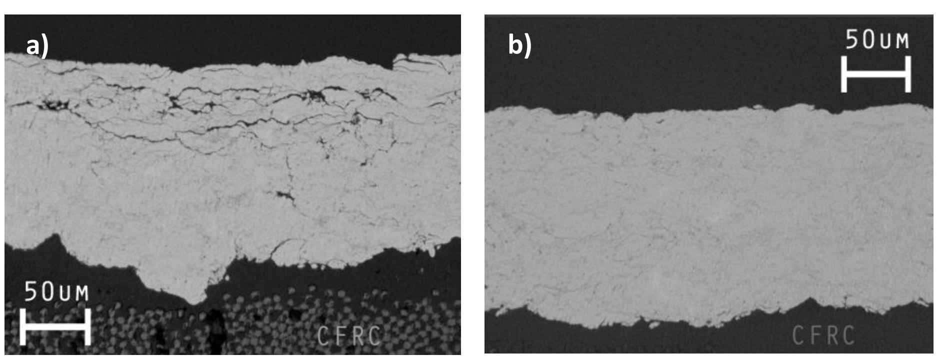

Figure 94 - RL 1.7: Cross-section image of coating-CFRC: a) crack propagation from first to second layer, b) fully dense microstructure

4.1.8 Combination of Spray Parameters with Double 1st Layer

As learnt from experiment RL 1.7, it was envisaged that increase in the thickness of the first layer would slow down the crack propagation significantly before reaching the second layer, due to more energy being required for fracturing thicker material. Inspection of coating to mould cross-sections showed that the coating was fully dense with no signs of microcracks, nor vertical cracks (Fig. 95 a)). However, coating to CFRC samples showed similar results to those in experiment RL 1.7. Crack propagation seemed slightly less severe, but still reached the second layer in some areas (Fig. 95 b)).

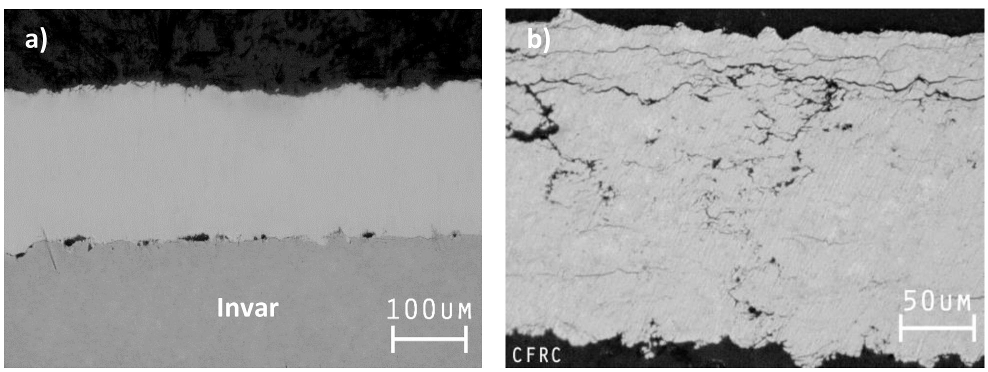

Figure 95 - RL 1.8: Cross-section image of: a) fully dense and crack-free as-sprayed coating on mould, b) coating on CFRC, showing crack propagation from first to second layer

4.1.9 Combination of Spray Parameters with Double 2nd Layer

Another potential alternative to mitigate crack propagation is to double the second layer. Since the second layer exhibits better cohesive strength thanks to higher spray parameters, it would likely prevent cracks from propagating all the way through its thickness.

Inspection on coating on mould cross-sections showed that the coatings possessed a fully dense microstructure like that from the experiment RL 1.7 (Fig. 96). Coating to CFRC samples showed a reduction in crack propagation through the second layer (Fig. 97 a)), meaning that a thicker and better consolidated layer slowed down the propagation. Despite a reduction in fractures, minor microcracks were still observable in some areas within the second layer (Fig. 97 b)). It was overall difficult to control and predict the propagation in coatings made of dendritic copper powder.

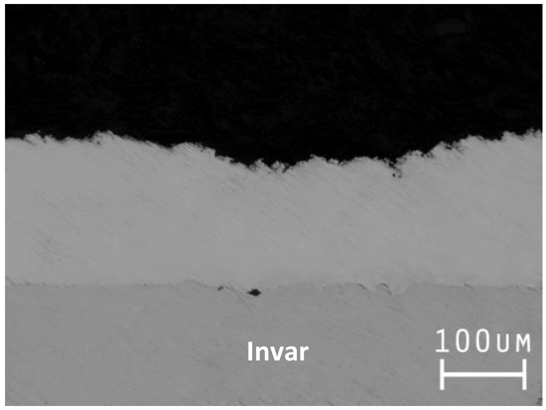

Figure 96 - RL 1.9: Cross-section image of coating as-sprayed on mould

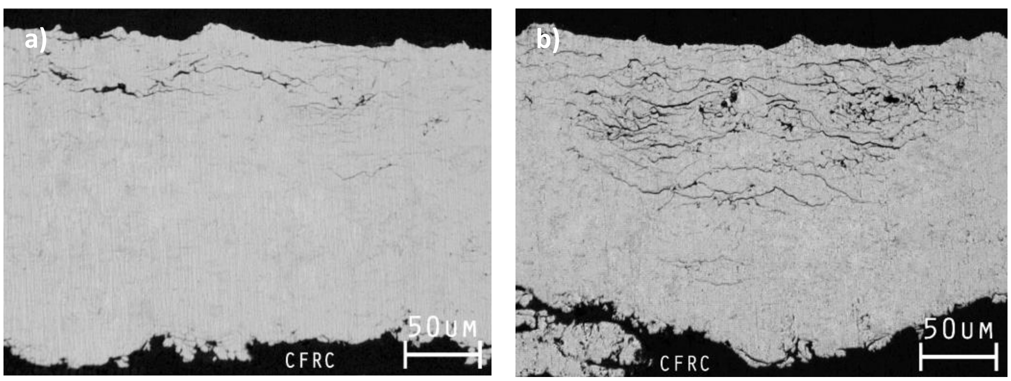

Figure 97 - RL 1.9: Cross-section image of coating to CFRC: a) crack propagation stopped near second layer, b) crack propagation from first to second layer

4.1.10 Attempt with Praxair Cu-159 Powder

Powders of spherical morphology are known to demand more deformation for adhering on substrates, compared with dendritic powders due to their geometry. In contrast to a tree-like dendrite, a sphere does not contain any sharp angle nor ramification that facilitates anchoring between valleys on the surface of a substrate or a coating. This property means that only the well-deformed particles may adhere and build-up on a substrate, resulting in dense and cohesively strong coatings.

Inspection of cross-sections revealed that the coating was fully dense on the mould (Fig. 98 a)) and remained unchanged after demoulding (Fig. 98 b)), with no signs of crack propagation. This indicated that the cohesive strength of the spherical powder coating exceeded that of the dendritic powder coating. Some cross-sections were etched after inspection for further investigation of the coatings' microstructure (Fig. 99). It can be noticed that the shperical particles were well deformed into pancake-like shapes.

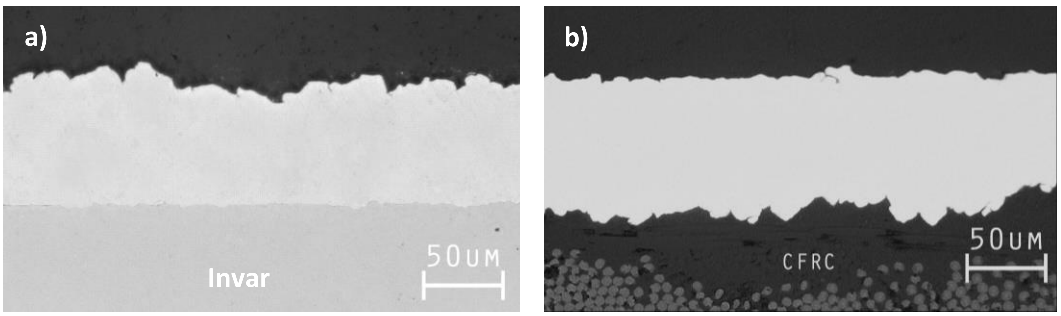

Figure 98 - RL 1.10: Cross-section image of: a) coating to mould, b) coating-CFRC

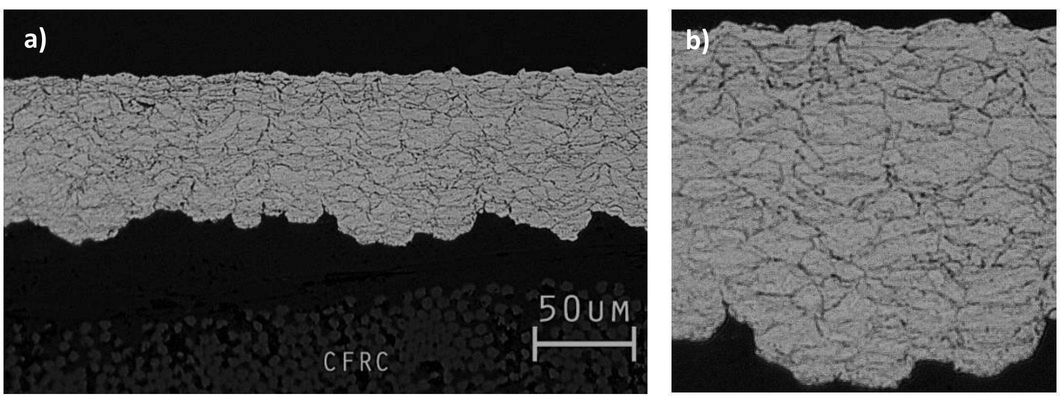

Figure 99 - RL 1.10: Cross-section image of etched coating-CFRC sample: a) general microstructure, b) magnification of a), showing well-deformed particles

In coating to mould adhesion tests, all coatings failed in adhesion at an average stress of 2.38 ± 0.43 MPa. In coating to CFRC adhesion tests, all coatings failed in adhesion at an average stress of 7.70 ± 0.38 MPa; this means that the cohesive strength of the copper coating was at least equal to that value, if not higher. Figure 100 shows an example of the coating to CFRC PATTI test after adhesion failure.

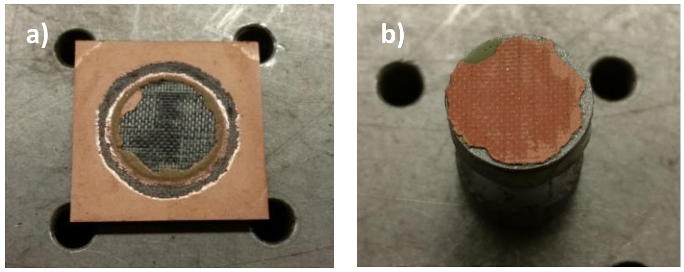

Figure 100 - Post-PATTI test: a) copper-CFRC, b) dolly with debonded copper coating from a)

The exact value obtained from this test is somewhat trivial because epoxy from CFRC plays an important role in retaining the coating; in other words, the epoxy acts as a glue that dictates the ultimate adhesion strength if the coating does not break in cohesive failure. Nevertheless, the test pointed to an improvement over the initial setup (2.61 ± 0.5 MPa, Experiment: RL 1.2 Dual Roughness Zone), and with the coatings showing potential for higher adhesion strengths. In comparison to aerospace-grade adhesives, the obtained adhesion resides in the same range [85].

4.2 Results for the GRIP Metal™ as Bond Coat Method

As mentioned in the literature review, GRIP Metal™ had never been investigated for aerospace applications as this new technology derives from backing plates used with brake pads. Therefore, no pre-defined requirements constrained this research, providing the freedom of deciding and designing both the manufacturing process and testing setup for GRIP Metal™-CFRC. The work was divided into two sections: phase 1 and phase 2. Phase 1 was an exploratory experimental series aiming at creating, applying and assessing the integration of GRIP Metal™ into CFRCs. From those results, phase 2 aimed at investigating the effect of using different hook configurations as offered by Nucap. The quality of GRIP Metal™ to CFRC laminates was evaluated in terms of two factors: adhesion strength of GRIP Metal™ to CFRC, and overall consolidation of metal to CFRC laminate. Beside these investigations, the study also included the characterization of GRIP Metal™ sheets as-received in terms of hook height, curvature and density.

4.2.1 Phase 1: GRIP Metal™ Characterization

An example of each GRIP Metal™ 3D topography is illustrated in Figure 101. Hook height of each GRIP Metal™ configuration was calculated in terms of median and median absolute deviation (MAD). Results appear in Table 25. According to the results obtained, the medians were similar for Nano hook sizes in both aluminium and steel (580 µm vs 639 µm), whereas a difference of around 50% was observed between the two materials in standard hook size (1051 µm vs 1590 µm). Aluminium hooks in Nano size had the highest MAD/Median value at 14.8%, suggesting that they had the least consistent hook heights.

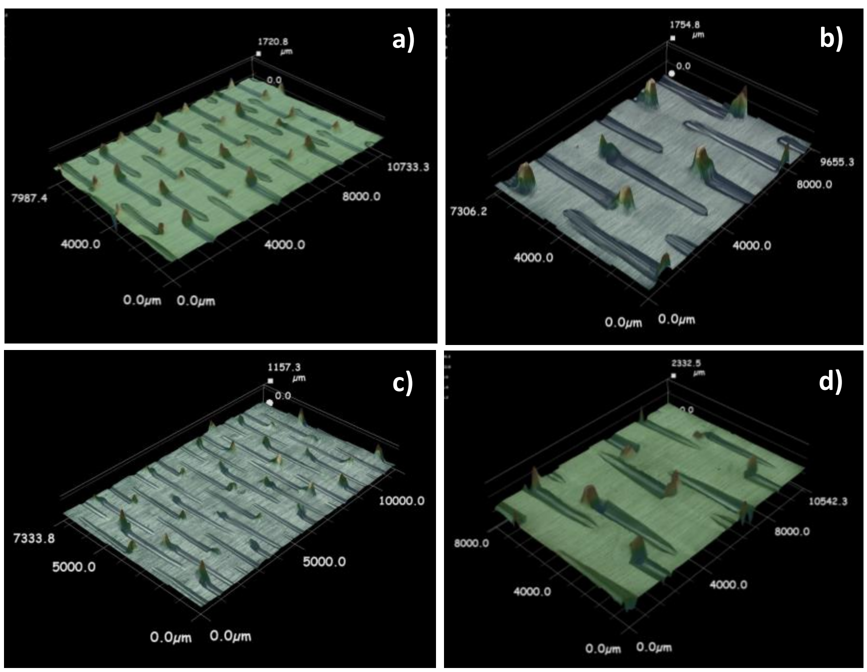

Figure 101 - Phase 1: Example of 3D topography of GRIP Metal™: a) Al 5052-H38, Nano hook size, b) Al 5052-H38 Standard hook size, c) AISI 1010 steel, Nano hook size, d) AISI 1010 steel, Standard hook size

Table 25 - Phase 1: GRIP Metal™ hook height

Material	Hook Size	Hook Curvature	Median (µm)	MAD (µm)	MAD/ Median
Al 5052-H38	Nano	Standard	580	80	14.8%
	Standard	Standard	1051	82	7.8%
AISI 1010 Steel	Nano	Standard	639	37	5.8%
	Standard	Standard	1590	62	3.9%

An example of hook curvature is illustrated for each GRIP Metal™ configuration in Figure 102. Curvatures were also calculated in terms of median and MAD (Table 26). The results show that the curvatures were similar within the same hook size category. As for the MADs, Nano size hooks had curvatures ranging from 380 to 660 μm whereas standard size hooks had curvatures ranging from 1700 to 3258 μm. The MAD/Median percentages were the largest for Nano size hooks in both aluminium and steel, at around 22%.

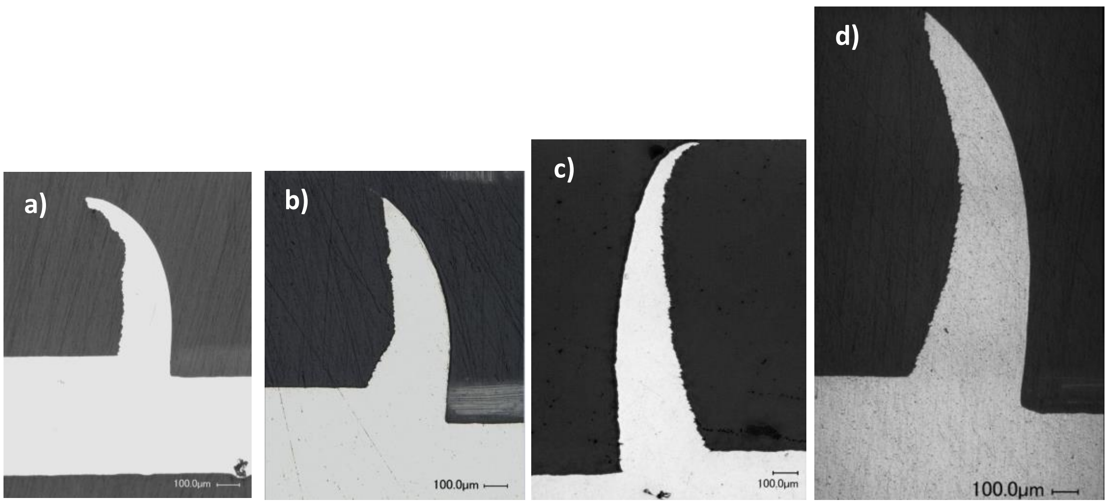

Figure 102 - Phase 1: Example of GRIP Metal™ hook curvature of: a) Al 5052-H38, Nano hook size, b) AISI 1010 steel, Nano hook size, c) Al 5052-H38, Standard hook size, d) AISI 1010 steel, Standard hook size

Table 26 - Phase 1: GRIP Metal™ hook curvature

Material	Hook Size	Hook Curvature	Median (μm)	MAD (μm)	MAD/Median
Al 5052-H38	Nano	Standard	484	105	21.7%
	Standard	Standard	2663	595	22.3%
AISI 1010 Steel	Nano	Standard	593	70	11.8%
	Standard	Standard	2100	367	17.5%

An example of hook density for each GRIP Metal™ configuration is illustrated in Figure 103. The densities were calculated in terms of mean and standard deviation (Table 27), due to the small size of the data population. The results show that all configurations differed, with Nano size hooks being denser than standard size hooks. From Figure 103, it could also be observed that all configurations had different hook length, noticeable by comparing their chiselling trails. Furthermore, standard steel hooks were significantly wider compared with any other configuration examined in phase 1.

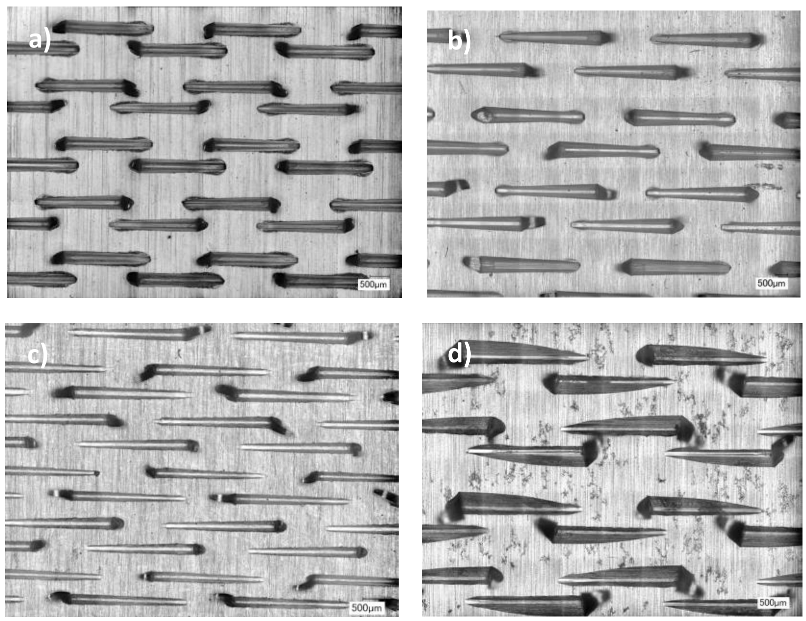

Figure 103 - Phase 1: Examples of 2D top view of GRIP Metal™: a) Al 5052-H38, Nano hook size, b) Al 5052-H38, Standard hook size, c) AISI 1010 steel, Nano hook size, d) AISI 1010 steel, Standard hook size

Table 27 - Phase 1: GRIP Metal™ hook densities

Material	Hook Size	Hook Curvature	Mean (Hooks/m^2)	SD (Hooks/m^2)	SD / Mean
Al 5052-H38	Nano	Standard	401589	9689	2.4%
	Standard	Standard	111719	2028	1.8%
AISI 1010 Steel	Nano	Standard	479276	10451	2.2%
	Standard	Standard	72505	876	1.2%

4.2.2 Phase 1: GRIP Metal™-CFRC Consolidation without Pre-compression

Visual inspection of the cured products revealed that visible gaps were present between the GRIP Metal™ and CFRCs (Fig. 104). Also, fibres in the top layers of the laminates seemed to be distorted in a wavy pattern caused by the intrusion of hooks.

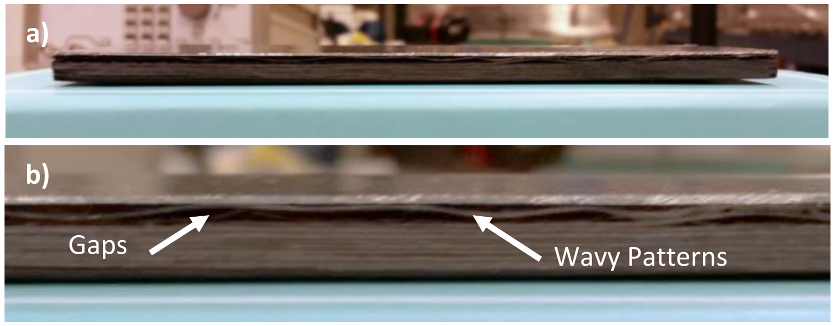

Figure 104 - Phase 1: Examples of: a) cured GRIP Metal™-CFRC assembly made without pre-compression, b) magnified image of a), showing gaps and wavy patterns

When correlating cross-section analyses (Fig. 105) with visual inspections, observations of the latter could be confirmed: all GRIP Metal™-CFRC interfaces featured large gaps caused by the failure of the hooks to penetrate fully through the laminate, that consequently left empty spaces. It was also observed that the fibres were pressed by the hooks, resulting in deviation in fibre directions in the top layers, which correspond to the wavy patterns seen in visual examinations.

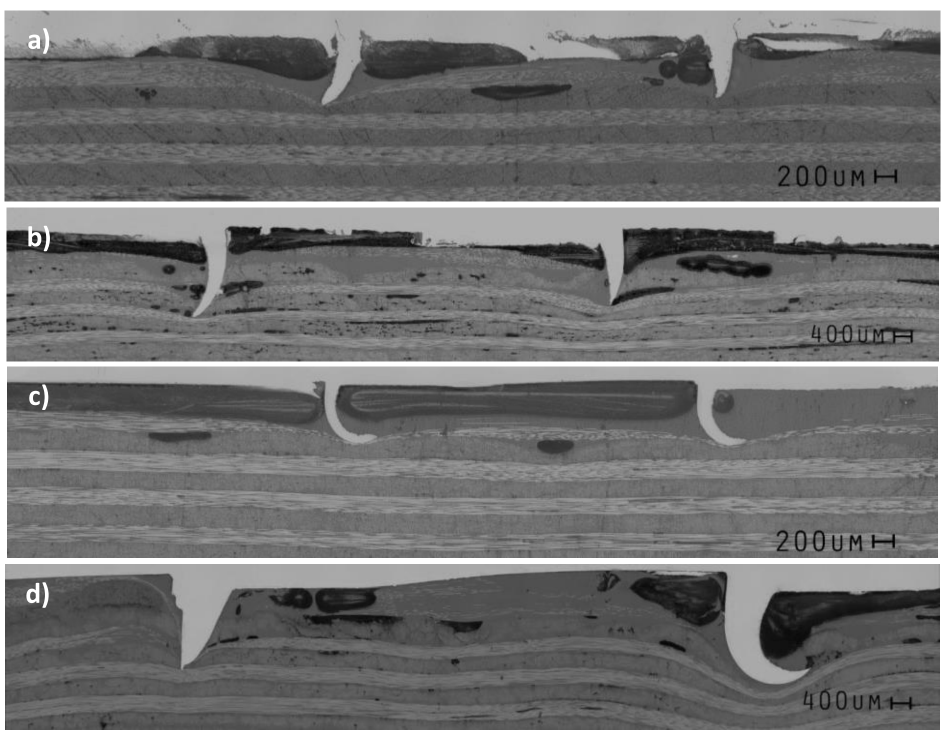

Figure 105 - Phase 1: Cross-section images of GRIP Metal™-CFRC without pre-compression: a) Al5052-H38, Nano hook size, b) Al5052-H38, Standard hook size, c) AISI 1010 Steel, Nano hook size, d) AISI 1010 Steel, Standard hook size

4.2.3 Phase 1: GRIP Metal™-CFRC Consolidation with Pre-compression

Following experiments conducted without pre-compression, it was thought that compaction pressure applied prior to consolidation would help the hooks to better penetrate through the CFRC. A manually operated hydraulic press was used, with compression pressure steadily increased up to 10 atmospheres, then held for 5 minutes before release. Afterwards, the assembly was put inside a vacuum bag and cured. Figure 106 shows an example of the cured GRIP Metal™-CFRC assembly. No noticeable gaps between GRIP Metal™ and CFRC were observed. It should be noted that the darker zone at the metal to CFRC interface was cured bled-out resin. The absence of any visible gap means that the additional pressure had a positive effect on pushing the hooks into the composite laminate.

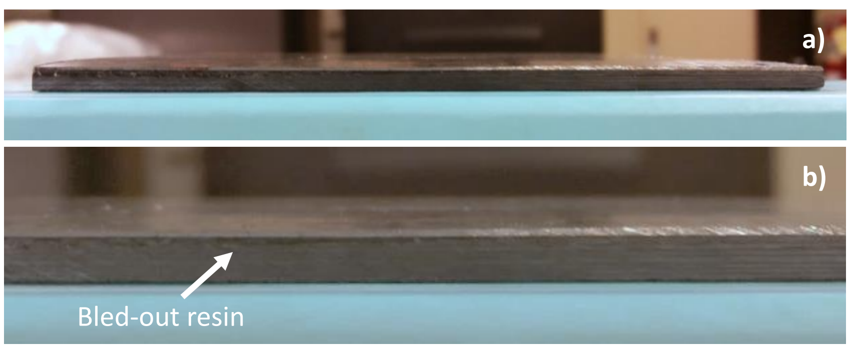

Figure 106 - Phase 1: Example of a) cured GRIP Metal™-CFRC assembly made with pre-compression, b) zoomed image of a), showing bled-out resin

Inspection of cross-sections (Fig. 107) confirmed that the pre-compression had a positive effect on hook penetration. A reduction in porosity near the interface was observed. The occurrence, size and geometry of these porosities were unpredictable. They were observed between fibre layers, at the hooks, within resin-rich zones, near and at the metal to CFRC interface.

Similarly to samples made without pre-compression, the hooks distorted fibres in the top layers, causing large voids for resin to fill, that ultimately led to the formation of resin-rich zones.

Most hooks successfully passed through the layers, with the exception of some in random areas of aluminium Standard hook size laminates (Fig. 108).

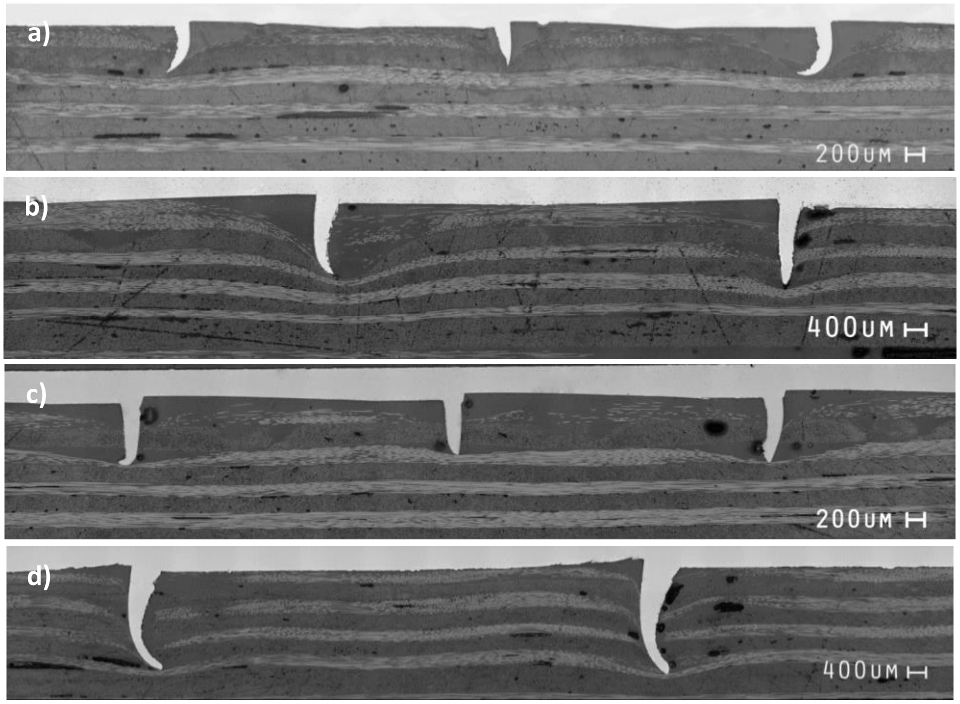

Figure 107 - Phase 1: Cross-section images of GRIP Metal™-CFRC with pre-compression: a) Al 5052-H38, Nano hook size, b) Al 5052-H38, Standard hook size, c) AISI 1010 Steel, Nano hook size, d) AISI 1010 steel, Standard hook size

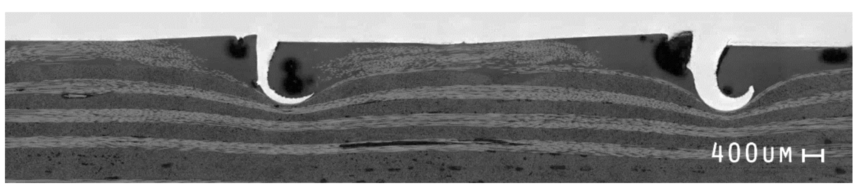

Figure 108 - Phase 1: Cross-section images of GRIP Metal™-CFRC with pre-compression: Al 5052-H38, Standard hook size, showing hooks that failed to penetrate through CFRC layers

4.2.4 Phase 1: GRIP Metal™-CFRC PATTI Test

All samples made without pre-compression failed at their metal to CFRC interface with no damage to hooks (Fig. 109). PATTI test results (Fig. 110) showed that the adhesion strength of GRIP Metal™ did not outperform that of a flat sheet of the same material. This led to the conclusion that the large gaps present at the metal to CFRC interface caused their poor performance. Whilst the Nano size aluminium hooks outperformed their standard size hook counterparts, values for both configurations were close to each other when considering their standard deviations. On the other hand, comparison between flat sheets only showed aluminium performed slightly better; no explanation can be provided as epoxy bonds differently to various metals [86].

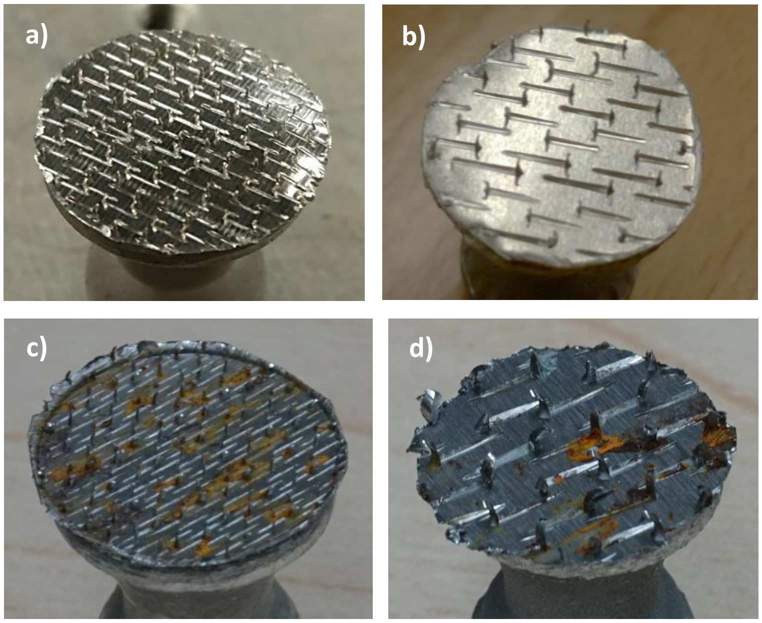

Figure 109 - Phase 1: GRIP Metal™ after PATTI test of samples made without pre-compression: a, b) Al 5052-H38, Nano hook size and Standard hook size respectively; c, d) AISI 1010 steel, Nano hook size and Standard hook size respectively

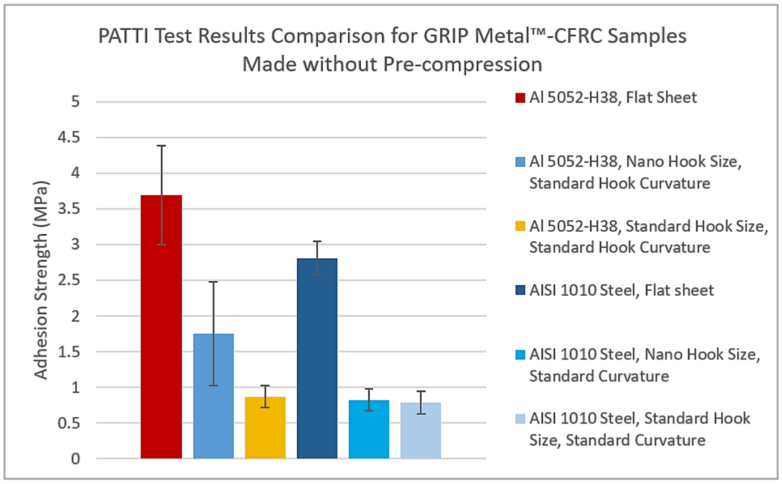

Figure 110 - Phase 1: PATTI test results for samples made without pre-compression

All samples made with pre-compression also failed at metal to CFRC interface, with no damage to the hooks (Fig. 111). PATTI test results (Fig. 112) showed that the adhesion strengths of GRIP Metal™ significantly increased for both steel and aluminium, from those obtained with samples made without pre-compression. AISI 1010 Steel GRIP Metal™ sheets outperformed their flat counterpart whereas aluminium 5052-H38 sheets did not. The best adhesion strength result was with steel GRIP Metal™ Nano hooks, with an average adhesion strength of 6.54 ± 0.82 MPa.

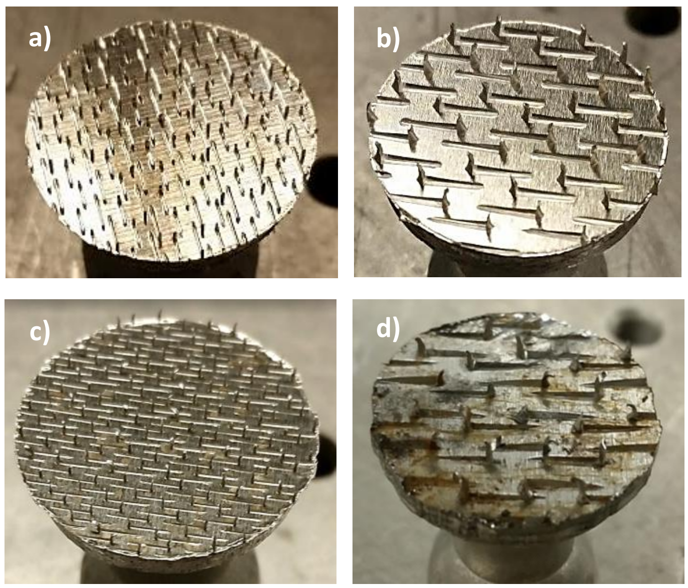

Figure 111 - Phase 1: GRIP Metal™ after PATTI test of samples made with pre-compression: a, b) Al 5052-H38, Nano hook size and Standard hook size respectively; c, d) AISI 1010 steel, Nano hook size and Standard hook size respectively

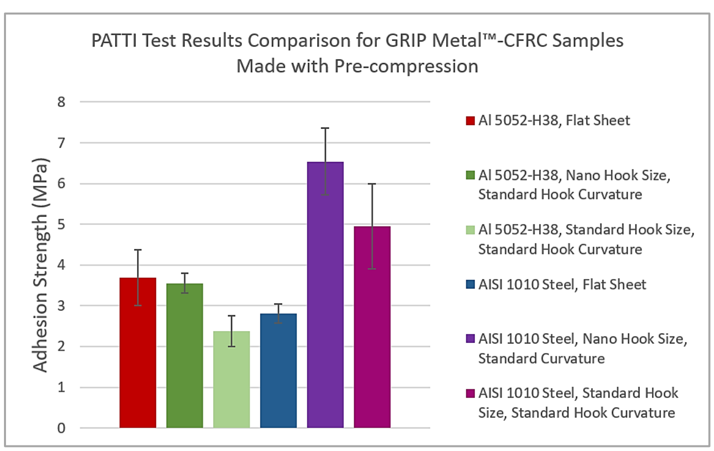

Figure 112 - Phase 1: PATTI test results for samples made with pre-compression

Rusted spots were found on all AISI 1010 steel GRIP Metal™ interfaces after adhesion test. It was believed that the air gaps between metal and CFRC oxidized the steel during curing process at high temperature. As such results present undesired characteristics, AISI 1010 steel was terminated from further investigation in Phase 2.

4.2.5 Phase 1: Observations from the Manufacturing, Inspection and Testing

Observations were made to assess the complete experimental procedure. Firstly, it was concluded that the procedure of the PATTI test whereby manually securing the dollies by cutting surrounding material may have induced significant shear stresses at the metal to CFRC interface. Since the hooks were anchored inside the laminate and prevented the GRIP Metal™ from moving, excessive stresses may have delaminated the metal from laminate with no clear sign of detachment.

Secondly, it was observed that manually operating the hydraulic press presented challenges in terms of pressure accuracy. Whilst the analogue pressure gauge had markers, its graduation unit was large, making accurate readings difficult.

Finally, when comparing hook heights measured with 3D topography versus cross-section imaging, it was realised that the hooks appeared around 200 μm shorter in 3D images. These differences occurred because the computer algorithm used for composing the 3D image might not perform well for complex geometries such as hooks.

4.2.6 Phase 2: GRIP Metal™ Characterization

Hook heights were calculated in terms of Median and MAD. Table 28 lists the results. The data show that hooks possessed similar heights within the same size category, with the exception of Nano size hooks with straight curvature. The MADs ranged from 5 to 11%.

Table 28 - Phase 2: GRIP Metal™ hook height

Hook Size	Hook Curvature	Median (µm)	MAD (µm)	MAD / Median
Nano	Straight	462	24	5%
	Standard	794	47	6%
	Over-bent	800	52	7%
Standard	Straight	1598	105	7%
	Standard	1291	137	11%
	Over-bent	1475	73	5%

In term of hook curvature, cross-section analyses (Fig. 113 for Nano size hooks and Fig. 114 for standard size hooks) showed that all configuration featured many hooks with curvatures ranging from lightly-bent to extensively-bent. Hooks of the same size category looked similar without distinctive features.

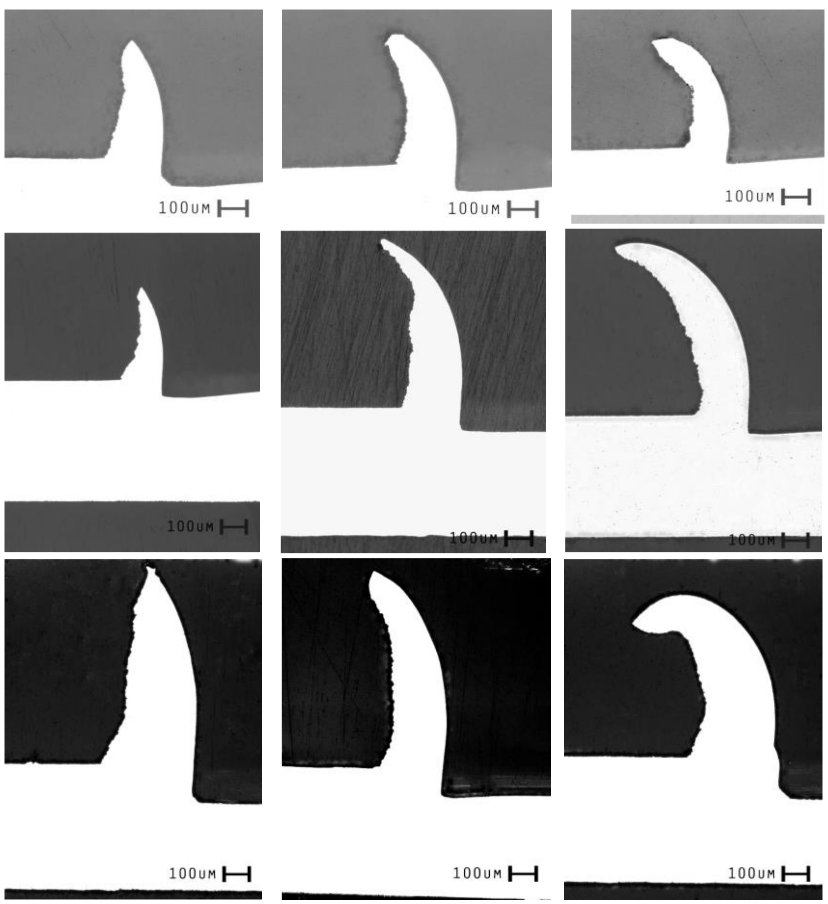

Figure 113 - Phase 2: Hook curvatures of Nano hook size: left) slightly-bent, middle) moderately-bent, right) extensively-bent; row 1: Straight hook curvature, Row 2: Standard hook curvature, Row 3: Over-bent hook curvature

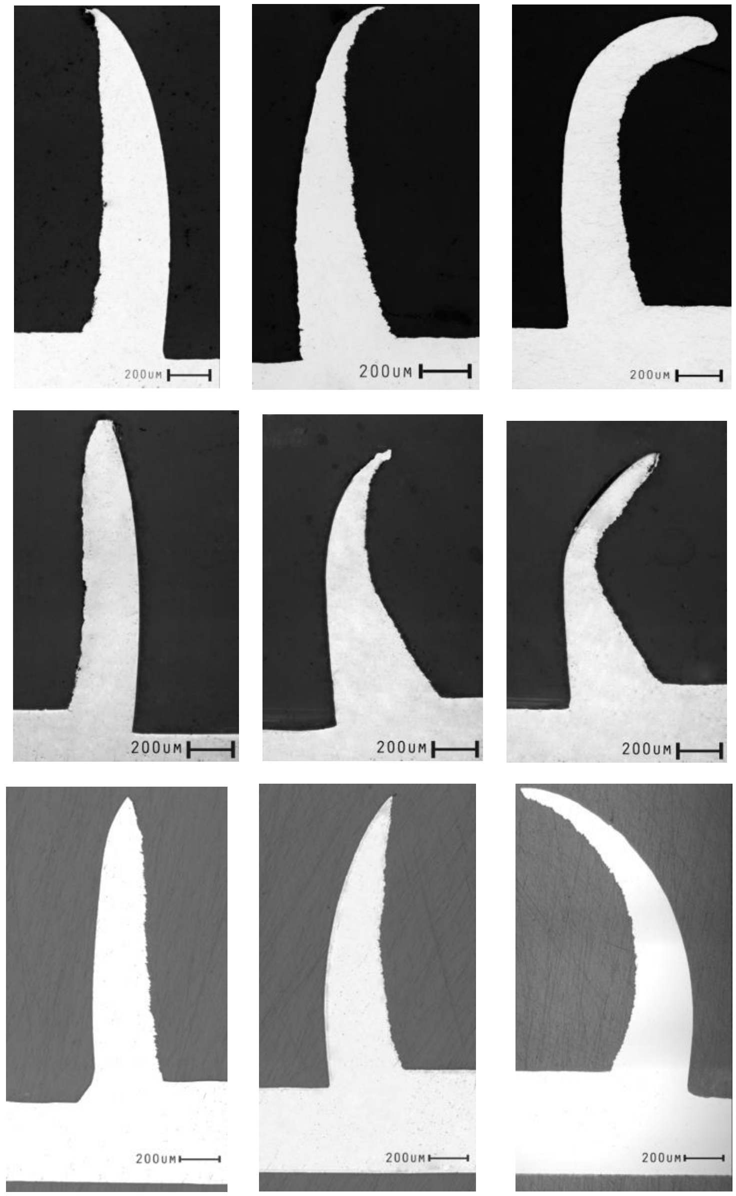

Figure 114 - Phase 2: Hook curvatures of Standard hook size: left) slightly-bent, middle) moderately-bent, right) extensively-bent; row 1: Straight hook curvature, row 2: Standard hook curvature, row 3: Over-bent hook curvature

Computed median and MADs (Tables 29 and 30) confirmed that hooks were of similar curvatures within the same size category. MADs ranged from 11 to 19% with the exception of standard size - standard curvature. Within standard hook size, over-bent hooks showed the smallest curvature amongst the three configurations; however, all values overlapped when considering their

MAD. The configuration: standard size - standard curvature had the highest MAD value, indicating significant inconsistences in curvature.

Table 29 - Phase 2: GRIP Metal™ hook curvatures, Nano hook size

Hook Size	Hook Curvature	Median (µm)	MAD (µm)	MAD / Median
Nano	Straight	531	59	11%
	Standard	566	104	18%
	Over-bent	578	106	18%

Table 30 - Phase 2: GRIP Metal™ hook curvature, Standard hook size

Hook Size	Hook Curvature	Median (µm)	MAD (µm)	MAD / Median
Standard	Straight	2123	362	17%
	Standard	2296	837	36%
	Over-bent	1707	328	19%

In term of hook density, the data showed that GRIP Metal™ contained on average 386000 hooks/m^2 in Nano size and 103000 hooks/m^2 in standard size (Table 31). Considering the potential measurement error, it may be stated that the densities were identical within the same hook size. Figure 115 shows an example of hook density for each GRIP Metal™ configuration.

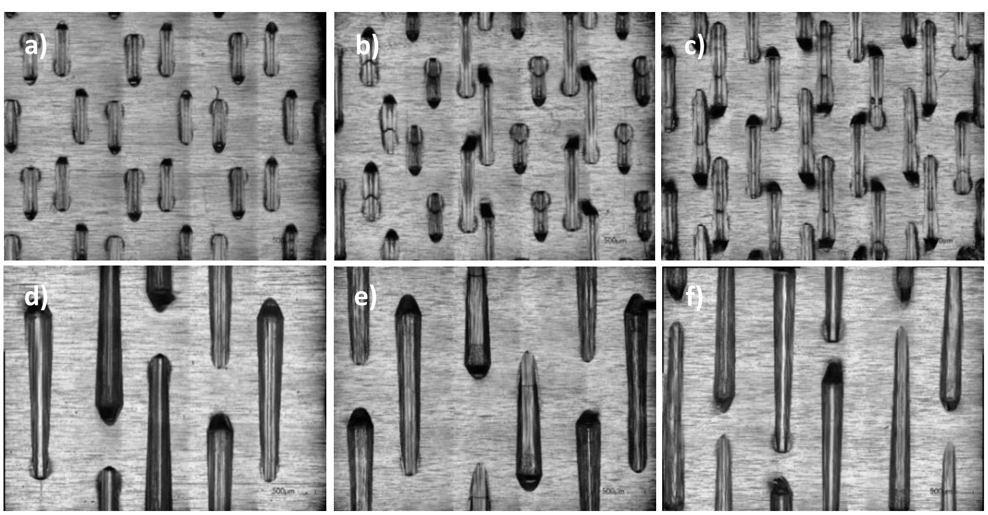

Figure 115 - Phase 2: Hook density: top row: Nano hook size with a) Straight hook curvature, b) Standard hook curvature, c) Over-bent hook curvature; bottom row: Standard hook size with d) Straight hook curvature, e) Standard hook curvature, f) Over-bent hook curvature

Table 31 - Phase 2: GRIP Metal™ hook densities

Hook Size	Hook Curvature	Mean (Hooks/m^2)	SD (Hooks/m^2)	SD / Mean
Nano	Straight	384591	7059	1.8%
	Standard	386026	7555	1.9%
	Over-bent	387720	7885	2.0%
Standard	Straight	103524	3987	3.8%
	Standard	101759	3118	3.1%
	Over-bent	104097	2790	2.7%

4.2.7 Phase 2: GRIP Metal™-CFRC Consolidation

The results for Nano hook size GRIP Metal-CFRC appear in Figure 116. In all these configurations, porosities were present near and at the metal to CFRC interface. Some hooks successfully penetrated through laminates whereas others remained at the top layer. It can be stated that those that did not pass through remained within the top layers and bent the fibres; however, it was difficult to determine if the hook tips were also bent and to what extent. The extensively bent fibres led to the formation of resin-rich zones. Samples with straight hooks had the least amount of visible voids amongst the three configurations due to their short hooks which required less penetration through the CFRC laminates.

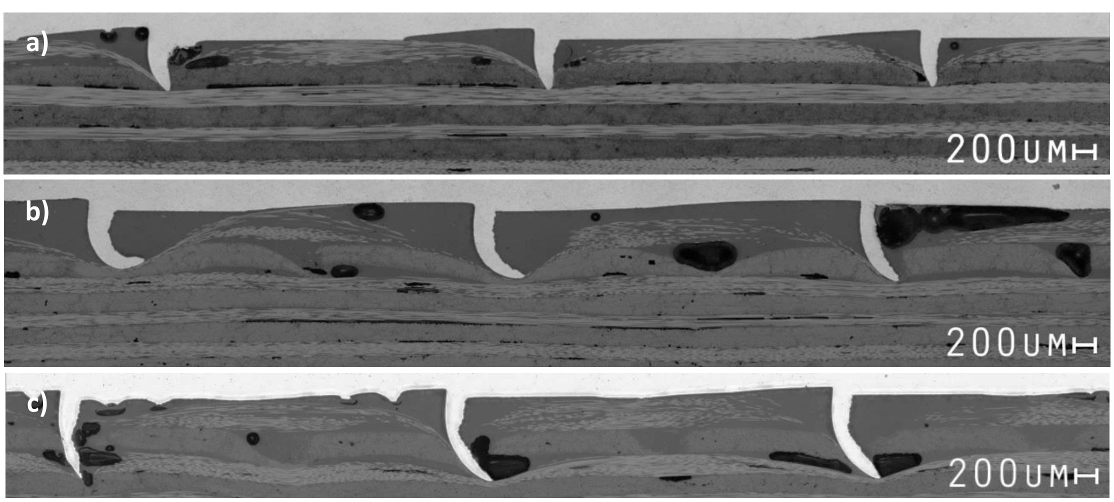

Figure 116 - Phase 2: Cross-section images of Al 5052-H38 GRIP Metal™-CFRC with Nano hook size, made with pre-compression by Instron: a) Straight hook curvature, b) Standard hook curvature, c) Over-bent hook curvature

Results for standard hook size GRIP Metal to CFRCs are shown in Figure 117. In all these configurations, porosities were also present near and at the metal to CFRC interface. Most hooks penetrated through the laminate where those that did not penetrate remained at the first layer and were severely bent. Figure 118 shows examples of these intensively distorted hooks and fibres.

Overall, the occurrence and intensity of both fibre distortions and internal porosities were unpredictable for all configurations tested. Porosities were observed between fibre layers, at the hooks, within resin-rich zones, near and at the metal to CFRC interfaces.

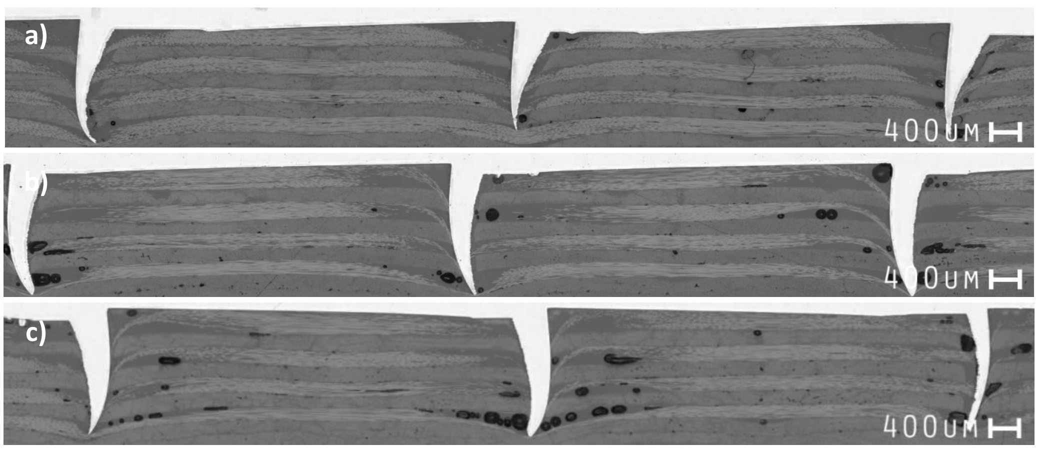

Figure 117 - Phase 2: Cross-section image of Al 5052-H38 GRIP Metal™-CFRC with Standard hook size made with pre-compression by Instron: a) Straight hook curvature, b) Standard hook curvature, c) Over-bent hook curvature

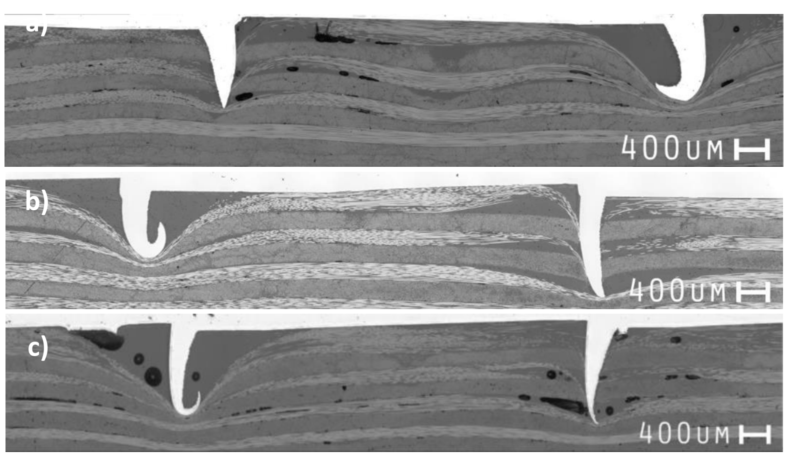

Figure 118 - Phase 2: Cross-section image showing examples of Standard size hooks that failed to penetrate through CFRC laminate: a) Straight, b) Standard and c) Over-bent hook curvatures

4.2.8 Phase 2: GRIP Metal™-CFRC ASTM C297 Test

Results from ASTM C297 tests showed that all GRIP Metal™ configurations failed at their metal to CFRC interfaces, with some fibres remaining attached to the metal (Fig. 120). No damage was observed in the hooks after failure. The amount of fibres attached did not correlate with the samples hook size, nor with their adhesion strengths, indicating that intensity of this behaviour was unpredictable. Figure 119 shows an example of sample failure.

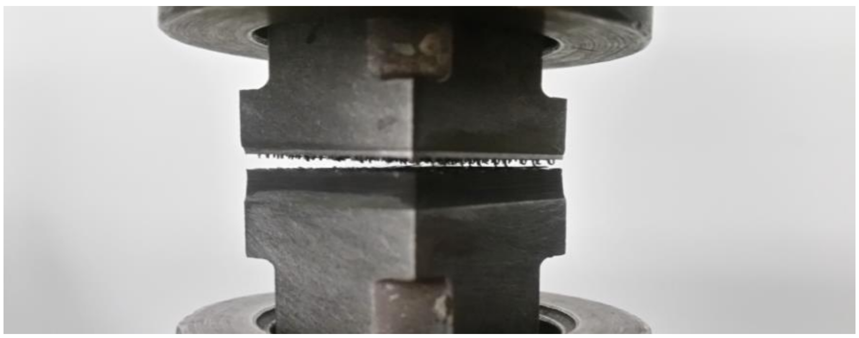

Figure 119 - Phase 2: Example of GRIP Metal™-CFRC after failure

Figure 120 - Phase 2: Examples of GRIP Metal™ interface after failure: a) Nano hook size, b) CFRC originally bonded to a), c) Standard hook size, d) CFRC originally bonded to c)

Values of adhesion strength were collected then computed into mean and standard deviations shown in Figure 121. The test results showed that all GRIP Metal™ configurations outperformed the flat aluminium sheets, with the exception of configuration Nano size - Straight curvature. This underperformance was potentially due to the shorter hook profiles of this configuration, in comparison to others in the same hook size category (462 μm vs 794 μm and 800 μm). It was noticed that all standard deviations were large and overlapping. The data were investigated towards finding possible failure patterns that would point out to a possibility of experimental errors; unfortunately, no conclusion could be made in this regard as the data were found to vary randomly.

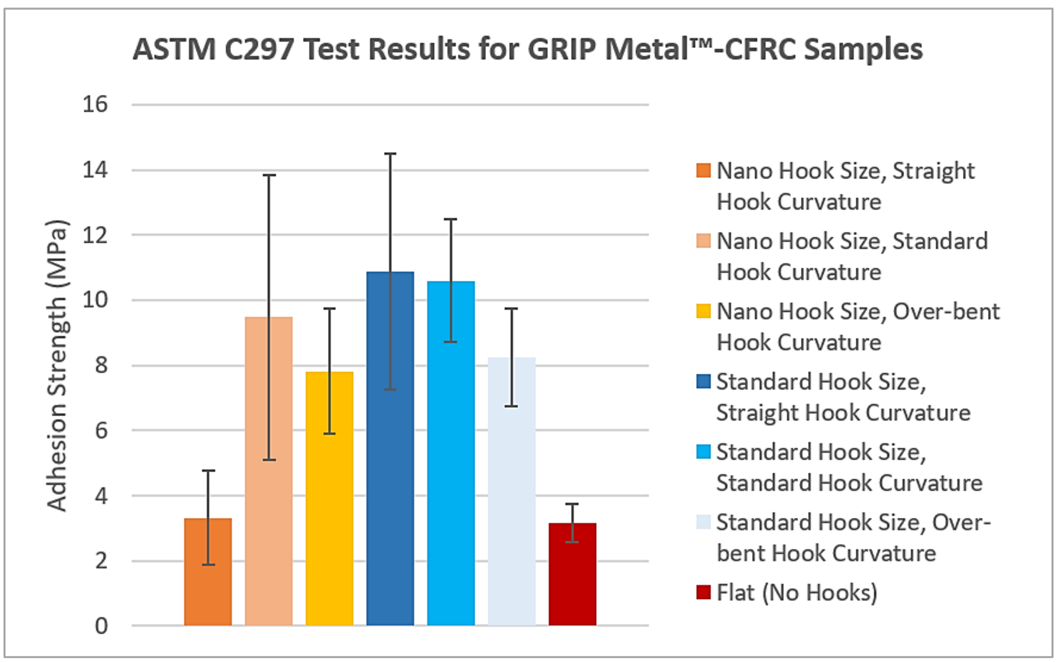

Figure 121 - Phase 2: ASTM C297 Test Results

In terms of standard deviations, all GRIP Metal™ samples performed similarly with the exception of the one configuration mentioned above. The highest value was achieved was with the standard size - straight curvature, at an average adhesion strength of 10.86 ± 3.62 MPa. In comparison, flat aluminium sheets performed only to an average of 3.16 ± 0.59 MPa.

Chapter 5

Discussion

5.1 Discussion on the Results of the Reverse Lay-up Method

5.1.1 Demoulding Technique

Metallic tapes (RL 1.1) could not sustain copper particles impingement and were abraded from the substrates. It was unclear how much adhesion strength would be needed for the tapes to stay adhered during spray. Success with this approach would depend on two parameters: tape to glue, and glue to mould interfacial adhesion strengths. A balance between the two would potentially avoid tape detachment. Although further investigation of this matter may lead to a better-defined answer, it was thought that a preferable alternative would be one that does not require an additional material for inducing interfacial defects.

The Dual Roughness Zone approach (RL 1.2) was successful and reproducible. This demoulding process requires only a small force to detach the coating from the mould. As zone Ra 2 had higher roughness than zone Ra 1, coatings should adhere less on the latter. Coating to mould adhesion strengths were tested for both zones and this assumption was confirmed, thence indicate that the coating to mould interfacial delamination begun from zone Ra 1 instead of Ra 2 during demoulding.

The Single Roughness Zone approach (RL 1.3) offered the benefit of reducing the number of steps required in surface preparations compared with RL 1.2. This would result in savings in labour costs and processing time. Roughness Ra 2 was used in this experiment instead of Ra 1 as the latter resulted in a coating adhesion that was too low for a complete build-up. The approach was proven equally successful and reproducible, meaning that roughness Ra 2 alone could ensure coating to mould interfacial delamination. It is reasonable to assume that a scenario where the coatings would not detach from the moulds occurs when coating to mould adhesion strengths are greater than either those of coating to CFRC, or than the coating's cohesive strength. In terms of incorporating this approach into industrial-scale CFRC manufacturing, overall complexity and additional costs remain low: the surface preparation is economical and easily achievable, and the protruding CFRC length requires simply a minor modification to mould design.

5.1.2 Coating Improvement: Dendritic Copper Powder

Results from depositing coatings at 300°C and 1.7 MPa (RL 1.4) showed that the low spray parameters identified from previous work could not generate a crack-free as-sprayed coating on the Invar substrates. Although most areas were found to be fully dense, others contained undesirable microcracks. This observation indicates that whilst dendritic copper particles could be deposited under given spray conditions, they did not deform extensively to form a firm bonding between themselves. The reason behind this discrepancy between the results obtained in previous and this work remain unclear.

Combining low and high spray parameters to generate a mixed coating microstructure (Code RL 1.5) showed that the as-sprayed coatings were fully dense on the moulds, with no sign of microcracks, nor visible distinction between the first and second layers. However, vertical cracks caused by thermal expansion coefficient mismatch between the copper and Invar were observed. As described briefly in section 4.1.5, the copper coatings were hot during spray and were cooled in ambient temperature. Volumetric contractions of the copper coatings were restricted by those of the Invar due to the significant difference in their TEC. Internal stresses generated inside the coatings resulted in these vertical cracks. Rises in temperatures were due to the slow gun traverse speed that let the gas stream to heat up both the coating and the substrate, over a relatively long period of time. This issue could be mitigated either by spraying at lower temperatures or by using faster traverse speeds; the latter option was chosen.

By increasing the spray parameters to 500°C and 3.45 MPa and spraying one layer only (RL 1.6), the as-sprayed coatings were fully dense on the moulds with no signs of microcracks. However, the coatings fractured after being demoulded along with the CFRCs. The coating to mould adhesion strengths were tested and an average of 6.12 ± 0.36 MPa was obtained. This value was too high for avoiding internal damages in the coatings during demoulding. This phenomenon occurs in case where the cohesive strengths between the coatings' particles are much lower than the coating to mould adhesion strengths. This hence proves that a compromise exists between coating to mould adhesion strengths, and the cohesive strengths of coatings.

The TEC mismatch issue was mitigated by spraying the second layer with doubled gun traverse speed (RL 1.7). The coatings as-sprayed on mould no longer showed signs of vertical cracks from the TEC mismatch. Etched coating cross-sections showed that many branches of the dendritic particles folded on themselves densely with no signs of gaps between their boundaries. Despite the as-sprayed coating being fully dense, the branches may not have bonded well to each other because the dendritic particles impact the substrate at high velocity, but their branches do not fold at equivalent speed. It is well-known that in cold spray, the impact velocity plays a critical role in the successful particle bonding [87]. Also, impinging particles can densify the coating by closing the gaps between the folds, but they do not necessarily contribute to bonding between folds. When the coatings were demoulded along with the CFRC, cracks were observed in the portion where the first layer is located. Cracks propagated from the first layer towards the second but decreased in intensity. This outcome indicated that the second layer had better cohesive strengths and hence impeded crack propagations.

Attempting to double either the first or the second layer (RL 1.8 and RL 1.9) failed to show significant difference to the results obtained in experiment RL 1.7. Overall it was difficult to predict and control the crack propagations in coatings made of dendritic copper.

5.1.3 Coating Improvement: Spherical Copper Powder

By using spherical copper powder (RL 1.10), trials led to immediate success whereby coatings had fully dense and crack-free microstructures on the mould and remained undamaged on the CFRCs through demoulding. The extra amount of deformation required for the spherical powder to adhere permitted that only the well-deformed particles stayed attached to the substrates, which created cohesively well bonded microstructures. Etched cross-sections confirmed that the particles were intensively deformed from spherical to pancake-shaped geometries.

Coating to CFRC adhesion strengths were tested and an average of 7.70 ± 0.38 MPa was obtained whereby all coatings failed in adhesion. This result indicates that the coatings had cohesive strengths that could withstand at least 7.70 MPa, which presents a significant increase in comparison with any tested coating-CFRC samples made with dendritic copper.

5.2 Discussion on the Results of GRIP Metal™ as Bond Coat Method

5.2.1 Phase 1: Characterization

Medians of hook heights were 580 μm and 1051 μm for aluminium 5052-H38 Nano size hooks and standard size hooks, respectively. The medians of hook heights were 639 μm and 1590 μm for AISI 1010 steel Nano size hooks and standard size hooks, respectively. All MADs were consistent within 8% from the median, with the exception of the configuration of aluminium Nano size hooks which was 14%. No specific comments on this peculiar deviation could be made, since no detailed information on the manufacturing process of the GRIP Metal™ sheets was disclosed by the supplier. These results indicate that the hooks in standard size were around 50% taller than those in the Nano size.

Medians of hook curvatures were 484 μm and 2663 μm in inner curvature radius for aluminium 5052-H38 Nano size hooks and standard size hooks, respectively. The medians of hook curvature were 593 μm and 2100 μm in inner curvature radius for AISI 1010 steel Nano size hooks and standard size hooks, respectively. The MADs were within 23% from the median for aluminium and within 18% for steel. These results indicate that the hooks in standard size were more straight than those in the Nano size.

The mean hook densities were calculated as 401 589 hooks/m^2 and 111 719 hooks/m^2 for aluminium 5052-H38 Nano size hooks and standard size hooks, respectively. The average hook densities were calculated as 479 276 hooks/m^2 and 72 505 hooks/m^2 for AISI 1010 steel Nano size hooks and standard size hooks, respectively. The standard deviation for each configuration was within a maximum of 2.5% from its mean value. These results indicate that the hook densities were unique to each GRIP Metal™ configuration.

All geometric values measured for hook profiles should be seen as comparative rather than deterministic due to the difficulty in assessing the accuracy of each measurement technique; all values collected contained some measurement error that could not be determined, hence measurement cannot be considered as exact. For example, hook curvatures were determined by matching value of the radius to the inner radius of each hook. Also, since each GRIP Metal™ configuration had unique hook density, the results cannot be compared directly, meaning that each GRIP Metal™ to CFRC assembly had its own characteristics in terms of consolidation and performance that cannot be used for establishing any direct, quantitative relationship to hook material, hook size, hook curvature, etc.

5.2.2 Phase 1: GRIP Metal™-CFRC Consolidation

Cross-sections of assemblies consolidated without pre-compression clearly showed that both the aluminium and steel hooks need more than 1 atm to penetrate deeply into the CFRC laminates. All samples made without pre-compression featured large voids at the metal to CFRC interfaces.

With pre-compression, the hooks penetrated deeper into the laminates, resulting in decrease in voids in the laminates. Whilst pre-compression generated better consolidated assemblies, porosities near and at the metal to CFRC interfaces were noticed. The occurrence and dimensions of these defects were unpredictable and therefore could not be quantified reliably. Steel hooks, being stiffer than aluminium, showed better penetration in both the Nano and standard configurations. It was observed that some standard size aluminium hooks were extensively bent and therefore could not pass through the laminates. These bent hooks distorted fibres severely. This phenomenon can be explained by the hooks' stiffness and length. Stiffer materials deform less than soft materials when a given stress is applied, which means that hooks made from AISI 1010 steel retained their shape better than aluminium 5052-H38 when sliding through the fibres. Also, long hooks are more susceptible to bending than short ones, in the similar manner than a cantilever beam.

The process of pre-compression with a manually operated hydraulic press was found to be less accurate than expected. Compression pressure was fluctuating during the operation, and needed constant re-adjustments. Moreover, the pressure gauge dial had large graduation unit that made accurate readings difficult.

5.2.3 Phase 1: GRIP Metal™-CFRC Adhesion Tests

All PATTI tests performed on consolidated GRIP Metal™-CFRC assemblies failed at the metal to CFRC interface with no damage to the hooks. Rust was found on all AISI 1010 Steel GRIP Metal™ samples on the hooked side (the one in contact with the CFRCs). This was most likely due to the air pockets at the metal to CFRC interfaces that oxidized the steel during curing at elevated temperatures.

Although PATTI tests showed different adhesion strengths for different configurations, the test results were potentially inaccurate due to the PATTI test setup process whereby dollies were isolated by cutting off surrounding material manually. This process may induce large amount of stresses at the metal to CFRC interfaces, and potentially engender delamination. Since the hooks still held the GRIP Metal™ in place, delamination could have happened without clear signs of occurrence when the samples were examined by eye.

5.2.4 Phase 2: Characterization

In phase 2, the medians of hook heights were 462 µm, 794 µm and 800 µm for straight, standard and over-bent configurations in Nano size hooks, respectively, whereas they were 1598 µm, 1291 µm and 1475 µm for straight, standard and over-bent configurations in standard size hooks, respectively. Comparing these results, it can be noticed that standard size hooks were anywhere from 1.6 to 3.5 times taller than Nano size hooks. The MADs were consistent within 7% from the median, except for the configuration of standard size - standard curvature, at 11%. Overall, hooks of the same size category had similar heights. Nevertheless, it was noticeable that the configuration Nano size - straight curvature featured hooks that were significantly shorter than their counterparts of the same size category. Again, no comment on these deviations could be made, but it is believed that manufacturing inconsistencies caused this outcome.

Medians of hook curvatures were 531 µm, 566 µm and 578 µm in curvature radius for straight, standard and over-bent configurations in Nano size hooks, respectively, whereas they were 2123 µm, 2296 µm and 1707 µm in curvature radius for straight, standard and over-bent configurations in standard size hooks, respectively. The MADs were within 19% from the median with the exception of the configuration standard size -standard curvature, at 36%. Overall, the results showed that small hooks were more curved than larger ones. In terms of MADs, hooks had similar curvature radii within same hook size category.

Mean hook densities were 384 591 hooks/m^2, 386 026 hooks/m^2 and 387 720 hooks/m^2 for straight, standard and over-bent configurations in Nano size hooks, respectively, whereas they were 103 524 hooks/m^2, 101 759 hooks/m^2 and 104 097 hooks/m^2 for straight, standard and over-bent configurations in standard size hooks, respectively. The standard deviations showed that the hook densities were relatively consistent and within a maximum of 3.8% from their mean. With consideration of potential measurement error, it can be stated that the densities were identical within same hook size category.

5.2.5 Phase 2: GRIP Metal™-CFRC Consolidation

Pre-compression using the Instron machine was straight forward and consistent. Pressure decreased slightly during the 5-minute holding period, due to resin flow and fibre realignment, but the difference was re-adjusted accordingly.

Cross-section analyses showed that all configurations featured porosities near and at the metal to CFRC interfaces, and induced fibre distortion in the top layers of the laminate. All consolidated laminates of the same hook size category looked similar, except for Nano hooks of straight curvature (GM P2 Al1), since the latter had much shorter hooks. Larger hooks did penetrate deeper into the CFRC laminates, but in some areas, some large hooks failed to penetrate and therefore bent their tip intensively, causing significant distortion to fibres. As seen in phase 1, fibre distortion and porosities were unpredictable in terms of location and quantity, which made their quantification challenging.

5.2.6 Phase 2: GRIP Metal™-CFRC Adhesion Tests

ASTM C297 test results showed that all configurations, with the exception of the configuration Nano size - straight curvature (GM P2 Al1), outperformed flat metal sheets in term of metal to CFRC interfacial adhesion, averaging in the range between 8 to 11 MPa. However, the standard deviations were overlapping. The underperformance seen in experiment GM P2 Al1 was likely due to the shorter hook profile used with that configuration.

When considering the overlapping standard deviations, all configurations performed similarly except for the particular configuration mentioned above. No damage to the hooks was observed, but in some cases, chunks of fibres remained attached to the metal interfaces. These chunks came from CFRC interlayer delamination, which was likely as a result of the interlayer porosities induced by hook penetration.

Adhesion strengths may not have been optimal due to the presence of porosities, particularly voids at the metal to CFRC interfaces that contribute in delamination. Nevertheless, GRIP Metal™ sheets increased metal to CFRC interfacial adhesion thanks to their hooks that added extra bonding surface areas for the epoxy resin. Nevertheless, this increase traded off the consolidation quality of the CFRCs to the porosities and fibre distortions.

5.3 Comparison between the Methods

Both methods aimed at solving the vulnerabilities of CFRCs, each in its own way. When comparing overall complexity of integration into existing CFRC manufacturing procedures, the Reverse Lay-up Method offers an advantage due to its ability to adapt to existing processes. The Reverse Lay-up Method only requires spraying a coating on the mould whereas GRIP Metal™ would still need stretch-forming in addition to chiselling hooks from the surfaces of the metal sheets. Furthermore, the Reverse Lay-up Method does not induce any defect into the CFRC laminate. In contrast, GRIP Metal™ hooks create fibre distortions in the top layers of the laminates, and porosities near and at metal to CFRC interfaces. In term of metal to CFRC adhesion strength, both methods generated similar results with laminates created using GRIP Metal™ as Bond Coat Method slightly outperforming laminates made using the Reverse Lay-up Method.

Chapter 6

Conclusions

In this work, two metallization techniques were investigated for the protecting CFRCs against erosion and lightning strikes: Reverse Lay-up Method and GRIP Metal™ as Bond Coat Method. Objectives pertaining to each method were reached:

Reverse Lay-up Method

1. Development of a reliable demoulding process
2. Development of dense and crack-free copper coatings on CFRCs

GRIP Metal™ as Bond Coat Method

1. Characterization of GRIP Metal™ sheets
2. Assessment on GRIP Metal™ integration into CFRCs

6.1 Conclusions of Reverse Lay-up Method

A reliable demoulding process was developed whereby an extra length of CFRC was added to the composite component's original size. The extra material protruded one edge of the mould and hence served as a cantilever for initiating the demoulding. The demoulding process was nearly effortless, and no visible coating damage was observed when examined by eye.

Coating quality improvement was attempted using different spray parameters for dendritic copper powder, and a satisfactory coating was ultimately achieved using spherical copper powder. For dendritic copper, the results showed that low spray parameters (RL 1.4) generated as-sprayed coatings with low coating to mould adhesion but cracked microstructures, whereas high spray parameters (RL 1.6) generated as-sprayed coatings with high coating to mould adhesion but crack-free microstructures. Both cases did not produce satisfactory coatings on CFRC. Attempts with layer combinations (RL 1.5, 1.7 -1.9) showed improvements in mitigating microcracks; crack propagation induced by demoulding was impeded by the dense second layer thanks to the better cohesive strength of the latter. Ultimately, spherical powder (RL 1.10) generated the desired coating microstructures that were dense and crack-free both in as-sprayed and in post-demoulding states. Two major factors contributed to this success: low coating to mould adhesion and high cohesive strength of the coating. Coating to CFRC adhesion strength tests showed that all coatings made of spherical copper powder failed in adhesion at an average of 7.70 ± 0.38 MPa.

6.2 Conclusions of GRIP Metal™ as Bond Coat Method

GRIP Metal™ products were characterized in terms of hook height, hook curvature and hook density. It was found that some GRIP Metal™ configurations had significant inconsistencies in hook height and/or hook curvature. Also, all configurations in phase 1 featured unique hook densities.

The integration of GRIP Metal™ into CFRC was investigated. In phase 1, samples made with and without pre-compression were compared. Results showed that more than 1 atm pressure was required to push hooks adequately into uncured CFRC laminates. GRIP Metal™-CFRC samples made without pre-compression featured large voids at the metal to CFRC interfaces, whereas those made with pre-compression had significantly less. The results also revealed that intrusion of hooks into CFRC induced fibre distortions that led to the formation of resin-rich zones and porosities. In phase 2, aluminium GRIP Metal™ configurations with different hook sizes and curvatures were probed. Characterization revealed that configurations within the same hook size category showed similar hook profiles without distinctive features. GRIP Metal™-CFRC samples in phase 2 were tested using ASTM C297 standard; all configurations showed significant increase in metal to CFRC adhesion in comparison to flat aluminium sheets, with the exception of configuration Nano size - straight curvature. In comparison to the Reverse Lay-up Method, GRIP Metal™ slightly outperformed in term of metal to CFRC adhesion strength.

6.3 Future Work

For the Reverse Lay-up Method, the next step will consist in generating copper coatings of variable thicknesses on complex mould geometries. Knowledge gained in this work can also be transferred to other coating materials, such as titanium. The layer combination approach opens the possibility of generating hard coating materials on CFRCs, for example using a low-adhesion first layer of copper by cold spray and dense second layer of ceramic material by HVOF spray.

For the GRIP Metal™ as Bond Coat Method, the next step will consist in mitigating fibre distortions and porosities. It would also be interesting to study the potential increase in interfacial shear bond strength and the feasibility of GRIP Metal™ integration into complex CFRC geometries. Plus, coatings should be deposited on the bond coats and be examined subsequently.

References

[1] S. Putić, P. S. Uskoković and R. Aleksić, "Analysis of Fatigue and Crack Growth in Carbon-Fiber Epoxy Matrix Composite Laminates," *Strength of Materials - Springer,* vol. 35, no. 5, 2003.

[2] B. Zettl, H. Mayer, C. Ede and S. Stanzl-Tschegg, "Very High Cycle Fatigue of Normalized Carbon Steels," *International Journal of Fatigue,* vol. 28, no. 11, pp. 1583-1589, 2006.

[3] A. P. Cysne Barbosa, A. P. P. Fulco, E. S. S. Guerra, F. K. Arakaki, M. Tosatto, M. C. B. Costa and J. D. D. Melo, "Accelerated Aging Effects on Carbon Fiber/Epoxy Composites," *Composites Part B: Engineering,* vol. 110, pp. 298-306, 2016.

[4] "Modern Airliners," 2015. [Online]. Available: http://www.modernairliners.com/boeing-787-dreamliner/boeing-787-dreamliner-specs/. [Accessed 24 10 2017].

[5] "GE Aviation," General Electric, [Online]. Available: https://www.geaviation.com/commercial/engines/ge90-engine. [Accessed 24 10 2017].

[6] E. Kwon and J. Damazo, "Lightning protection research partnership," Boeing, [Online]. Available: http://www.boeing.com/features/innovation-quarterly/aug2017/feature-technical-lightning.page. [Accessed 25 10 2017].

[7] A. Papyrin, "Cold Spray Technology," Ktech Corporation, Alburquere, 2001.

[8] M. Guagliano, M. Dao, S. M. Hassani-Gangaraj and A. Moridi, "Cold spray coating: review of material systems and future perspectives," *Surface Engineering,* vol. 36, pp. 369-395, 2014.

[9] H. Assadi, T. Schmidt, H. Richter, J.-O. Kliemann, K. Binder, F. Gartner, T. Klassen and H. Kreye, "On Parameter Selection in Cold Spraying," *Journal of Thermal Spray Technology,* vol. 20, no. 6, pp. 1161-1176, 2011.

[10] H. Che, P. Vo and S. Yue, "Metallization of carbon fibre reinforced polymers by cold spray," *Surface & Coatings Technology,* vol. 313, pp. 236-247, 2016.

[11] R. Lupoi and W. O'Neil, "Deposition of metallic coatings on polymer surfaces using cold spray," *Surface & Coatings Technology,* vol. 205, pp. 2167-2173, 2010.

[12] A. Ganesan, M. Yamada and M. Fukumoto, "Cold Spray Coating Deposition Mechanism on the Thermoplastic and Thermosetting Polymer Substrates," *Journal of Thermal Spray Technology,* vol. 22, no. 8, pp. 1275-1282, 2013.

[13] M. Gagne, Properties of Lightning Strike Protection Coatings, Montreal: Universite de Montreal, 2016.

[14] G. Archambault, B. Jodoin, S. Gaydos and M. Yandouzi, “Metallization of carbon fiber reinforced polymer composite by cold spray and lay-up molding processes,” *Surface & Coatings Technology,* vol. 300, pp. 78-86, 2016.

[15] S. Mileiko, A. Rudnev and M. Gelachov, “Carbon-Fibre/Titanium Silicide Interphase/Titanium-matrix Composites: Fabrication, Structure and Mechanical Properties,” *Elsevier,* vol. 55, no. 3, p. 1, 1995.

[16] “Matweb,” 2017. [Online]. Available: http://www.matweb.com/search/QuickText.aspx?SearchText=carbon%20fibre. [Accessed 24 10 2017].

[17] “ASM - Aluminum 7075-T6; 7075-T651,” MatWeb, [Online]. Available: http://asm.matweb.com/search/SpecificMaterial.asp?bassnum=MA7075T6. [Accessed 25 10 2017].

[18] Hexcel, 2017. [Online]. Available: http://www.hexcel.com/Resources/DataSheets/Carbon-Fiber. [Accessed 24 10 2017].

[19] “MatWeb,” [Online]. Available: http://www.matweb.com/search/DataSheet.aspx?MatGUID=1c74545c91874b13a3e44f400cedfe39&ckck=1. [Accessed 24 12 2017].

[20] C. Michael Hudson, “A Study of Fatigu and Fracture in 7075-T6 Aluminum Alloy in Vacuum and Air Environment,” NASA, Hampton, Va., 1973.

[21] J. Yu, Y. Liu and R. Shi, “Studies on Crack Propagation of Carbon Fiber Reinforced Epoxy Resin Composite,” Trans Tech Publications, Switzerland, 2009.

[22] FAA, “Chapter 7: Advanced Composite Materials,” in *AMT Handbook - Airframe*, U.S. Department of Transportation, 2012, pp. 7-3.

[23] D. P. Avery, D. D. Samborsky, J. F. Mandell and D. S. Carins, “Compression Strength of Carbon Fiber Laminates Containing Flaws with Fiber Waviness,” *42 nd AIAA Aerospace Sciences Meeting and Exhibit (2004), pp. 54-63 Key: citeulike:6792719,* pp. 54-63, 2004.

[24] A. Thiruvengadam, “The Concept of Erosion Strength,” *Erosion by Cavitation or Impingement,* pp. 22-41, 1967.

[25] B. Bochman, “AirInsight,” Dexmet Corp, 2013. [Online]. Available: https://www.airinsight.com/down-the-supply-chain-dexmet-corporations-lightning-strike-protection/. [Accessed 25 10 2017].

[26] "Airship.net," [Online]. Available: http://www.airships.net/delag-passenger-zeppelins/. [Accessed 24 10 2017].

[27] IATA, "IATA," 2 February 2017. [Online]. Available: http://www.iata.org/pressroom/pr/Pages/2017-02-02-01.aspx. [Accessed 24 October 2017].

[28] IATA, "IATA," 16 July 2013. [Online]. Available: http://www.iata.org/pressroom/pr/Pages/2013-07-16-01.aspx. [Accessed 24 October 2017].

[29] R. Hedayati and M. Sadighi, "An Experimental, Theoretical and Numerical Investigation," *Bird Strike,* pp. 9-33, 2016.

[30] J. Hanna and J. Thomas, "CNN, U.S.+," CNN, 9 8 2015. [Online]. Available: http://www.cnn.com/2015/08/08/us/delta-emergency-landing-hail/index.html. [Accessed 24 10 2017].

[31] J. Johnson, "Twitter," 8 8 2015. [Online]. Available: https://twitter.com/jwjohnson99/status/629953153434193920/photo/1?ref_src=twsrc%5Etfw&ref_url=http%3A%2F%2Fmashable.com%2F2015%2F08%2F09%2Fhail-storm-delta-flight%2F. [Accessed 24 10 2017].

[32] LoireTech, 2017. [Online]. Available: http://www.loiretech.com/forming-and-stretching-technologies. [Accessed 24 10 2017].

[33] "http://theatlasgroup.biz," The Atlas Group, [Online]. Available: http://theatlasgroup.biz/capabilites/stretch-forming-capabilities/. [Accessed 12 12 2017].

[34] "Static Electricity - Lesson 4 - Electric Fields," PhysicClassRoom, [Online]. Available: http://www.physicsclassroom.com/class/estatics/Lesson-4/Lightning. [Accessed 25 10 2017].

[35] "Lightning Strikes: Protection, Inspection and Repair," The Boeing Company, 4 2014. [Online]. Available: http://www.boeing.com/commercial/aeromagazine/articles/2012_q4/4/. [Accessed 25 10 2017].

[36] "General Aviation Lightning Strike Report and Protection Level Study," U.S. Department of Transportation Federal Aviation Administration, Springfield, Virginia, 2004.

[37] "Boeing examines expanded metal foils for lightning protection of composite structures," SAE, 8 1 2014. [Online]. Available: http://articles.sae.org/12712/. [Accessed 12 12 2017].

[38] "Copper Expandaded Mesh," IndiaMart, [Online]. Available: https://dir.indiamart.com/impcat/expanded-mesh.html. [Accessed 12 12 2017].

[39] "Nitric Acid," PubChem, 16 9 2004. [Online]. Available: https://pubchem.ncbi.nlm.nih.gov/compound/nitric_acid#section=Taste. [Accessed 25 10 2017].

[40] S. Gao, M. Fan and W. Guiping, "Copper Plating on the Carbon Fibers by Double Pulse," *Applied Mechanics and Materials,* Vols. 148-149, pp. 928-931, 2012.

[41] H. Zhongsheng, L. Yihan, Y. Guangchun, W. Lei, M. Jia and L. Lisi, "Preparation and Characterization of Nickel-Coated Carbon Fibers by Electroplating," *Journal of Materials Engineering and Performance,* vol. 21, no. 3, pp. 324-330, 2012.

[42] K. L. Chopra, P. D. Paulson and V. Dutta, "Think-film Solar Cells: An Overview," *Progress in Photovoltaics: Research and Applications,* vol. 12, pp. 69-92, 2004.

[43] C. Maurer and U. Schulz, "Erosion resistant titanium based PVD coatings on CFRP," *Wear,* 2013.

[44] S. Stokes, "Chemical Vapor Deposition," CNX.org, [Online]. Available: https://archive.cnx.org/contents/9bbbe39c-a840-4461-882ce31f8a0125e6@2/chemical-vapor-deposition. [Accessed 25 10 2017].

[45] Z. Guo, L. Sang, Z. Wang, Q. Chen, L. Yang and Z. Liu, "Deposition of copper thin films by plasma enhanced pulsed chemical vapor deposition for metallization of carbon fiber reinforced plastics," *Surface and Coatings Technology,* vol. 307, pp. 1059-1064, 2016.

[46] A. Abidin, R. Kozera, M. Hohn, I. Endler, M. Knaut, A. Boczkowska, A. Czulak, P. Malczyk, N. Sobczak and A. Michaelis, "Preparation and characterization of CVD-TiN-coated carbon fibers for applications in metal matrix composites," *Thin Solid Films,* vol. 589, pp. 479-486, 2015.

[47] J. Affi, H. Okazaki, Y. Motohiro and M. Fukumoto, "Fabrication of Aluminum Coating onto CFRP Substrate by Cold Spray," *Materials Transactions,* vol. 52, no. 9, pp. 1759-1763, 2011.

[48] M. Fukumoto, A. Ganesan, M. Yamada and Y. Tsunekawa, "Thick Metallic/Composite Coating on C-FRP Substrate by Plasma Spraying," in *International Symposium of Plasma Chemistry,* Queensland, 2013.

[49] "Daimler Technology," Daimler AG, 31 8 2011. [Online]. Available: http://media.daimler.com/marsMediaSite/en/instance/ko/Friction-losses-minimised-by-NANOSLIDE-technology-Mercedes-Benz-innovation-NANOSLIDE-for-lower-consumption.xhtml?oid=9915751. [Accessed 25 10 2017].

[50] A. Liu, M. Guo, M. Zhao, H. Ma and S. Hu, "Arc sprayed erosion-resistant coating for carbon fiber reinforced polymer matrix composite substrates," *Surface & Coatings Technology 200,* 2005.

[51] M. Ivosevic, R. Knight, S. R. Kalidindi, G. R. Palmese and J. K. Sutter, "Adhesive/Cohesive Properties of Thermally Sprayed Functionally Graded Coatings for Polymer Matrix Composites," *Journal of Thermal Spray Technology,* 2004.

[52] A. McDonald, N. Huonnic, M. Abdelghani and P. Mertiny, "Deposition and characterization of flame-sprayed aluminum on cured glass and basalt fiber-reinforced epoxy tubes," *Surface & Coatings Technology,* vol. 205, pp. 867-873, 2010.

[53] "GE Global Research," General Electric, 07 11 2013. [Online]. Available: http://www.geglobalresearch.com/blog/cold-spray-ge-technology. [Accessed 25 10 2017].

[54] T. Jerman and J. Langus, "Calculating cold gas microthruster velocity flow using finite volume analysis," University of Ljubljana, Ljubljana, 2011.

[55] M. Grujicic, C. Zhao, W. DeRosset and D. Helfritch, "Adiabatic shear instability based mechanism for particles/substrate bonding in the cold-gas dynamic-spray process," *Materials & Design,* vol. 25, no. 8, pp. 681-688, 2004.

[56] T. Hussain, D. McCartney, P. Shipway and D. Zhang, "Bonding Mechanisms in Cold Spraying: The Contributions of Metallurgical and Mechanical Components," *Journal of Thermal Spray Technology,* vol. 18, no. 3, pp. 364-379, 2009.

[57] E. Maev, V. Leshchynsky, E. Strumban and D. Dzhurinskiy, "Influence of Grit Blasting on the Interface Roughness and Adhesion Strength of Cold Sprayed Copper Coatings," in *International Thermal Spray Conference and Exposition 2015*, Long Beach, 2015.

[58] H. Assadi, F. Gartner, T. Stoltenhoff and H. Kreye, "Bonding mechanism in cold gas spraying," *Acta Materialia,* vol. 51, no. 15, pp. 4379-4394, 2003.

[59] B. DuBose, "Cold Spray Technology Designed to Repair Commercial Aircraft Parts," MaterialPerformance.com, 1 6 2017. [Online]. Available: http://www.materialsperformance.com/articles/material-selection-design/2017/06/cold-spray-technology-designed-to-repair-commercial-aircraft-parts. [Accessed 26 10 2017].

[60] "Case Study - Cold Spray, Landing Gear," COC Aerospace, 3 9 2016. [Online]. Available: http://www.materialsperformance.com/articles/material-selection-design/2017/06/cold-spray-technology-designed-to-repair-commercial-aircraft-parts. [Accessed 26 10 2017].

[61] H. Bu, M. Yandouzi, C. Lu and D. MacDonald, “Cold spray blended Al + Mg17Al12 coating for corrosion protection of AZ91D magnesium alloy,” *Surface and Coatings Technology,* vol. 207, pp. 155-162, 2012.

[62] M. Kumar, H. Singh, N. M. Chavan, S. Kumar and S. V. Joshi, “Development of Erosion-Corrosion-Resistant Cold-Spray Nanostructured Ni-20Cr Coating for Coal-Fired Boiler Applications,” *Journal of Thermal Spray Technology,* vol. 24, no. 8, pp. 1441-1449, 2015.

[63] E. Calla, S. Pabla and R. Goetze, “Turbine rotor fabrication using cold spraying”. USA Patent US 20110078896 A1, 7 10 2009.

[64] “Producing seamless pipes in less steps,” CSIRO, 9 12 2016. [Online]. Available: https://www.csiro.au/en/Research/MF/Areas/Metals/Cold-Spray/Manufacturing-pipes. [Accessed 12 12 2017].

[65] C. Yannick, D. Philippe, B. Jodoin and A. Corbeil, “Pyramidal Fin Arrays Performance Using Streamwise Anisotropic Materials by Cold Spray Additive Manufacturing,” *Journal of Thermal Spray Technology,* vol. 25, no. 1-2, pp. 170-182, 2016.

[66] B. Wu, J. Zheng, J. Qiu, Z.-q. Zou, K.-b. Yan, X.-l. Chen, L.-m. Hu, K.-s. Zhang and R.-g. Chen, “Preparation of the projectile rotating band and its performance evaluation,” *Journal of Adhesion Science and Technology,* vol. 30, no. 11, pp. 1143-1164, 2016.

[67] D. Cormie, “uO Research,” 2015. [Online]. [Accessed 25 10 2017].

[68] V. Bortolussi, F. Borit, A. Chesnaud, M. Jeandin, M. Faessel, B. Figliuzzi, F. Willot, K. Roche and G. Surdon, “Cold spray of metal-polymer composite coatings onto carbon fiber-reinforced polymer (CFRP),” in *Inter-national Thermal Spray Conference 2016,* Shanghai, 2016.

[69] H. Che, X. Chu, P. Vo and S. Yue, “Cold spray of mixed metal powders on carbon fibre reinforced polymers,” *Surface & Coatings Technology,* vol. 329, pp. 232-243, 2017.

[70] X.-T. Luo, C.-J. Li and Y.-J. Li, “Dependency of deposition behavior, microstructure and properties of cold sprayed Cu on morphology and porosity of the powder,” *Surface & Coatings Technology,* vol. 328, pp. 304-312, 2017.

[71] W. Wong, P. Vo, A. Irissou, N. Ryabinin, J.-G. Legoux and S. Yue, “Effect of Particle Morphology and Size Distribution on Cold-Sprayed Pure Titanium Coatings,” *Journal of Thermal Spray Technology,* vol. 22, no. 7, p. 1140–1153, 2013.

[72] B. Jodoin, L. Ajdelsztajn, E. Sansoucy, A. Zúñiga, P. Richer and E. Lavernia, “Effect of particle size, morphology, and hardness on cold gas dynamic sprayed aluminum alloy coatings,” *Surface & Coatings Technology,* vol. 201, pp. 3422-3429, 2006.

[73] "YouTube," Nucap Brakes, 20 11 2015. [Online]. Available: https://www.youtube.com/watch?v=ItgkU61myuU. [Accessed 24 10 2017].

[74] "Backing Plates," NUCAP, [Online]. Available: http://www.nucap.com/products/backing-plates/nrs. [Accessed 12 12 2017].

[75] D. Dickson, "www.sme.org," The Boeing Company, 30 8 2007. [Online]. Available: www.sme.org/uploadedFiles/Events/Webinars/layup_tooling.pdf. [Accessed 15 11 2017].

[76] C. Ltd., "SupersonicSpray," 4 2015. [Online]. Available: http://supersonicspray.com/knowledge-docs/en/SST-TDS-C5003-PR-1_3-0415.pdf. [Accessed 12 11 2017].

[77] P. S. Technologies, "Praxair," 23 7 2014. [Online]. Available: http://www.praxairsurfacetechnologies.com/components-materials-and-equipment/materials/thermal-spray-powders/pure-metals-and-metal-alloys. [Accessed 12 11 2017].

[78] "GRIP Metal," Nucap, [Online]. Available: http://www.gripmetal.com/. [Accessed 22 12 2016].

[79] "Gurit - SE70," 17 08 2014. [Online]. Available: http://www.gurit.com/-/media/Gurit/Datasheets/se-70.ashx. [Accessed 12 11 2017].

[80] "Gurit - SA70," 15 05 2016. [Online]. Available: http://www.gurit.com/-/media/Gurit/Datasheets/sa-70.ashx?la=en&hash=7F094852696A99E226C39780B6E0CAA2AE32B0F2. [Accessed 12 11 2017].

[81] H. Hirakata, T. Kitamura and D. V. Truong, "Initiation of interface crack at free edge between thin films with weak stress singularity," *Thin Solid Films,* vol. 515, pp. 3005-3010, 2007.

[82] A. International, "ASTM," 2016. [Online]. Available: https://www.astm.org/Standards/C297.htm. [Accessed 10 11 2017].

[83] "MatWeb - Copper, Cu; Cold-worked," [Online]. Available: http://www.matweb.com/search/DataSheet.aspx?MatGUID=ca486cc7cefa44d98ee67d2f5eb7d21f. [Accessed 25 10 2017].

[84] "MatWeb - Carpenter Invar 36 Alloy, Cold Drawn Bars," Carpenter Technology Coporation, [Online]. Available: http://www.matweb.com/search/datasheet.aspx?matguid=b6fb00b235f0442da4d31a0cd04671c9&ckck=1. [Accessed 25 10 2017].

[85] Henkel Aero, “LOCTITE metal & honeycomb bonding,” 2018. [Online]. Available: http://www.henkel-adhesives.com/aerospace/metal-honeycomb-bonding-50417.htm. [Accessed 23 5 2018].

[86] “Design Guide for Bonding Metals,” Henkel Loctite, 2014. [Online]. Available: chrome-extension://oemmndcbldboiebfnladdacbdfmadadm/https://www.ellsworth.com/globalassets/literature-library/manufacturer/henkel-loctite/henkel-loctite-design-guide-bonding-metals.pdf. [Accessed 10 11 2017].

[87] F. Raletz, M. Vardelle and G. Ezo'o, “Critical particle velocity under cold spray conditions,” *Surface & Coatings Technology,* vol. 201, no. 5, pp. 1942-1947, 2006.